Study of Flow and Transport in Fractured Granitic Rock

by

Cliford Ndiweni

Thesis submitted in fulfillment of the requirements

for the degree of

Doctor of Philosophy

in the Faculty of Agricultural and Natural Sciences

(Institute of Groundwater Studies)

University of the Free State

Bloemfontein, South Africa

May 2012

Declaration

I declare that this thesis is my own, unaided work. It is being submitted for the degree of Doctor of Philosophy in the University of the Free State, Bloemfontein. It has not been submitted before for any degree or examination at any University.

....

Dedication

To

My Dear Wife Nthabiseng
&

My Boys

Thandwa and Bakithi

I love you all for making the difference in my life
You are so special. I am so proud of you

Abstract

The hydrogeology of the Tono basin, Japan, is strongly influenced by the hydraulic properties of faults, especially the main Tsukiyoshi fault, which extends through the centre of the assessment area and has an E-W strike. According to the results of borehole investigations, the fault has $N80^0W$ strike, 70^0 dip, $10 - 30m$ width and approximately $30m$ vertical off-set. Hydraulic head discontinuities over the main fault in the basin are about 40 m as a result of the low permeability of the fault acting as a barrier to flow perpendicular to it. The fracture data from the Tono basin was analysed in order to establish a correlation between geologic/geometric attributes of a fracture and associated permeability of the interval that contains the fracture, if any. Pressure response transients to excavation of two shafts that are monitored at various boreholes within the study site show that proximity to a fault is a key attribute that determines the ability of the fracture to conduct water. The responses in boreholes that are close to the fault are vertically invariant, indicating a large vertical permeability. This is not the case in boreholes that are further from the main fault, where there is depth dependence in the pressure responses. Near the fault, the damage zone seems to be equilibrating the heads between otherwise unconnected aquifers. The Tsukiyoshi fault therefore acts as barrier to flow perpendicular to it but also acts as conduit to vertical flow and flow parallel to the fault.

A three-dimensional model that simulates groundwater flow in the Tono basin is constructed in order to study the dynamic fluid flow before and after it was disturbed by production and the excavation of the shafts. In the steady-state calculation, the model predicts that the hydraulic head at depth in boreholes near the fault is near the land surface. This condition indicates high vertical permeability in those boreholes.

This thesis introduces a new approach of using pressure response data to do an inversion calculation for the effective porosity of the granite. Pressure response transients have been analysed using a numerical inversion procedure to estimate the specific storage of the granite. The specific storage was calculated using the pressure response data and ranged from 4.12×10^{-7} to $8.93 \times 10^{-6} m^{-1}$.

These values of the specific storage were used to do a transport calculation in order to study the impact of the main fault on the transportation of hypothetical contaminants in the basin. Particle tracking was used to investigate and demonstrate the effects of the fault on path lines. The fault was found to have a strong influence on the transportation of contaminants. The general trend of the transportation of the contaminants follows groundwater flow from the northern high elevations toward the southern low elevation. This shows that the contaminants are transported mainly by advection. However, this trend is interrupted by the Tsukiyoshi fault that blocks horizontal flow and sends water toward the surface. An interesting feature demonstrated by the model is that, within the fault core, no contaminants were

found. The contaminants rise through the high-permeability damage zone and cross over the fault through the weathered granite. However, at depths where the water changes direction slowly because of the fault barrier to horizontal flow, the contaminants seem to be able to cross the fault. The explanation is that diffusion becomes the dominant mode of transport at the point where the water moves at slow velocities.

Acknowledgments

I would like to begin my story of the study of flow and transport in granitic rock on the first day I contacted my thesis advisor, Dr Kenzi Karasaki (this is probably the best decision I have ever made in my life!). When I approached Dr. Karasaki to see if he would be interested in supervising a PhD thesis in this subject, it did not take him long to agree and suggest a project. I was very excited – such a project combined physics, geology and computers – a perfect combination of three different subjects, all of which I found particularly interesting.

I would also like to observe that the long-term study and analysis of groundwater flow and transport in granitic rock was and is an exacting task that requires a maximum of patience, insight and scientific rigor. I have always felt that there was no one more suited to this study than the person who I have had the honour of having as my thesis co-supervisor. I am therefore very grateful to Kenzi for all he has done for me. To me, he is not only a thesis advisor but also a friend and brotherly figure. From him I have learnt the way of thinking and doing.

I take this opportunity to sincerely thank Dr Christine Doughty of the Lawrence Berkeley Laboratory (LBL) for all her guidance and patience with me when I did not understand what now appears obvious. For all the e-mails and long discussions when I visited her at LBL, I will be forever grateful. Chris has been a real teacher

to me in groundwater modelling, pointing out the subtleties that were not clear to me and giving me the encouraging words: 'It will be clear to you as you gain experience'. I have also quoted extensively from her and Kenzi's reports, which are the foundations of my thesis.

I would like to express my deep and sincere gratitude to my supervisor, Professor GJ van Tonder, not only for agreeing to stand in as my supervisor, but also for his insistent enthusiasm and his valuable contributions to this work. His wide knowledge and logical way of thinking have been of great value to me. His understanding, encouragement and personal guidance have provided a good basis for the completion of this thesis.

I want to thank my family for their patience and encouragement while I pursued this project. In particular, I want to mention my boys Thandwa and Bakithi (to whom, along with my wife, this thesis is dedicated), with the hope that this work might inspire them in their own education. Finally I want to sincerely thank my long-suffering wife, Nthabiseng Dieketseng Ndiweni, for her steady support since way back when. My sincere thanks also go to my grandparents, whose views and teachings have had the greatest influence of all on my outlook, goals and accomplishments, including this work.

Contents

List of Figures

List of Tables

Introduction

Groundwater models are powerful tools for evaluating the impact of human activities on groundwater resources. Models allow the water resource engineer or geo-hydrologist to evaluate, for example, the sustainable capacity of a groundwater system, the effect of land use changes on the water balance, the appropriate extent of the protected capture zone for a well, the effects of competing activities on the resource, the consequences of contamination as a result of a spill or the effectiveness of groundwater remediation measures. State-of-the-art models can now handle complex situations such as heterogeneous or fractured materials, as well as large aquifer systems in 3-D, extending over many hundreds of square kilometres. By means of models, the engineer or planner can assess the impact of management decisions before they are implemented, and thereby assure the long-term sustainability of the resource.

Another important application of models is the planning and design of waste disposal facilities. Regulatory agencies require that all risk arising from the facility be quantified and shown to be within acceptable levels. Modern groundwater models are the only tools that allow the comprehensive evaluation of the impact of such facilities and the effects of measures to control the impact, and their use is often mandatory in the approval process.

Models can be used at regional as well as local scale to investigate detailed problems. The accuracy of the model results is limited only by the detail and accuracy of the available geological and hydrogeological data. It is therefore very important to exercise care in obtaining the necessary field data.

Modern groundwater models have evolved over the last few decades in parallel with the advent of the computer. Early methods for the quantitative analysis of groundwater systems include graphical methods for the determination of equipotential lines and flow lines (limited to two dimensions) and electrical analogue models consisting of networks of resistors and capacitors representing the transmission and storage capacities of an aquifer, as well as physical sandbox models. While these models were reliable in the hands of a skilled practitioner, they were laborious and inflexible in that a change of the parameters or boundary conditions required reconstruction of the model, and they were limited to very simple conditions. By contrast, a digital model, once it has been set up, can be effortlessly rerun for a number of parameter combinations or boundary conditions, handling virtually any complexity.

Digital models are developed mathematically, starting with the governing partial differential equations describing the physical process. These equations are generally an expression of mass conservation over the solution domain. For idealized conditions, it is often possible to find an analytical solution to the governing equation (such as the Theis solution for flow to a well) (Theis, 1935). Unfortunately, most analytical solutions are limited to very simple geometries and constant parameters. Most real groundwater systems, on the other hand, are complex in the sense that the boundary conditions may be irregular, the hydraulic conductivities may be heterogeneous, and there may be processes such as transport, degradation or chemical reactions taking place in the aquifer. Under such complex conditions, the solution of the governing equations requires numerical methods.

Before discussing the different approaches to modelling fractured terrain, it is important to note that in all cases it is crucial that the conceptual models, including the modelling approaches used to describe the geological media and the numerical models that are built, closely resemble the real situation as much as possible. Building a model of a large body of heterogeneous rock requires great effort on the part of the modeller, more so if the rock is fractured. The modeller needs to have access to geohydrologic data of high integrity. More often than not, available hydrologic data are limited and insufficient. Ijiri et al. (2009) point out that a conceptual model can greatly affect uncertainty regarding groundwater flow and transport. It is extremely challenging to scale up detailed, small-scale measurements and to predict and verify large-scale behaviour. Unless there is an underlying known property that extends over scales, measurements conducted at a certain scale can only be used to describe the processes at the same scale. To overcome this difficulty, a geostatistical approach to predict the range of the model outcomes has been proposed by Schwartz et al. (1983). However, the more heterogeneous the rock, the larger the uncertainty.

Building a geohydrologic model of a large area involves many uncertainties from various sources, from the conceptual model to input parameters. Although Ijiri et al.(2009) have addressed the uncertainty in models created through different approaches uncertainty studies applied to the creation of a conceptual model are limited. The most important element of a reliable model is unquestionably the correct conceptual understanding of the hydrologic process within the area, which comes after a long progression of models involving much trial and error.

A major difficulty facing countries with nuclear power plants is the disposal of nuclear waste—commonly divided into low-, intermediate- and high-level waste. In South Africa low- and intermediate-level wastes are disposed at Vaalputs, the National Nuclear Disposal Facility, situated approximately 80 km southeast of the town Springbok in Namaqualand, while high-level waste is stored in ponds at the Koeberg power station and the Thabana Pipe Store, an interim storage facility at Pelindaba near Pretoria (Andreoli et al., 2006). Although a few attempts have been made to search for a site suitable for the geological disposal of high-level waste, especially spent nuclear fuel (SNF), the investigations were discontinued mainly because of the lack of funding (Andreoli et al., 2006). However, the facilities at Koeberg are now reaching their limits, while the power station itself is approaching its design-life span. This means that Eskom, the operator of Koeberg, must begin to look for a suitable site to dispose the SNF.

Although there are other procedures that can be used for the disposal of high-level nuclear waste, many countries today favour geological disposal in principle, as it seems to offer many advantages in terms of safety and security for this category of radioactive materials, and as a way to address ethical concerns (Andreoli et al., 2006; IAEA, 2007). Research in this field was consequently initialized at individual sites around the world as early as the 1970s (OECD/NEA, 2002). As shown by these investigations, the planning and development of a geologic repository typically proceeds through several stages (IAEA, 2007), involves a large number of disciplines and is a costly exercise. No attempt will therefore be made to address the activities associated with the planning and development of a geological repository here. However, as a closer examination of the concept shows,

the main purpose of such a repository is to isolate and contain radioactive waste for many thousands of years. This objective can only be addressed by projecting the performance of the facility far into the future. The only way known today to achieve this is through computer models (IAEA, 2007). Of particular importance from the South African point of view at this time is the transport of leached waste from the repository through the geosphere to the biosphere of the earth (Andreoli et al., 2006).

The geospheres at depth of the major sites considered for the disposal of high-level nuclear waste in South Africa mainly consist of fractured rocks. The invitation of Dr Kenzi Karasaki to work on with him on the hydrogeology of the basement rocks underlying the Mizunami Underground Research Laboratory (MIU) and the nearby Shobasama site in the Tono region of Japan was greatly appreciated.

The investigations originally began with the drilling of an extensive network of deep boreholes on the Shobasama site, 1,5 km to the west of the MIU Laboratory, which is owned by the JAEA, with the view that all investigations and facility construction would be carried out on the site. However, due to difficulties experienced in obtaining permission to begin construction and excavation at Shobasama site, JAEA concluded in 2002 a contract with the Mizunami City for the lease of the city-owned land at Akeyocho and decided to construct the research galleries and related facilities for the project at this site.

1.1 Purpose of the Thesis

As pointed out above, models form an integral part of investigations related to the disposal of radioactive waste. This applies in particular to the understanding of how radionuclides

might migrate away from the repository through the surrounding geosphere. In this thesis, an attempt is made to develop a model for the basement rocks underlying the MIU Laboratory and the nearby Shobasama site, thereby contributing towards the hydrogeology of the MIU project. The strategy followed to achieve this can be briefly summarized as follows:

1. Examine available fracture data from the Mizunami Underground Research Laboratory (MIU) site in Japan. These fracture data are collected from the shaft walls and drill cores as well as using a digital borehole camera. Attempts will be made to find correlation between geologic/geometric attributes of a fracture and associated permeability of the interval that contains the fracture, if any. It is anticipated that the traditional approach of discrete fracture network modeling, where fractures are binned by dip and orientation into sets and the permeability is assumed to be a function of fracture density, will need to be improved. Proximity to a nearby fault is potentially a key attribute that determine the ability of fracture to conduct water. Vertical fractures from horizontal drifts and boreholes will be analyzed to examine the effects of vertical fractures on the permeability that are often ignored.

2. Analyze the pressure data from boreholes at various distances/depths/directions from the shafts being excavated. Construct a numerical model based on available geohydrologic information. The PEST inversion code in Feflow code will be used to estimate the parameters/structure of the groundwater flow system that can explain the observed pressure responses.

3.   Attempt to develop a methodology to estimate the large-scale hydraulic effective

porosity of the granite based on the long-term pressure responses. Design a large-scale

field test to verify the methodology.

1.2 Scope of the Study

The procedure followed in achieving the previously stated purpose of the thesis was to study

the geology of the area, discussed in Chapter 3. This is followed by a discussion of the field

investigations in Chapter 4. The proposed hydrogeological model is discussed in Chapter

5 and its steady-state and transient implementations in Chapters 6 and 7 respectively. The

effects of the Tsukiyoshi fault on the hydydrogeological conditions in the Tono area are

addressed in Chapter 8. The thesis is concluded with a summary of the main conclusions

and recommendations in Chapter 9.

Chapter 1
Approaches to Fracture Modelling

In the characterization of deep geological repositories for spent nuclear fuel, flow and contaminant transport in fractured aquifers are of paramount concern. Currently, many of the sites in the world that are earmarked for or are being investigated as possible sites for spent fuel disposal are located in fractured granitic rock. The main characteristic of naturally fractured sub-terrain is that the main storage of fluids is in the rock matrix, while the main transport medium is the fractures. This means that a different approach from that used with conventional porous media has to be adopted (Muskat, 1937, 1949). Various approaches related the scale of the modelled area have been developed. Berkowitz et al. (1988) divides the approaches into three subdivisions based on the size of the modelled area, the level of interconnection in the fractures and the location of the source. These investigators have come up with the following subdivisions: the 'very near field' which is at the scale of a single fracture; the 'near field', which is a domain with a relatively small number of fractures in the vicinity of the source; and the 'far field', where the entire domain can be treated as an equivalent porous medium, the so-called effective continuum model.

Historically, the study of flow and transport in fractured sub-terrain was addressed by Barenblatt and Zheltov (1960) and Barenblatt et al. (1960). They developed the double-porosity model, which views the porous matrix and fracture network as overlapping and mutually communicating continua. The work of Barenblatt et al. (1960) motivated other workers, as the topic is of great industrial importance. Warren and Root (1963) mod-

elled fractured porous media as a system made up of individual, rectangular porous parallelepipeds separated by an orthogonal network of fractures. The model neglects flow through the matrix block system. This simplification generally yields satisfactory results if the permeability of the matrix system is negligible compared with that of the fracture network. As Berkowitz et al. [1988] have pointed out; the problem with the Warren-Root approach is that it requires the formation of a fluid exchange function. This function is constructed using quasi-steady or simple unsteady flow approximation and involves a geometry dependent parameter, which, as mentioned above, is based on an assumed uniform size and shape of the porous block. Such porous block cannot be found in the field. Odeh [1965] extended this approach for reservoirs in which the pattern of fractures is not known. The equations have been thoroughly studied in the literature, with many boundary conditions. It is not the purpose of this thesis to review them here; the interested reader may consult the following references: van Golf-Racht (1982), Chen (1989, 1990), Pinder et al. (1993).

Alder and Thovert [1990] have presented other approaches. One of the more useful is probably the multi-scale analysis of flow through fractured porous media that was initiated by Aifantis (1980) and extended by Arbagast et al. (1990), Levy (1988,1990) and Panfilov (1990,1994).

1.1 Discrete Fracture Networks Approach

Among the alternative approaches to Warren-Root upon which much effort has been expended is that using discrete fracture networks. Initially, the approach adopted was an enumerative one, first studying flow behaviour in an individual fracture (Lomize, 1951;

Baker, 1955; Huitt, 1956); then studying flow behaviour in relatively simple and regular

fracture networks of definite sizes and configurations (Romm, 1966; Snow, 1969; Parson,

1966; Wilson and Witherspoon, 1974); and finally considering flow behaviour in a natu-

rally fractured reservoir.

The history of discrete fracture networks goes back many years, an example being

the two-dimensional model of Long et al. (1982). The MAFIC package, in the FRACMAN

suite of Golder and Associates, still uses this approach (Dershowitz and Fidelibus, 1999).

This approach has been popular, as it seemed quite natural and reasonable at first glance.

For example, a research group at Lawrence Berkeley Laboratory spent a long time devel-

oping this approach to model fluid flow in naturally fractured reservoirs (Long et al. 1985;

Long and Billaux 1987).

When we discuss the problem of fluid flow through a network of fractures where

the rock is assumed to be essentially impermeable, there are two issues: (1) determining

the permeability of the fracture system, and (2) establishing whether or not such networks

behave like porous media. In the past, methods developed by Snow (1965, 1969) have been

applied. In such techniques the orientation and apertures of the fractures intersected by a

borehole were determined in the field. The fractures were assumed to be infinite in length,

and an equivalent porous medium permeability was then computed as an accumulation of

individual fracture permeabilities.

However, field observations suggest that a fractured rock mass contains sets of dis-

continuous fractures with irregular geometry. The fractures are finite in size: they do not

extend indefinitely within the same plane. As a result, the degree of interconnection be-

tween the assemblages of discontinuous fracture planes is a critical feature that contributes to the hydraulic conductivity of the total system. Although it is assumed that the fractures are interconnected, this not necessarily always true in reality. Bear (1993) argues that the interconnectedness of the fractures depends on the density of the fractures in any given case. This assumption, at first glance and without using real field data, seems plausible. It seems obvious that as the density of the fractures (that is, the number of fractures per unit of fractured rock) or fracture area becomes smaller, the chance of a fracture intersecting a neighbouring one is reduced. This subject has been investigated by researchers using percolation theory, which attempts to determine the percolation threshold, defined as the density of fractures above which the connection of fractures is sufficient to enable flow through the network, at least through part of the fractures. Several investigators (Robinson, 1984; Charlaix, 1985; de Marsily, 1985) studied the issue of connectivity in fractured rock, using percolation theory. The aperture of each fracture, of course, determines its individual permeability, and the orientation of the fracture determines those directions along which fluids may flow within the rock mass. Thus, in discrete fracture networks, the characterization of the fracture system is considered complete when each fracture can be described in terms of its (1) size, (2) location, (3) effective aperture and (4) orientation.

Saga and Runchal (1982) have extended Snow's (1969, 1965) theory of the permeability of fractured systems in an attempt to account for the finite size of fractures. The authors assumed that flow in any fracture is independent of flow in other fractures, and that flow in fractures is dependent only on their size and orientation in the overall field. For this, Saga and Runchal (1982) concluded that 'any fracture which does not appear on

the boundary of the rock element considered is of no interest in the calculation of equiva-
lent permeability.' While these assumptions may be correct for the infinite fracture system
analysed by Snow, they are not applicable to the discontinuous networks to which they
were applied, because they ignore the effects of interconnection and heterogeneity.

In order to study only the effect of interconnection, Long and Witherspoon (1985) ex-
amined two-dimensional networks of fractures in which all the fractures in any given net-
work had the same aperture and length. As such networks are homogeneous, any decrease
in permeability from that predicted by Snow's theory is due to lack of interconnection.

Researchers have long realized that the concept of discrete fracture networks can only
be realistically employed at a laboratory scale and not on a regional scale, where the scale
of interest is over 100 m. The basic problem here is that of establishing homogeneity. Ho-
mogeneity has been studied by Hubbert (1956), Fara and Scheidegger (1961), Toth (1967),
Bear (1972) and Freeze (1975). Freeze pointed out that there is really no such thing as a
truly homogeneous medium in geology. However, in order to do the analysis in a hetero-
geneous medium, a scale of measurement (macroscopic scale) must be found for which
a porous medium is seen as a continuum (Hubbert 1956). Hubbert (1956) introduced the
concept of a representative elementary volume (REV). If one can take sufficiently large
samples of fractured material at different locations within the domain, one shall find in
each of them a rock matrix and a fracture. If a sample centred at a point is to represent
what happens at that point and in its close neighbourhood, it is obvious that the size of
the sample should not be too large. On this scale, the medium is said to be homogeneous.
The scale at which analysis is possible – the volume at which the parameter of interest, in

most cases permeability, first ceases to vary – is defined as the REV. With respect to permeability, the REV of a medium can be sought by measuring the average permeability of increasing volumes of rock until the value does not change significantly with the addition or subtraction of a small volume of rock. Troth (1967) shows that as the volume increases still further, the value of parameter may start to vary again and then become constant again.

Discrete fracture networks may be suited to those situations where only several fractures are of significance. As pointed out by Berkowitz et al. (1988), it is virtually impossible to determine the precise locations of and characteristics of all fractures. Even though there have been attempts to overcome this difficulty by using a stochastic approach to modelling mass transport in fractured reservoirs (Schwartz et al., 1983), the shortcomings are apparent. Karasaki et al. (2010) point out that if the scale of interest is over 100 m and time and resources are limited, it is virtually impossible to measure the properties of individual fractures. Moreover, they make the bold statement that they 'do not believe that scaling up, of small-scale measurements to predict large-scale properties will work.' The discrete approach is also not feasible for investigating transient flow in naturally fractured rock, where a number of matrix blocks with different sizes and irregular shapes are separated by numerous fractures randomly distributed throughout the formation. In fact, the sizes and configurations of the fracture networks themselves can hardly be sufficiently defined from the rather limited data that is available.

1.2   Continuum Approach

The continuum approach for naturally fractured rocks, as described in some detail in Section 1.1, was introduced by Barenblatt et al. (1960). The double porosity models they introduced have been extended by others (Warren and Root, 1963; Odeh, 1965; Kazemi, 1969; Streltsova, 1983). This simplification normally yields satisfactory results for transient flow because the flow from the matrix can be approximated by one-dimensional flow to and from fractures.

An important drawback is that models of this kind do not treat fractures near the well explicitly. If there are only a small number of fractures intersecting the pumping well, a single continuum approximation may not be appropriate, because the conditions of the well test cause flow to converge into the few fractures that intersect the well. The fractures will also experience a large hydraulic gradient. The properties and the geometries of these few fractures therefore control flow in the vicinity of the active well. The characteristics of the fractures close to the well must be accounted for, especially if the hydraulic parameters of these fractures are significantly different from the average values of the entire system.

On the other hand, if the reservoir is extensively fractured and if a large number of fractures intersect the well, the fracture system probably can be approximated by a single continuum,, depending on the geometry of the fracture system as well as the scope of the test. Karasaki et al. (1988) have proposed a composite system with two concentric regions (Figure 1 and Figure 2). The inner Region1 contains a finite number of fractures, and flow to the well is assumed to be linear. The outer Region 2 is a fractured system with enough interconnection, or enough matrix permeability, that it can be treated as the classical

porous medium where only radial flow takes place. Similar composite models have been investigated by others (Larkin, 1963; Bixel and van Poolen, 1967; Ramey, 1970), but none has considered a linear-radial flow.

Karasaki *et al.* (1988) assume an isothermal system in a homogeneously fractured formation of uniform thickness h and infinite radial extent (Fig. 1.1). The well is pumped at a constant rate q, and no wellbore storage or skin effect is considered. The conceptual model of the flow system consists of two zones (Fig. 1.2). In the inner Region 1, the flow is assumed to be linear through a finite number of fractures n. These fractures have the same hydraulic aperture b, permeability k_1 and storage capacity $(\phi c_t)_1$. In the outer Region 2, the flow is radial and the permeability and storage capacity are k_2 and $(\phi c_t)_2$, respectively.

The fractures are assumed to be vertical and to extend from the top to the bottom of the formation. The well has a radius r_w and the radius of the boundary between the inner and outer regions is r_f. The latter radius specifies the distance from the wellbore where the radial flow dominates the system's response under well test conditions. In practice, r_f is related to but not necessarily equal to the fracture length. It is assumed that there is an infinitesimally thin ring of infinite permeability between the two regions, so that otherwise incompatible regions can be matched.

1.3   Effective Continuum Approach

In the continuum approach, some average characteristics of the medium and the flow taking place over a REV are introduced, and the basic laws governing the process are formulated

Flow Direction

Well bore

XBL 856-10595
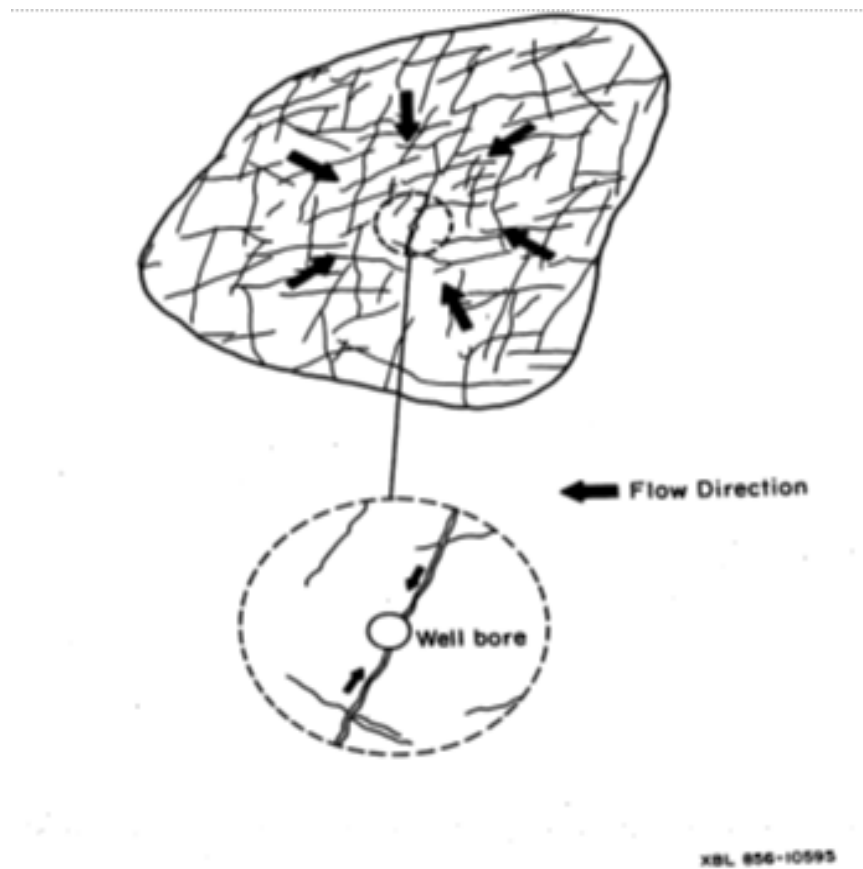
Fig. 1.1. Flow to a well in a fracture-dominated system (Karasaki et al, 1988)
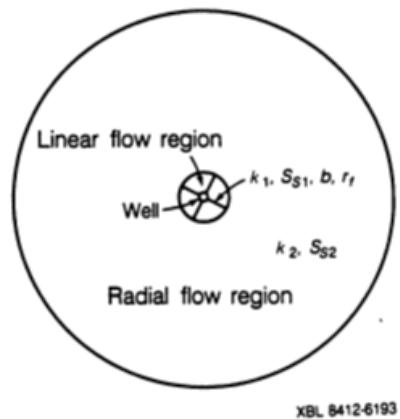
Fig. 1.2. Composite model of a fracture-dominated system, with linear and radial flow (after Karasaki et al 1988)

in terms of these average characteristics. In the dual-porosity approach or dual continuum (DCM) (Fig. 1.3 (b)) and (Fig. 1.3(c)), each grid block is divided into two sub-grid blocks, one representing the fracture network and the other representing the rock matrix. Fracture grid blocks are connected to one another to create the fracture network, and each fracture grid block is connected to one matrix grid block to represent fracture—matrix interactions. If the matrix grid blocks are not connected to one another, the model is known as a dual-porosity model (Fig. (1.3 (b)) (i.e., the matrix continuum contributes additional porosity to the model, but not additional permeability for global flow). If the matrix grid blocks are connected to one another, the model is known as a dual-permeability model (Fig. 1.3 (c)) (the matrix contributes both additional porosity and additional permeability for global flow). When matrix permeability is much smaller than fracture permeability, as is the

case for the present problem, global matrix flow tends to be quite small, and dual-porosity models give comparable results to dual-permeability models.

Under steady flow conditions, for a dual-porosity model, flow occurs through the fracture network only, meaning that the dual continuum model and effective continuum model (ECM) give identical results. In contrast, under transient flow conditions, for a dual-porosity model the fracture network and rock matrix respond at their own time scales. Typically, the lower permeability of the rock matrix causes its response to be slower than that of the fracture network. Heat flow occurs by convection through the fracture network and by conduction through both fracture and matrix, with a delayed matrix response possible. Tracer transport occurs by advection through the fracture network and by diffusion between fractures and matrix. In spite of all the progress made in the theory of fluid flow through double porosity, dual permeability systems, a number of unsolved problems remain. One of the drawbacks of this approach is the requirement to establish the REV and then do some 'scaling up' of the small-scale measurements to predict large-scale properties.

In the multiple interacting continua model (MINC) (Fig. 1.3 (d)), each grid block is divided into one fracture sub-grid block and multiple matrix sub-grid blocks, enabling a transient response that propagates away from fractures through the matrix. In contrast, for a dual continuum model, the response of the matrix is considered quasi-steady, as a single number represents the average behaviour over the entire grid block. For highly transient problems, a MINC model is more accurate than a DCM, however, it is computationally much more expensive.
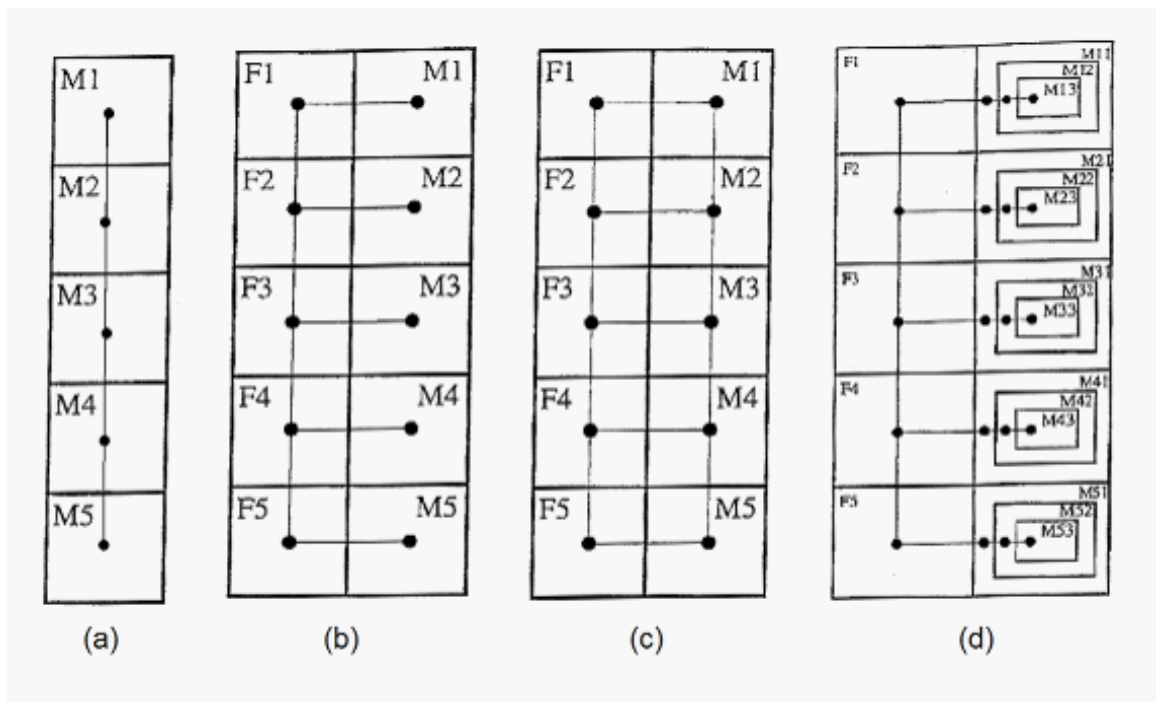
Fig. 1.3. Schematic diagram of a 1-D column of grid blocks, modelled as (a) single continuum or ECM (b) dual-porosity with one matrix grid block per fracture grid block, (c) dual permeability with one matrix gridblock per fracture gridblock and (d) multiple interacting continua model (MINC). The fracture elements are labeled as F and the matric elements labeled as M. (Modified from Zimmerman et al., 1996)

The approach used in this thesis is the effective continuum model (ECM) adopted by Doughty and Karasaki (1999). In the ECM (Fig. 1.3 (a)), one grid block represents both the fracture network and the rock matrix, which are assumed to be in pressure equilibrium at all times, with no driving force for flow between fractures and matrix. Generally, the grid-block permeability and porosity represent the fracture network, with flow through the matrix assumed to be negligible. However, the grid-block porosity can also represent the aggregate void space of both the fracture network and the matrix, so the matrix contributes an additional storage term for transient fluid flow (with the same time-dependence as the fracture-network response). For vadose-zone problems, one assumes capillary equilibrium between fractures and matrix to partition liquid between continua. This allows calculation of relative permeabilities in each continuum and consequently the total mobility of the fracture plus matrix system. Heat flow occurs by convection through the fracture network and by conduction through both the fractures and the matrix, with instantaneous thermal equilibration between fractures and matrix within a grid block. Tracer transport occurs by advection through the fracture network. If porosity also includes a contribution from the matrix, this implies that the tracer moves through the matrix concurrently, which may or may not be realistic.

The approach here is not to use the fracture parameters such as fracture transmissivity, fracture aperture and other statistical information on the fracture geometry. Although the geometric data are useful, it is only regarded as soft data. The reasons are: (1) It is virtually impossible to test individual fractures to measure and determine their transmissivity in the field. Therefore, the fracture transmissivity quoted in the literature is invariably in-

ferred from borehole tests, making certain assumptions regarding the flow geometry. The measured value is likely to be the effective transmissivity of a collection of interconnected fractures at unknown distances and directions. (2) Fractures are generally not planar, circular or square. (3) Variability of the hydraulic conductance (transmissivity) within a fracture is likely to be larger than the variability among fractures. (4) Correlations between the parameterized fracture geometry and the hydraulic properties of the fractured rock mass may or may not exist. Furthermore, even if accurate information on the flow and transport of properties were available, there is only a limited spatial regime in which modelling individual fractures (a discrete fracture network model) is useful. At small scales or low fracture densities, the few individual fractures present may be modelled explicitly, but it is quite likely that there will be no connected fracture flow path across the model. At large scales and high fracture densities, the many fractures present are likely to be well connected, and thus can be more efficiently represented as an effective continuum. For the study area considered in this thesis, the model extent (9 km by 9 km by 3 km) is far greater than the typical measured fracture spacing ($8m^{-1}$). Hence, the choice is made to construct an effective continuum model to simulate the groundwater flow and tracer transport.

The approach used in this thesis to model flow and transport in fractured rock is to construct a conceptual model by inverting the field hydrologic test data (hard data), such as responses during flow tests and pressure interference tests. How the inversion of some of the specified parameters works in constructing an effective continuum model (ECM) is described. In this approach and in the model, a stochastic permeability distribution is used to represent the fractured rock block as an effective continuum. However, large-scale

features such as fault zones, lithological layering, natural boundaries and surface topology are incorporated deterministically.

1.4 Effective Porosity

Fracture porosity is an important parameter used in the modelling of transport processes in rock formations. Fracture porosity plays a critical role in determining transport velocities in problems that range from contaminant migration and radioactive waste isolation to aquifer resource evaluation in fractured media. The determination of fracture porosity for rock formations can be extremely challenging. Fracture porosity may vary by several orders of magnitude within the same lithostratigraphic unit and may exhibit little or no spatial correlation. This is the case of the Tono area, Japan, which is investigated as part of this research. The Tono MIU site is solely a basic R&D site for a future high-level radioactive waste geological repository (which will be located elsewhere), and as such, the accurate understanding of flow and transport through the granitic rock aquifer is critically important.

The term porosity describes the volume of voids contained within the total volume of a bulk medium. The bulk volume contains both the volume of solids and the volume of the voids that are typically filled with liquids and/or gases. Intrinsic to the notion of porosity is that, like any local property that may vary spatially, the value is an average over a specific domain.

The porosity of importance for determining advective transport velocities within a geological medium is referred to as the effective or kinematic porosity. The effective porosity consists of the volume of voids that are connected together to form a connected network

of open channels available for flow. The determination of the effective porosity is complicated by the large difference in times scales that may occur when comparing transport through different domains within a geologic medium. These different domains arise from lithological and structural variations in the formation.

In rock formations such as the granitic rocks in the Tono area, which consists of both a matrix and large-scale features such as fractures, the low-permeability rock matrix behaves very differently than the higher permeability interconnected fractures. The rock matrix may have a very low permeability; orders of magnitude below the bulk permeability exhibited by the fracture network, and still have a high porosity. A transient inflow into the formation, such as an episodic infiltration event, may be transported rapidly through the high-permeability fracture network, with little movement into the low-permeability matrix. Conversely, a very slow diffusion-dominated process may be controlled by the matrix porosity, while the low porosity, high permeability fractures are relatively inconsequential to the process. Neretnieks (1980) observed that contaminant transport in fractured medium undergoes three distinct stages: the first stage is fracture-dominated transport, the second is the double porosity transport and the third and final stage is the total porosity.

In this study, a methodology will be developed to estimate the large-scale hydraulic effective porosity of the granite, based on long-term pressure responses. The effective porosity approach assumes that some portion of the available matrix porosity in the fractured medium is immediately accessible to solutes in the fractures. In general, if it is assumed that the matrix diffusion will completely saturate matrix blocks in the groundwater flow system over the time of transport from the release point to the accessible environment,

then a value of the effective porosity equal to the matrix porosity is used. Again, if it is assumed that matrix diffusion will be extremely limited in the system of interest, then a value of the effective porosity equal to the fracture porosity is used. In this thesis, it is assumed that intermediate values of effective porosity approximate the situation in which some fraction of the total solute storage capacity of the fractured medium has been filled by diffusion. The effective porosity approach adopted here thus implicitly considers the effects of diffusion from fractures into the matrix; however, it is applied in an ad hoc manner. In reality, the portion of the matrix porosity available for solute storage changes as a function of time because the volume of influence gets larger in pressure transients, and because there may be precipitation and/or dissolution. The effective porosity, as calculated in present work, is a 'lumped' parameter that incorporates uncertainty in underlying processes and results in an approximate solution for solute transport.

1.5   Previous Work

The Japan Atomic Energy Agency (JAEA) has initiated a multi-national project to investigate the uncertainties involved in the prediction of flow and transport behaviour of a fractured rock mass. In the initial stage of the project, known as the CORE Collaborative Study (Oyamada and Ikeda, 1999; Doughty and Karasaki, 1999), several research organizations conducted numerical simulations of tracer transport through a hypothetical fractured rock mass at the 100 m scale. Each group was provided with the same hydrogeological data set and was requested to use the same boundary conditions. The groups' results were compared to identify and quantify uncertainties in model predictions. The study found that

discrete fracture network (DFN) models and effective continuum models (ECM) produced comparable results for mean values of flow through the model and tracer travel times, but that DFN models showed greater variability among stochastic realizations than did ECM.

The second stage of the project took a similar approach, but provided site-characterization data for a real field site, a 4 km by 6 km by 3 km region surrounding the Mizunami Underground Research Laboratory (MIU) site in the Tono area of Gifu, Japan, and left the choice of boundary conditions up to the research groups. The main results of the different groups' models were the predicted particle travel times from specified release points to the model boundary. Doughty and Karasaki (2001) developed an ECM and predicted relatively short travel times on the order of tens of years. That work is summarized in Ijiri et al. (2009) and Doughty and Karasaki (2001). There are no comparable field data available to directly validate the models, so, as in the first stage, model uncertainty was assessed by comparing the results of different models (Sawada et al., 2001). Although the general features of the flow paths from the release points to the model boundaries were similar for all the models, travel times varied over a huge range, from 1 to 10,000,000 years. Much of this variation could be attributed to the large range of fracture porosities assumed by the different groups, but direct comparison between models was difficult because of differences in how boundary conditions were assigned.

For additional modelling of the region surrounding the MIU site, JAEA specified a set of common boundary conditions for all the groups to use, so that differences in results could be related directly to the modelling approach and property assignments. In addition to examining steady-state flows and transport, they also did a transient-flow analysis

by simulating the long-term pump test (LTPT), and thermal analysis of steady-flow conditions. The thermal analysis proved a valuable means of discriminating between alternative model boundary conditions. This work is summarized in Doughty and Karasaki (2002). Comparison of the results of the isothermal studies with those of the other research groups is presented in Sawada et al. (2003)

Subsequent to the LTPT, they analysed pressure transients collected before, during and after the LTPT itself. Strong pressure transients were observed in a number of wells in response to the removal of a packer in well MIU-2, which enabled flow across the Tsukiyoshi fault. Doughty and Karasaki (2002) refer to the packer removal and subsequent replacement as the 'inadvertent MIU-2 well test' and modelled it numerically by increasing permeability (packer removal) then subsequently decreasing permeability (packer replacement) of the grid block representing the intersection of Well MIU-2 and the Tsukiyoshi Fault. They calibrated the model to observed pressure transients to infer permeability and porosity information for the vicinity of the Tsukiyoshi Fault (Doughty and Karasaki, 2003). A key finding of the study was that pressure responses occur more slowly than their original model predicted, necessitating an increase in model porosity to effectively increase model storativity, and thereby slow model pressure responses. This porosity increase then acted to lengthen predicted tracer travel times by about a factor of ten compared with their previous model.

Next, the lateral domain of the model was increased to 9 km by 9 km. This extension enabled lateral boundaries to coincide with geographic features that provide a sound basis for assigning lateral boundary conditions. They modelled the steady-state head distribu-

tion, groundwater flow and tracer transport from selected release points. They developed

models for a base case and several sensitivity study cases with additional faults included,

stochastic distributions of flow properties or different surface recharge rates. The models

were calibrated to steady-state head profiles in several wells, followed by a thermal analy-

sis in which modelled and observed temperature profiles were compared (Doughty and

Karasaki, 2005).

Chapter 2
Fracture Attributes and Associated Permeability

In the traditional approach of discrete fracture network modelling, the fractures are binned by dip and orientation into sets and the permeability is assumed to be a function of fracture density. Thus, the characterization of a fracture system is considered complete when each fracture can be described in terms of its (1) size, (2) location and (3) effective aperture.

One example of the modelling approach is to use a random fracture mesh generator that produces random realizations of populations of fractures in a region called the generation region. Several fracture sets are generated, and each set is generated independently. For each set, the density (number of fractures per unit area) is supplied to determine the number of fracture centres to be generated. Then, normally distributed orientations are randomly assigned to each centre. The fractures are randomly truncated such that the lengths are distributed according to a log–normal or negative exponential distribution, and those particular fractures crossing the boundaries of the generation region are truncated at the boundary. Finally, log–normally distributed apertures are randomly assigned to each fracture and sets are superimposed. Some geostatistical methods are then used to correctly incorporate the partial variability found in field data into the fracture network model (Long and Billaux, 1987). When all the sets have been generated, a flow analysis is performed using either a finite element analysis or finite difference method.

In the discrete fracture network approach the fractures are considered planar, circular or square, which may not be true in the field. Mostly sub-horizontal fractures are therefore considered because boreholes are mostly vertical and the contribution of vertical fractures to flow is not well reflected. The approach also assumes the existence of correlations between the parameterized fracture geometry and the hydraulic properties of the fractured rock formation. Above all, the theory is not based on field observations.

In the present work the above assumptions will be tested using real (hard) data from the Mizunami Underground Research Laboratory (MIU) in the Tono region, Gifu, Japan. The details about the area, the background, investigations and the geology are described in Chapter 3. An attempt is made to find the correlation between geologic/geometric attributes and the associated permeability of the interval that contains the fracture. Data are available from the MIU site and the Shobasama site, a sister site about 15 km west of MIU. These fracture data are collected from borehole walls and drill cores using a digital borehole camera.

The field data, from which this analysis is based, consist of 59 hydraulic conductivity values inferred from slug tests and pumping tests using packed-off intervals in 4 boreholes, and 59 fracture density measurements made from borehole core analysis in 4 boreholes.

Fig. 2.4 to Fig. 2.7 show plots of fracture density versus $\log K$ for each of the packed-off zones in wells DH-6, DH-7, DH-8 and MIU-3. The K values were obtained from slug tests and pumping tests in the packed-off zones in each of these boreholes. As can be seen, these data show that there is no perfect correlation between fracture density and associated permeability as is assumed in the discrete fracture network approach. Fig. 2.8 is a plot of

the fracture density versus permeability for each of the lithological layers in the study area. Again, here there is no obvious correlation between fracture density and conductivity in all the lithological layers considered.

DH-6

Fig. 2.4. Plot of fracture density versus log K in each of the packed-off zones in DH-6 well

Fig. 2.9 and Fig. 2.10 show hydraulic head responses to excavation in the main shaft and the ventilation shafts observed at DH-2 and Dh-15 at the MIU site. Fig. 2.9 shows large responses at all sensors in granite, and the response is uniform in DH-2. Sensors in DH-15 show moderate response, with sensors in sediment and granite responding uniformly as shown in Fig. 2.10. The responses in the boreholes close to the fault (DH-2 and DH-15) are

DH-7

Fig. 2.5. Plot of fracture density versus log K in each of the packed-off zones in DH-7 well

Table 2.1. Measured hydraulic parameters in MIU-4 well

Interval (mabh)	K (m/s)	Temp (^{o}C)	Remarks
68.45-78.02	2.13×10^{-11}	20.0	
82.50-88.65	5.14×10^{-8}	19.5	
95.02-134.47	2.44×10^{-7}	21.5	
314.95-316.95	1.47×10^{-5}	23.0	
582.25-647.11	9.13×10^{-7}		Large amount pumping for WS with drill rods
584.00-647.11	1.22×10^{-6}	28.0	
183.20-254.20	5.70×10^{-8}	21.0	
754.50-790.10	6.00×10^{-7}	31.0	
669.50-677.00	2.06×10^{-7}	30.0	Tsukiyoshi Fault
690.50-753.00	3.54×10^{-8}	30.0	
500.30-562.80	8.26×10^{-7}	27.0	
361.60-424.10	4.40×10^{-7}	24.5	

DH-8
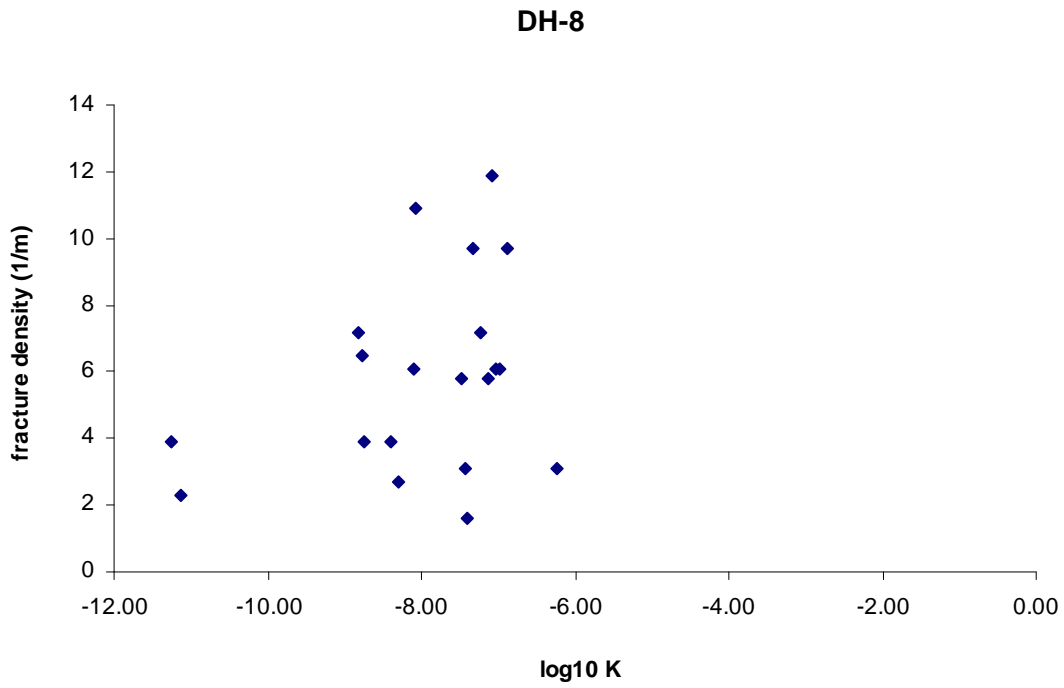
Fig. 2.6. Plot of fracture density versus log K in each of the packed-off zones in DH-8 well

Table 2.2. Measured hydraulic parameters in MIZ-1 well

Interval (mabh)	K (m/s)	S_s (m^{-1})
191.00-226.41	8.37×10^{-8}	1.17×10^{-8}
662.20-706.23	2.35×10^{-7}	4.26×10^{-7}
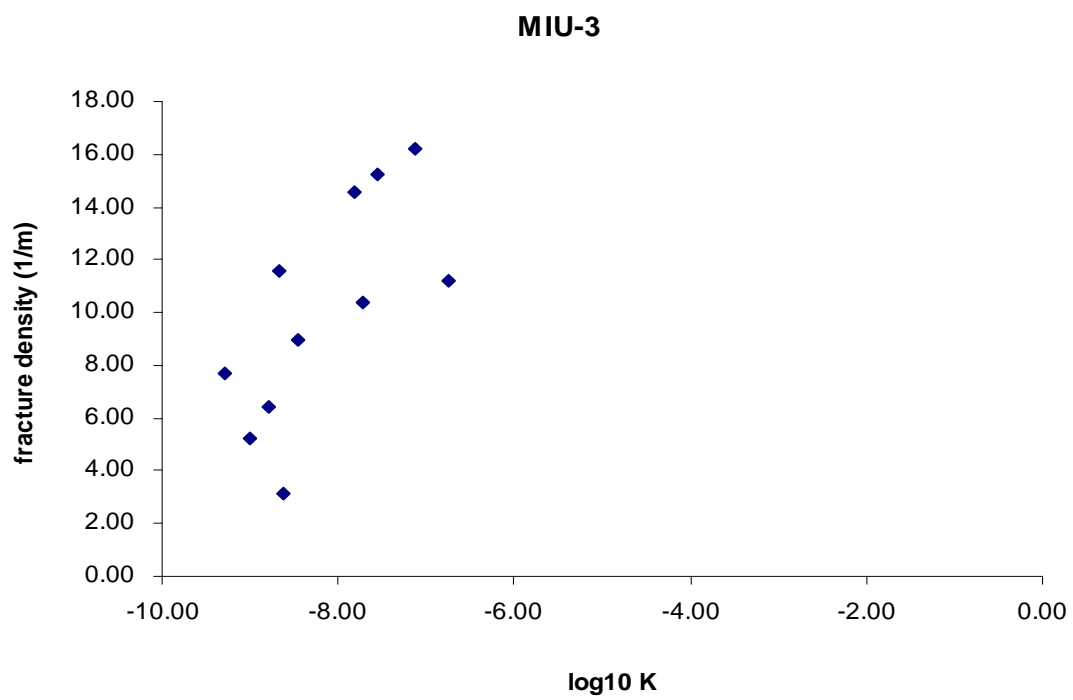
Fig. 2.7. Plot of fracture density versus log K in each of the packed-off zones in MIU-3 well
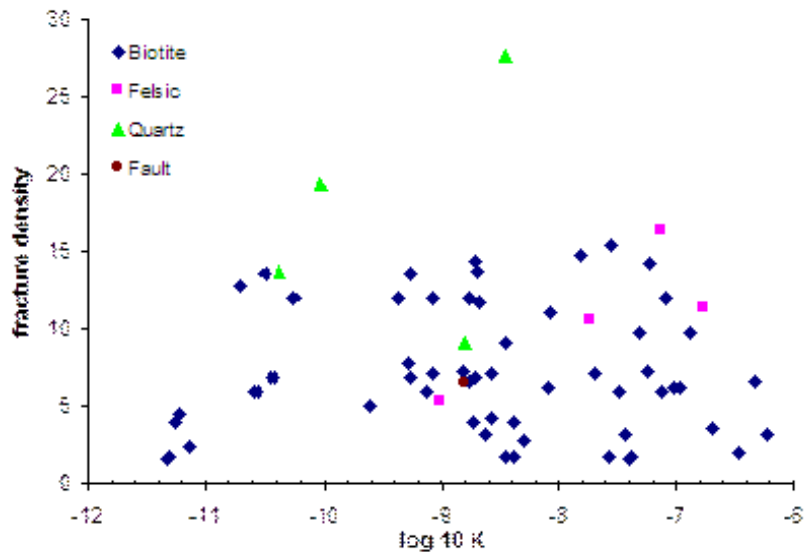
Fig. 2.8. Plot of fracture density versus logK in each of the lithological layers in the study area

vertically invariant, indicating large vertical permeability. This is in contrast to responses in

borehole AN-3, which is farther from the fault: here the responses show depth dependence

(Fig. 2.11). These wells are close to the Tsukiyoshi fault, which is semi-vertical and may be

positioned in the damage zone of this fault. This suggests that the faults are controlling the

hydrology there. Although the extent of the damage zone is not clearly understood, work

currently under way to characterize faults at LBL (Karasaki et al., 2010) suggests that in the

damage zone there are too many fractures and it is impossible to characterize each fracture

as the discrete fracture network entails. In the bigger picture therefore, evidence suggests

that there are fault-associated high-permeability zones along faults, and that the faults are

semi-vertical. Table 2.1 and Table 2.2 show high permeability values for sensors in MIU-

4 and MIZ-1, which are inclined boreholes. The fact that a high water is observed from

these horizontal boreholes indicates that the vertical fractures are permeable. These vertical

fractures enhance the connectedness of otherwise unconnected non-vertical fractures.

Fig. 2.9. Hydraulic head responses observed in the field in borehole DH-2
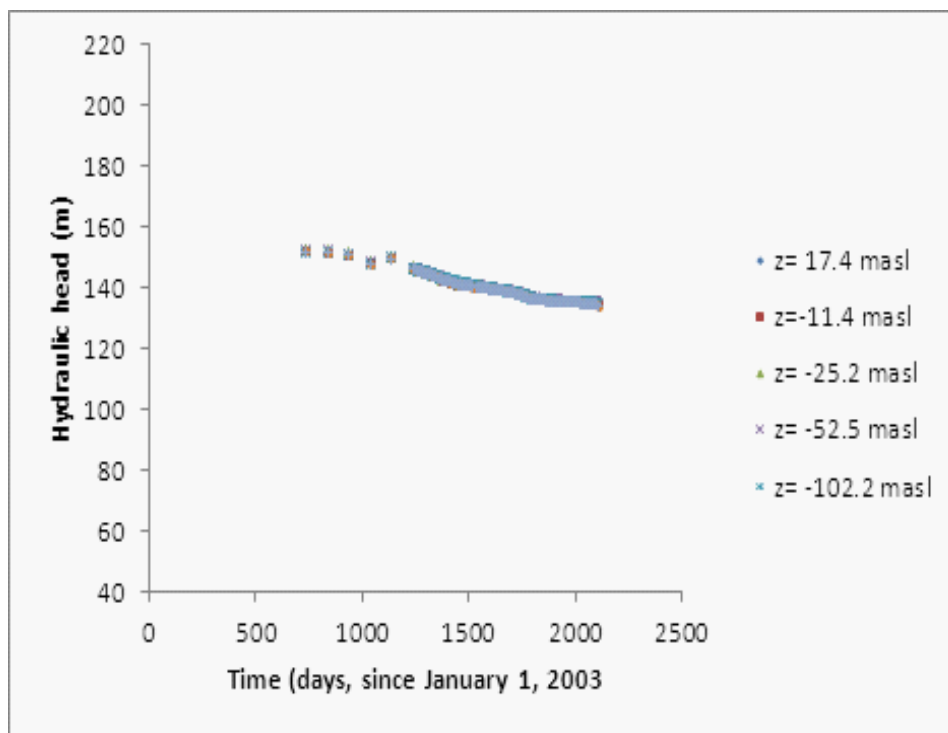
Fig. 2.10. Hydraulic head responses observed in the field in borehole DH-15
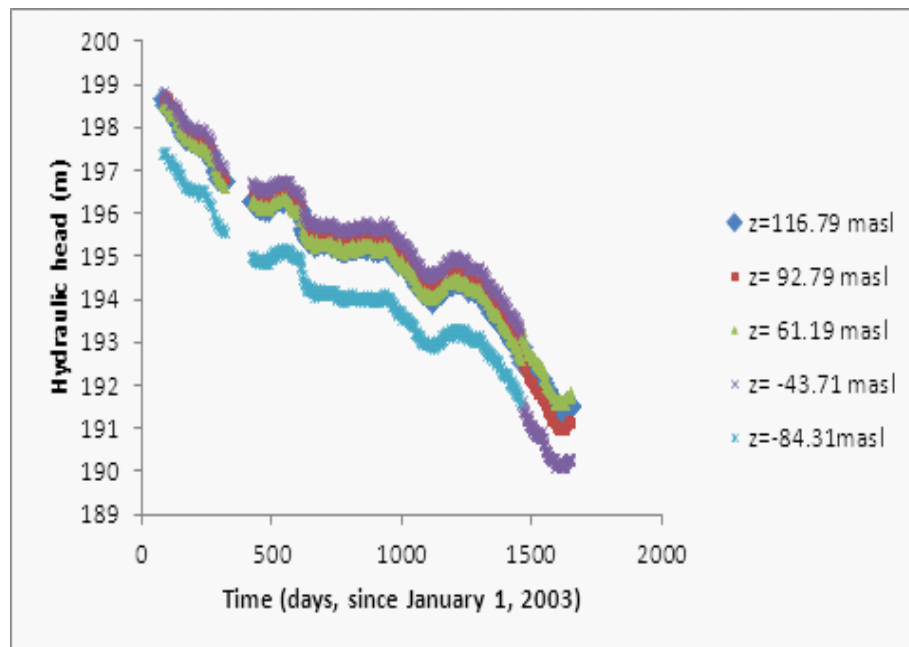
Fig. 2.11. Hydraulic head responses observed in the field in borehole AN-3

Chapter 3
Geology of the Tono Area

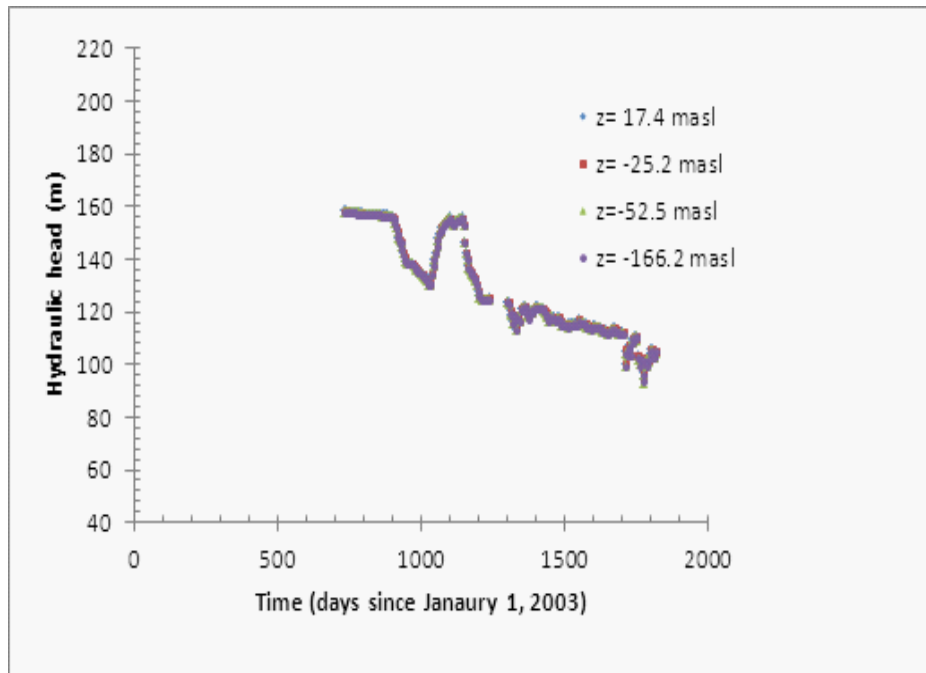The setting of the Tono region within the Japanese islands, and the aerial views of MIU and Shobasama sites within the Tono region are shown in Fig. 3.12 to Fig. 3.16. The MIU project was commissioned to establish the steps to be taken and the roles of concerned organizations for the final disposal of high-level radioactive waste. The long-term program requires the Japan Atomic Energy Agency (JAEA) to 'steadily carry on research and development activities to verify the reliability of geological disposal technologies and to establish a safety assessment method, using research facilities for deep geological environment.' It also states that 'these research facilities for deep geological environments will serve not only as a place for scientific investigation but also as a place for deepening public understanding of research and development activities related to the disposal of waste.' Accordingly, the research facility was to be distinguished from the disposal facility.

In the Mizunami Underground Research Laboratory (MIU) project, located in the Tono region (Fig. 3.12), a wide range of geoscientific research and developmental activities are being performed. The geoscientific research of the MIU project is being conducted at the MIU construction site, where two shafts (the main shaft and ventilation shaft) are being excavated and the Shobasama site, a sister site, 1.5 km to the west (Fig. 3.13), where an extensive network of deep boreholes were used for the initial investigations of the local geology.

The Shobasama site is located on a land owned by JAEA. It was initially selected as the site for all investigations and facility construction. An intensive characterization program was carried out and currently the site has an extensive borehole network suitable for on-going research and long-term monitoring. However, due to difficulties in obtaining permission to begin construction and excavation at the Shobasama site, JAEA concluded a contract in 2002 with Mizunami City for the lease of the city-owned land at Akeyo-cho, Mizunami City. It was decided that the research galleries and related facilities for underground research should be constructed at this site.

The main goals of the MIU project are:

1. To establish comprehensive techniques for investigation, analyses and assessment of the deep geological environment. The geoscientific research being carried out for the MIU project is primarily focused on the study of the granite at the site, as granite is the most widely distributed crystalline rock type in Japan. Currently two shafts (the main shaft and ventilation shaft) are being excavated at the MIU site.

2. To develop a range of engineering techniques for deep underground applications.

The working program is divided into the following investigation fields: borehole drilling and shaft excavation, geology, hydrogeology, hydrogeochemistry and long-term monitoring. This thesis is a contribution to the hydrogeology effort and is concerned only with flow and transport in the basement rocks.
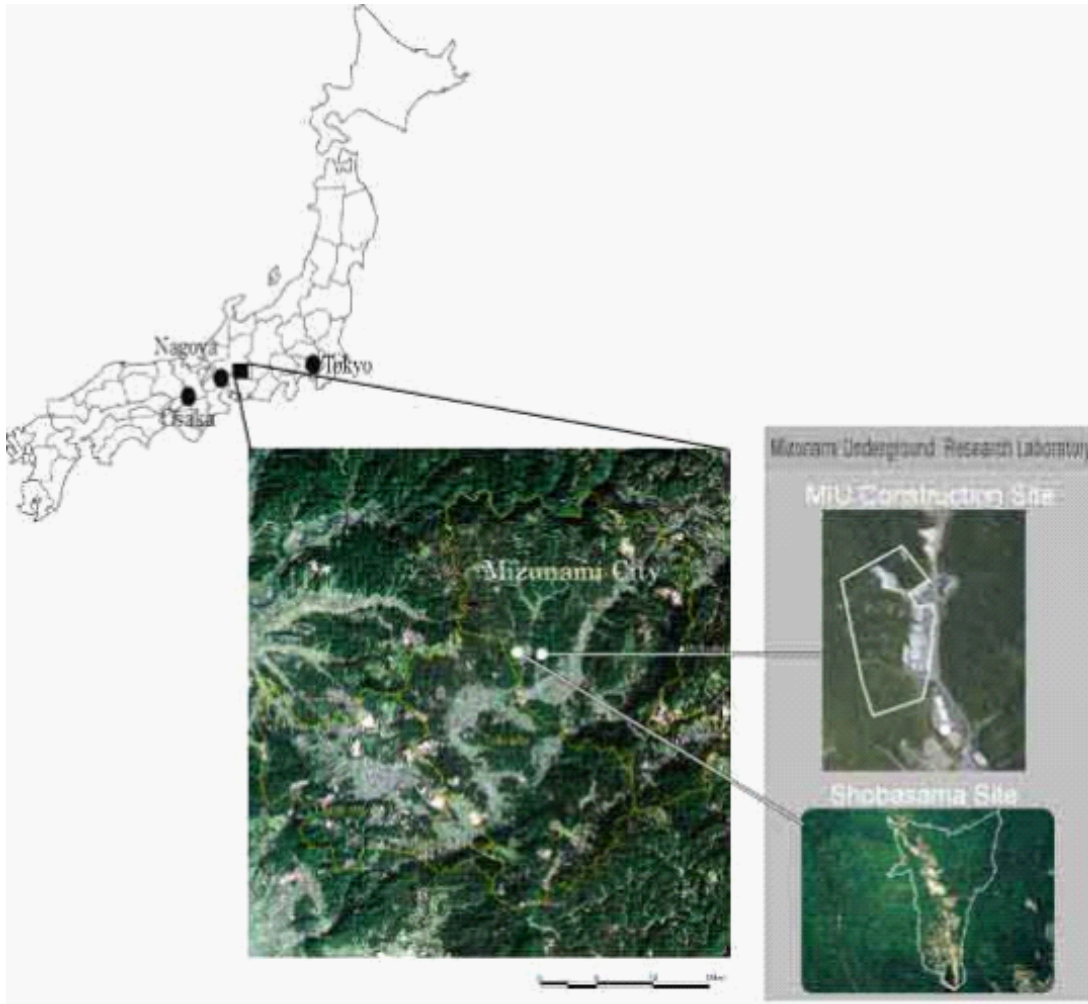
Fig. 3.12. Location of the Tono area in Japan and the location of the MIU and Shobasama sites in Tono.
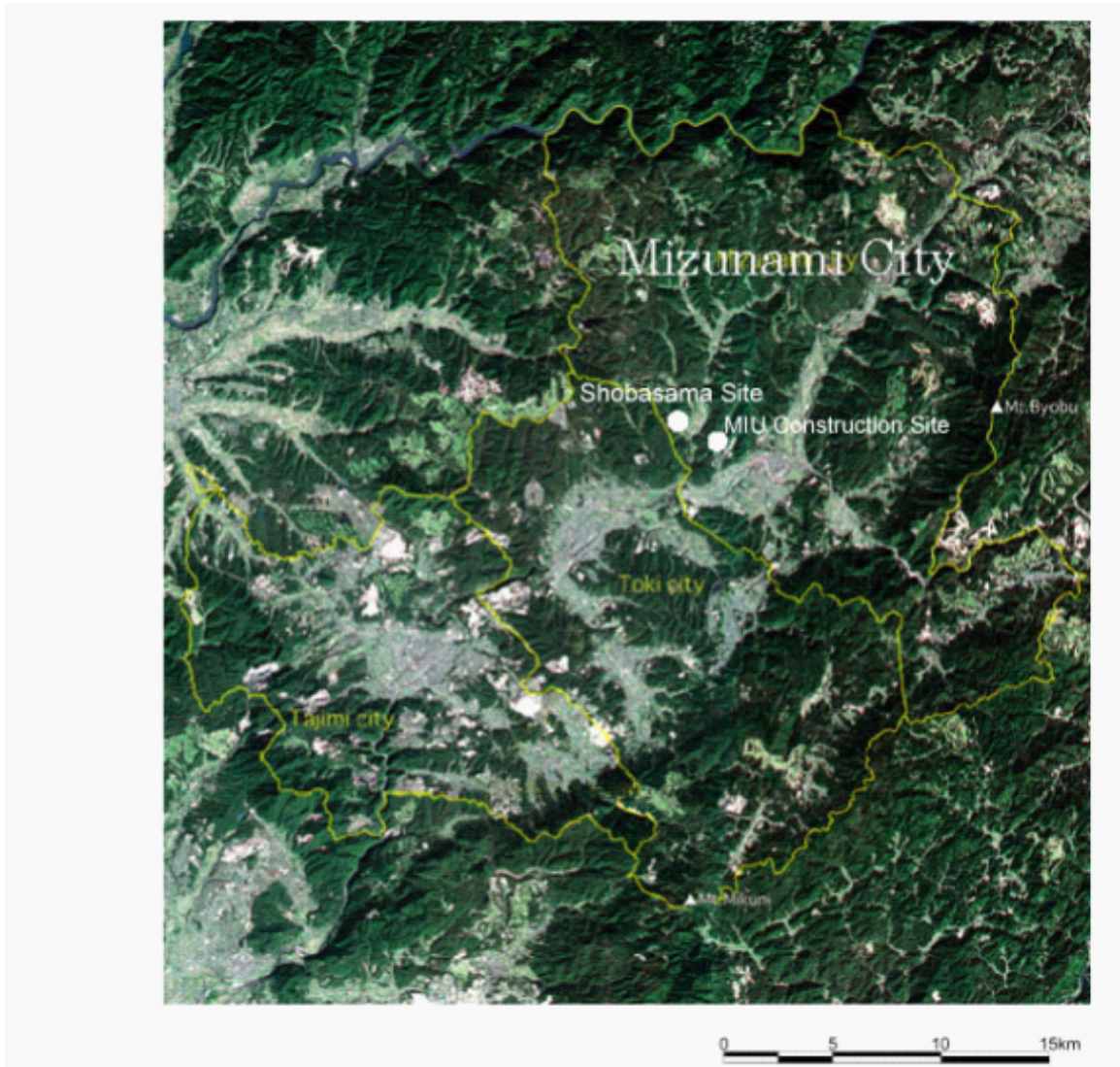
Fig. 3.13. Location of the MIU and the Shobasama sites in the Tono region (detailed view of Figure 12)

Fig. 3.14. Aerial view of the MIU site
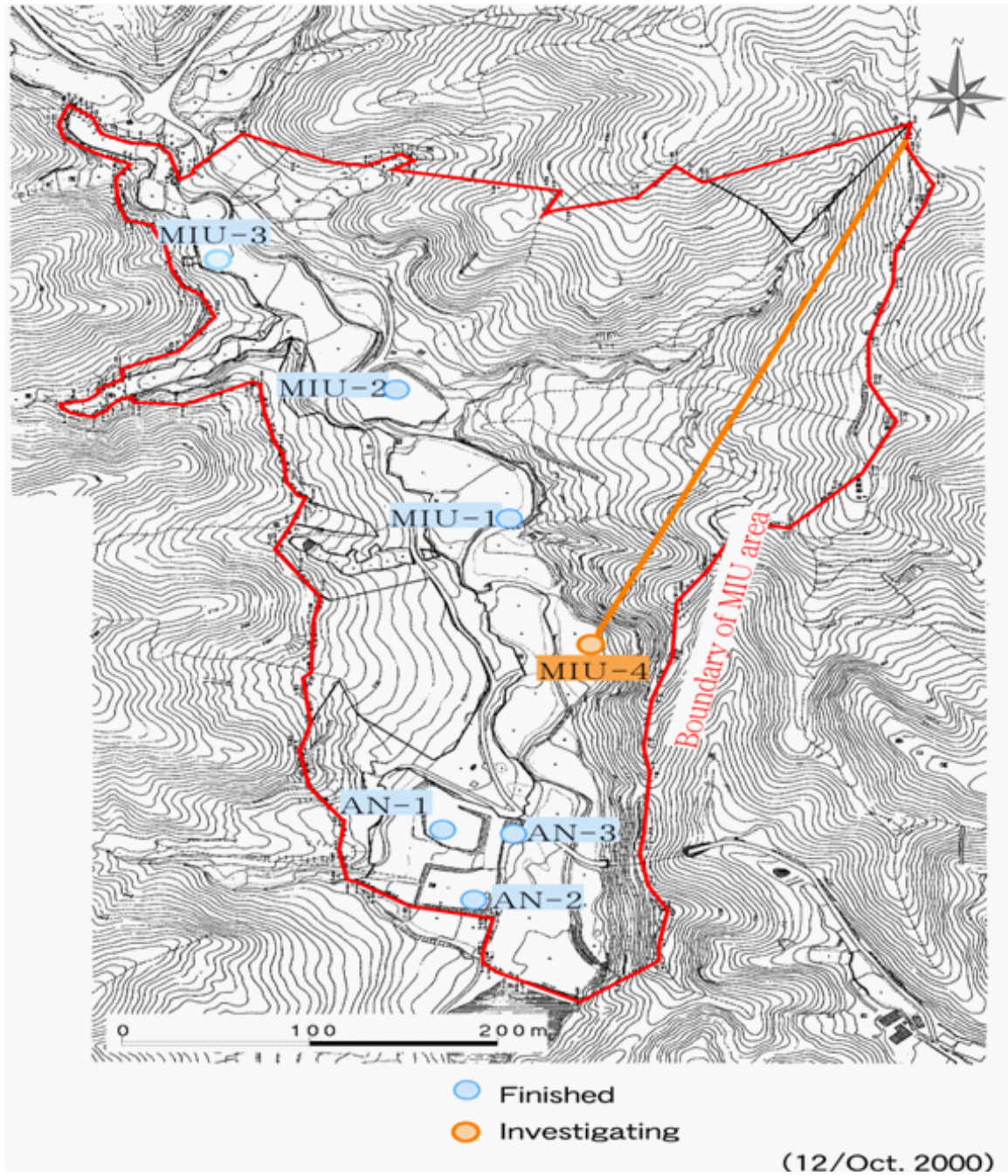
Fig. 3.15. Location of boreholes for pressure response test at the Shobasama site

3.1 Geology

The Tono region is a terrain that forms a bowl shape with a NE-SW axis surrounded by the Mino-Hida mountain district in the northwest and the Mikawa mountain district in the southwest. The Kiso River flows in the north of the terrain and the Toki River flows from the northeast to the southwest in the central region. The study area that is used for the regional groundwater flow analysis is a terrain bounded by the Kiso River in the north and Toki River in the south. The area gently slopes from the northeast to the southwest at maximum slope of 4%, at an altitude 150–400 m (see Fig. 3.16). There is a clear relationship between the geology and the topography. The mountainous regions, the hilly regions and hilltops correspond to the Mesozoic basement rocks, Niogrene/Quaternary sedimentary rocks and the Pliocene Seto Group, respectively.

The Kiso River forms a deep valley cutting through the northern mountains. The boundary between the southeastern mountains and the boat-shaped hills is clearly marked by the northeast-southwest oriented Byobusan Fault, named after Mount Byobusan (794.1 m). The fault can be identified in the northeast by the presence of a steep cliff with talus deposits, although this cliff is less distinct towards the southwest. In the central part of this region, the Toki River flows from the northeast towards the southwest. Terraces developed along the Toki River and its tributaries are composed of flat lying, alluvial deposits

The geology of the Tono area consists of sedimentary rocks of the Mino Belt (Jurassic to Cretaceous), granite and rhyolite (Cretaceous) and later sedimentary rocks (Miocene and Pliocene). As shown in Fig. 3.17 and Fig. 3.18, the Neogrene sedimentary rocks unconformably overlie the Mesozoic basement rocks. The Mesozoic basement rocks consist
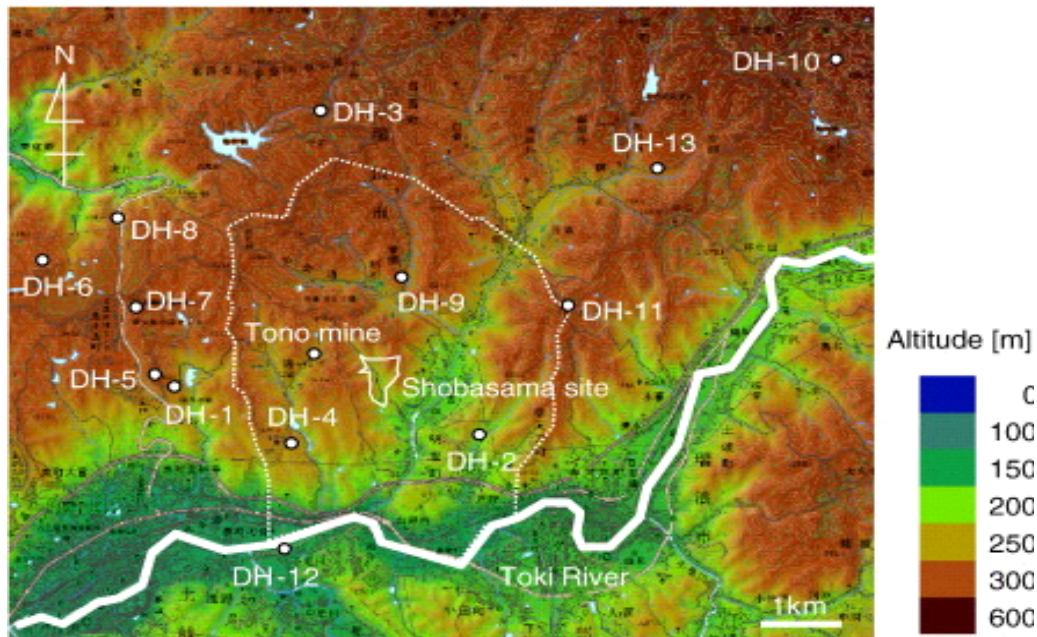
Fig. 3.16. Topographic map of the Tono area showing some of the borehole locations and the Toki River

of sedimentary rocks that belong to the Mino belt, the Nohi rhyolite that overlies the sedimentary rocks and the late Cretaceous Toki granite that intrudes above both rock types. The Toki granite occupies most of the basement rock area in the domain and consists of fine-to-coarse-grained biotite granite.

The Neogrene sedimentary rocks consist of the Miocene Mizunami Group and Pliocene Seto Group. The Seto Group unconformably overlies the Mizunami Group. The Mizunami Group consists of marine sedimentary rocks derived from transgression. The Mizunami Group slopes toward the south and is divided into four formations. The Toki lignite-bearing formation consists of lignite-bearing mudstone and sandstone and unconformably overlies basement rock with a conglomerate layer. The Hongo formation is composed of tuffaceous sandstone-siltstone-mudstone alternations along with conglomerate. The Akeyo formation

is composed of tuffaceous sandstone-mudstone that has a thin layer of tuff in the middle. The Oidawara formation consists of unstratified siltstone, the fine tuffaceous mudstone and conglomerate with medium-coarse sandstone in the basal horizon. The Seto Group is horizontally distributed throughout the study area and consists of clay and gravelly sand.
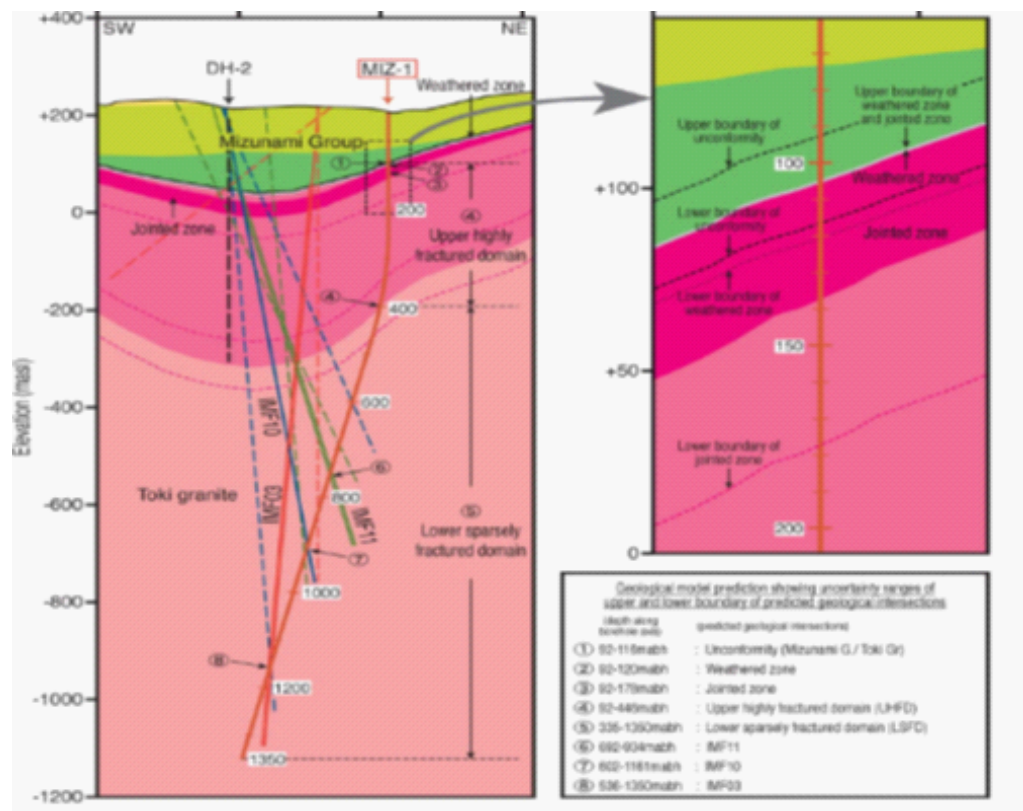
Fig. 3.17. Geological profiles along the DH-2 and MIZ-1boreholes

The regional basement of the area around the modelled site is mainly composed of the Toki granite that has intruded into the Paleozoic and Mesozoic formations (Kumazaki et al., 2003; Nakano et al., 2003). The top of the granite varies in elevation from 50 to 150 masl, in the Tono region. A thin layer in the upper part of the Toki granite is highly

(a)   **Geological map**

(b) **Cross section of the line A-B in the geological map**
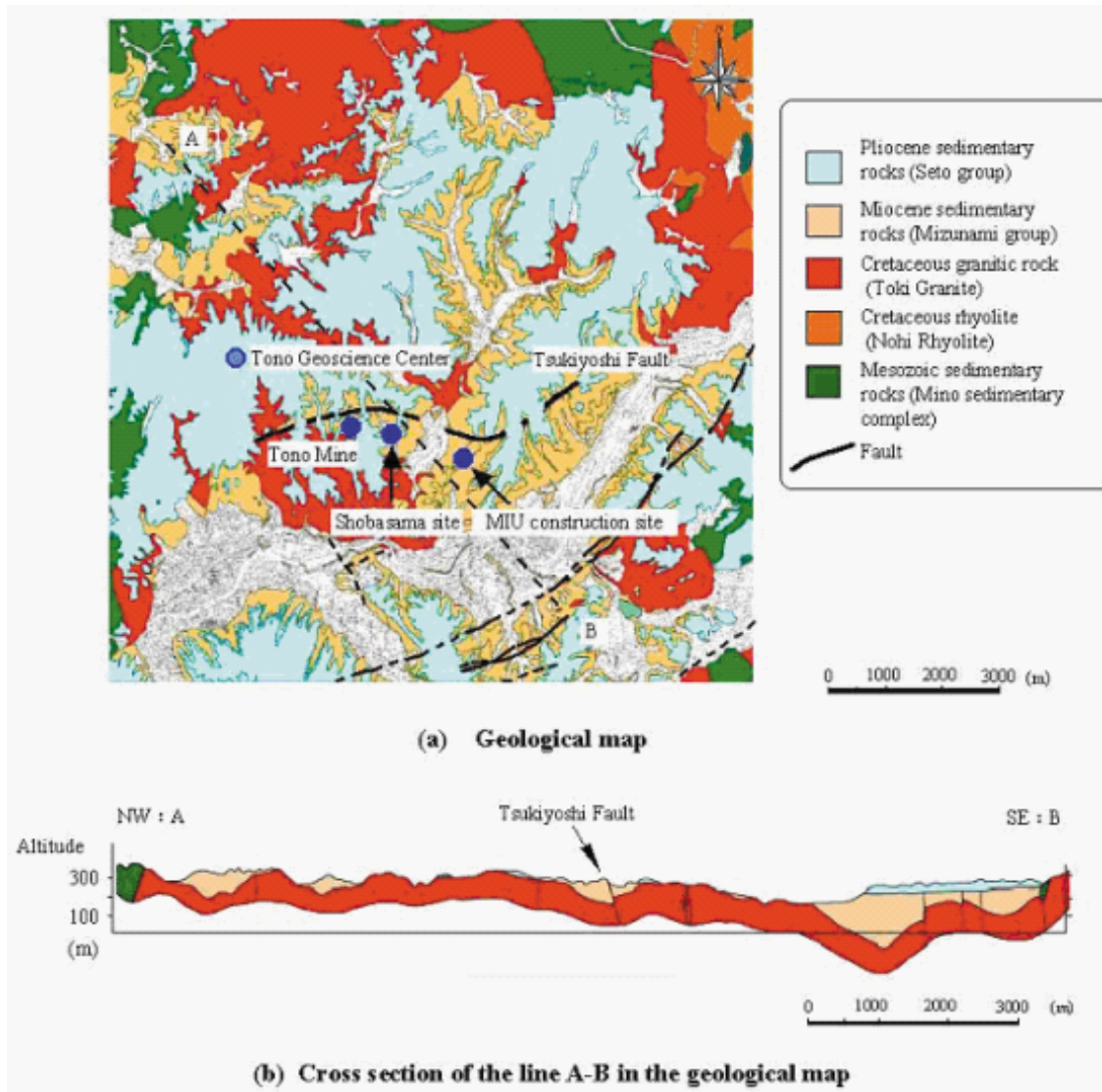
Fig. 3.18. Geological map of the Tono region

weathered. The thickness of the weathered layer observed along the MIZ-1 borehole is about 10 m, but this thickness varies from place to place.

The major rock forming minerals of the Toki granite are quartz, plagioclase, k-feldspar and biotite, and are accompanied by accessory minerals such as fluorite and pyrite. The dominant oxides present in sedimentary and granite rock samples collected in the Tono area were reported by Uozumi et al., 2005. Iwatsuki and Yoshida, (1999), studied the mineralogy of the fracture system in deep granitic rock of the Tono area to understand the chemical evolution of groundwater. Geological studies revealed that the fracture system within the granitic rock is mostly associated with hydrothermal alteration and can be classified into three categories based on the degree of fracturing: intact zones, moderately fractured zones and intensely fractured zones. In the moderately fractured zones, there is a small alteration, and the filling minerals are mainly of chlorite, montmorillonite and pegmatitic textures. The intensely fractured zones are associated with a strongly altered rock matrix, showing alteration to clay minerals such as kaolinite. X-ray powder diffraction showed that the carbonate minerals on the fractures are mainly calcite (Iwatsuki et al., 2002)

The Tsukiyoshi fault extends through the centre of the assessment area, having an E-W strike. According to the results of borehole investigations, the Tsukiyoshi fault has N80^{0}W strike, 70^{0}S dip, 10–30 m width and approximately 30 m vertical displacement. From the results of stratigraphic studies it is assumed that the Tsukiyoshi fault was active during the periods between the deposition of the Oidawara formation and the Seto Group. In addition, the Tsukiyoshi fault is considered to a have a low permeability zone near its

centre because pore water pressure is approximately 40 m higher in the footwall than in the

hanging wall.

Chapter 4
Field Testing at Tono

The field testing investigations were conducted in the Tono area. The study area is 9 km by 9 km in lateral extent, surrounded by ridges, which were considered hydrologic boundaries, and the Toki River to the south (Fig. 3.16). The bottom impermeable boundary was set at an altitude of -3000 masl for the numerical model, taking account of allowance of the depth because a previous study (Saegusa et al., 1998) demonstrated that groundwater flow was minimal in the zone deeper than an altitude of -2000 masl. The area being studied in the present work encompasses the Shobasama site and the MIU construction site shown in Fig. 3.13. In the Shobasama the boreholes considered in this study are the 1000 m deep MIU-1, -2, -3, -4, AN-1 and AN-3. At the MIU site, the following boreholes are considered: DH2, MIZ-1, MSB-1, MSB-2 and MSB-3. To the north of the Tsukiyoshi fault, DH-9, DH-11 and DH-13 are included in the study.

The different investigations that have been conducted at Tono are summarized in Table 4.3. As part of the aerial studies, Landsat imagery, SPOT imagery and aerial photography were employed to identify the distribution of lineaments (Fig. 4.19), because the observed lineaments substantially follow the distribution of trace length of faults distributed in Japan (Sawada et al., 2002).

Using surface-based investigations, the main geological structures such as a formation boundary, unconformity and the Tsukiyoshi fault were identified using seismic reflection and refraction profiling. The magneto-telluric (MT) method was used to identify the

50

Table 4.3. Details of site investigations at Tono

Survey	Method	Content
Literature survey	Topographic map	Topographic condition
	Geological map	Geological condition
Aerial investigation	Landsat imagery	Lineament
	Spot imagery	
	Aerial photos	
Ground investigation	Seismic reflection/refraction profiling	Major discontinuous structure condition
	MT method	Unconformity distribution
	Water balance observation	Precipitation, evapotranspiration, surface water discharge, from the Tono Mine
Borehole investigations	Core observation	Geological condition, fracture characteristics
	Borehole TV observation	Fracture depth, strike and dip, fracture aperture, crack sealed vein, Caliper logs, formation density logs, groundwater
	Borehole loggin	velocity, natural gamma logs, apparent resistivity, micro resistivity, neutron logs, neutron porosity, porosity, RQD, sonic logs, temperature logs,
	Lost circulation measurement	Water way condition (14 boreholes)
	Hydraulic head observation	Observed in total 158 boreholes
	Hydraulic pressure observation	Pore pressure distribution in vertical direction
	Hydraulic test	Pulse test, slug test, pumping test

spatial distribution of unconformities along the boundary between the Toki granite, which showed high resistivity, and Neogrene sedimentary rocks, which are identified by low resistivity. The parameters used to determine the recharge rate, such as precipitation, evapotranspiration, river discharge and mine discharge from the Tono Mine, were measured.

The geological characteristics of the site such as fracture characteristics, distribution of hydraulic conductivities, groundwater table and baseline pressure distribution were obtained through a series of borehole investigations. The borehole investigations consisted of: (1) core descriptions and borehole tele-viewer (acoustic) investigations to acquire detailed information on the location, orientation and size of fracture zones that are considered to be potential water conducting features in the granite; (2) hydraulic tests in 100 m sections

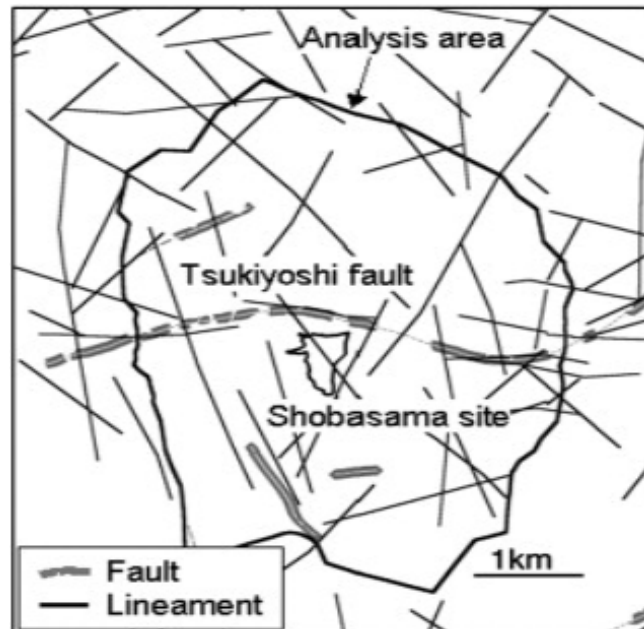Fig. 4.19. Lineament distribution in the Tono basin (with permision, Ijiri et al., 2009)

of packed-off sections to develop a comprehensive, albeit averaged database of hydraulic properties from near surface to depth and (3) hydraulic tests in sections several meters long to establish their hydraulic properties. The specific sections are potential water conducting features, fluid loss zones or major structures such as faults.

Chapter 5
Hydrogeological Model

The present study improves on a 9 km by 9 km by 3 km model as developed by Doughty and Karasaki (2008), to simulate the hydrologic response to the pumping accompanying excavation of the two shafts, which was monitored in nine wells with distances ranging from about 20 m to 2 km from the shaft. This is almost an unprecedented scale of transient pressure testing in fractured granite.

Hydraulic head was monitored at multiple depths in nine wells while two shafts (the main shaft and ventilation shaft) were excavated from the surface to 200 m depth. Excavation began in mid-2003 (January 1, 2003 is denoted day 0), with continuous pumping occurring until October 27, 2005 (day 1031), when pumping ceased abruptly. Pumping resumed on a small scale in early 2006 and at full scale on February 20, 2006 (day 1147). Fig. 5.20 shows the shaft water level as a function of time for the main shaft and the ventilation shaft. It is assumed in this study that the excavation level coincides with the water level (that is, water is pumped just enough to keep the excavated shaft dry).

Hydraulic head observations begin at different times for different wells, and continue through the end of 2007 (day 1826). This excavation can be considered a large-scale pump test, and this study aims to improve our understanding of the regional-scale hydrology by monitoring the pressure response in both nearby and distant wells. The pressure responses throughout the site reflect the permeability and storage capacity of a large volume of fractured rock.
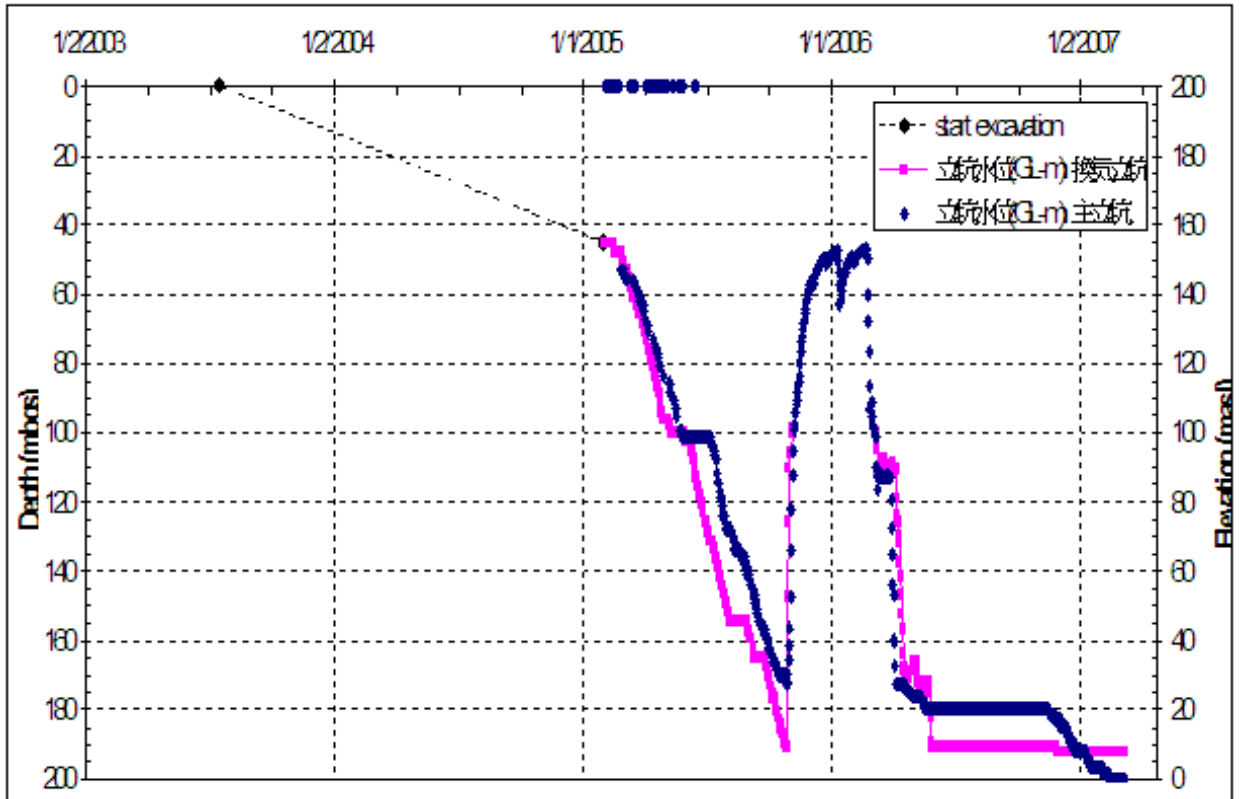
Fig. 5.20. Shaft water level as a function of time (from Doughty and Karasaki, 2008)

The difficulties and limitations of properly estimating the surface boundary conditions when the model is very large (several square kilometres) have been documented previously (Karasaki et al., 2009). In that paper, Karasaki et al. also discuss the challenges of determining the actual recharge from rainfall or river data for such an area. Moreover, taking a recharge value calculated from observations in the vicinity of a small area and then assuming that the recharge rate in the large area is the same may not be realistic. For example, Karasaki (personal communication, 2010) points out that he had found, to his surprise, that the amount of rainfall at the Berkeley Laboratory and downtown Berkeley (two locations that are about 5 km apart) were very different.

In their model, Doughty and Karasaki (2008), the top surface is a constant head boundary condition. Therefore, as the pressure in the model decreases due to pumping, the flow of water into the model representing infiltration and recharge may increase, but this would not be realistic. However, they point out that a better representation would be to specify constant fluxes for grid blocks that show inflow (representing infiltration/recharge) and constant heads for grid blocks that show outflow (representing spring discharge). Such an assignment is not a trivial problem, considering the irregular distribution of inflow and overflow over the top of the model.

In this work, as an improvement on the Doughty and Karasaki model, the top boundary of the recharge rate at the ground surface was specified. The recharge rate of 102.2 mm/year (JAEA), the mean calculated from observations carried out from 1990 to 1997 in the vicinity of the Tono Mine, was applied to the steady-state simulation. This recharge rate was decreased until the model heads matched the observed head data.

In the model of Doughty and Karasaki (2008), the computational grid is rectangular with lateral grid spacing of 100 m. Vertical grid spacing ranged from 50 m in the upper portion of their model to 100 m over most of the model, to 250 m for the deepest (1000 m). This lateral grid spacing is much too coarse to accurately model pressure transients for the monitoring locations in wells 05ME06, MSB-3, DH-2, MSB-1 and MIZ-1, which are less than 200 m from the shafts. The two shafts themselves are 40 m apart and each has a diameter of 6 m. The use of grid blocks of 100 m means that the shafts are lumped together in one column of grid blocks. Additionally, it is difficult to accurately represent the Tsukiyoshi fault or any other fault with such a coarse mesh. Thus, it cannot be expected that the Doughty and Karasaki (2008) model would capture all the details of the pressure transients in the field.

In this thesis, a new finite element model with local grid refinement around the wells and shafts is developed and applied to the Tono area. Due to local mesh refinement, this model therefore avoids lumping together the two shafts in one column of elements and is therefore able to include the two shafts as separate entities. In order to better represent the Tsukiyoshi fault and other structures, local mesh refinement around these geological structures is also implemented. This was not possible in the previous model of Doughty and Karasaki (2008), where they ended up with a fault core that is about 300 m wide, which is not realistic. Apart from just the geometric representation of the faults, local refinement will capture and help in the understanding of the flow field in and around the faults where there may be steep hydraulic gradients.

Doughty and Karasaki (2001) concluded that the effective porosity of the granite in the Tono region is one of the most uncertain model parameters that still needs to be understood. The transient model developed in this thesis will be used to estimate the large-scale effective porosity, based on the long-term pressure response to the shaft excavation in nine wells in the MIU and Shobasama sites.

5.1   Construction of the Conceptual Model

For this thesis, a conceptual model is defined as the conceptualisation of the system geometry and the controlling physical properties and a numerical model refers to incorporation of the conceptual model into a computer program that simulates the physical process such as fluid flow and transport in the identified system geometry. Therefore, the numerical model consists of input data and the numerical code. Numerical models have the advantage of being able to simulate flow and transport in complexly fractured systems at scales larger than those represented by a single borehole or aquifer test, and may be used for the testing of hypothesis about flow through fractured rock.

Starting with the regional geographic, geologic and subsurface hydrologic and geophysical data, an effective continuum model is developed to simulate subsurface flow and transport in the 9 km by 9 km by 3 km thick fractured granite rock mass overlain by about 100 m of sedimentary rock. The model extends from ground surface (ranging from 100 to 600 m masl) to an elevation of -2000 masl. Lateral boundaries are irregular, following local topographic features such as the Toki River along the southern and eastern model boundaries, and the ridgelines along the western and northern boundaries. Fig. 5.21 shows

the perspective view of the conceptual model showing the different materials. Within each material, permeability and porosity are drawn from stochastic distributions.

The model is composed of four geological layers. The bulk of the model is fractured granite, which is underlain by deep, low permeability granite and overlain by weathered, more intensely fractured granite few hundred meters thick. Over much of the model, sedimentary rocks overlie the weathered granite. One major fault is included in the model, the E-W striking, sub-vertical Tsukiyoshi fault. Two additional sub-vertical faults are also included. The Tsukiyoshi fault is represented with a planar structure, in which a low permeability core is flanked on either side by relatively high permeability planes representing the damage zone. The structure is suggested by the geological and tectonic nature of the site and is supported by steady-state and transient pressure observations (Takeuchi et al., 2001; Doughty and Karasaki, 2003). The two additional faults are each modelled as a single plane. All faults extend from the ground surface to the bottom of the model. Fig. 5.21 shows a perspective view of the conceptual model showing all the faults modelled and the different lithologic layers. Fig. 5.22 is a schematic diagram that shows the boreholes that penetrate the Tsukiyoshi fault.

Individual fractures were not modelled explicitly. Rather, continuum permeability and porosity were assigned to the finite elements stochastically, based on the hydraulic conductivities determined from well-test data and fracture density measurements. Large-scale features such as lithological layering and fault zones were assigned deterministically. The top of the model coincides with ground surface, with topographic relief determined from a 20 m by 20 m resolution digital terrain map.
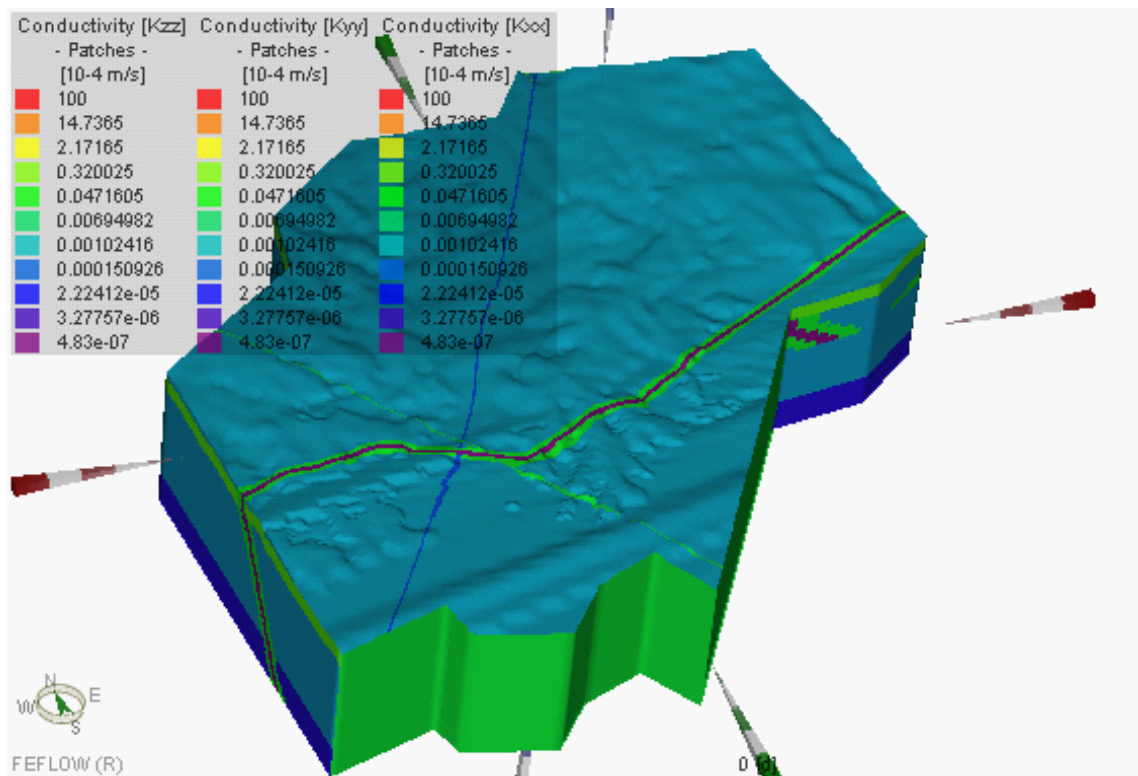
Fig. 5.21. Perspective of the conceptual model showing the different geolayers and the Tsukiyoshi fault and two other faults
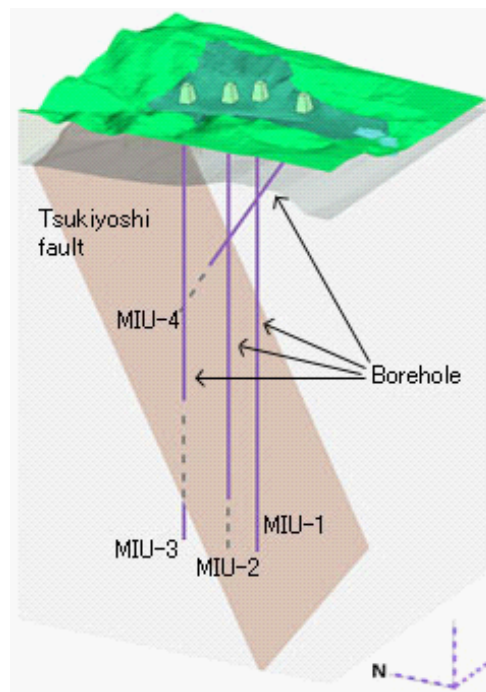
Fig. 5.22. Schematic diagram showing the wells that penetrate the Tsukiyoshi fault at the Shobasama site]

Table 5.4. Summary of material properties used in the model. For sedimentary rocks with no data available, typical stochastic properties are used. For deep granitic layers, the mean K is three times smaller than the overlying layer

Material type	Number of conductivity measurements	$\text{Log}_{10}K$ Mean	Std. Dev.	Type of distribution used for $\text{Log}_{10}K$
Alluvium	0	-7.9	1.6	Normal
Seto group	0	-7.9	1.6	Normal
Oidawara	1	-8.7	1.6	Normal
Akeyo	11	-7.9	0.8	Resampled
Toki lignite-bearing	21	-7.0	0.9	Resampled
Toki granite (biotite)	192	-7.1	1.7	Resampled
Toki granite (felsic)	46	-6.9	1.1	Resampled
Deep granitic layers	0	-8.0	1.6	Normal
Faults	12	-7.7	1.0	Tsukiyoshi resampled; other faults normal
Average over all rocks	283	-7.3	1.5	

Material type	Number of fracture density measurements	Fracture density (m^{-1}) Mean	Std. Dev.	Model Porosity Mean	Std. Dev.
Toki granite (biotite)	57	7.7	4.2	3.9E-4	5.9E-4
Toki granite (felsic)	4	10.8	4.2	3.5E-4	2.7E-4
Average over all rocks	67	7.9	5.0	3.2E-4	4.2E-4

The field data from which model permeabilities and porosities were derived consists of 283 hydraulic conductivity (K) values, inferred from slug tests and pumping tests at multiple zones sectioned using pneumatic packers in 14 boreholes, 67 fracture density (d) measurements made from borehole imaging and core analysis in 5 boreholes. The K values were not interpreted as representing individual fracture conductivities, but as representing effective continuum conductivities averaged over the length of the packed-off interval. The vertical elements in the model were chosen to be comparable to typical lengths of zones sectioned using pneumatic packers, and thus an assumption was made that there was no need to 'scale up' or 'scale down' K values measured during the well test, and that they directly represent the effective continuum conductivities required for the model. This is the same method used by Doughty and Karasaki (2002).
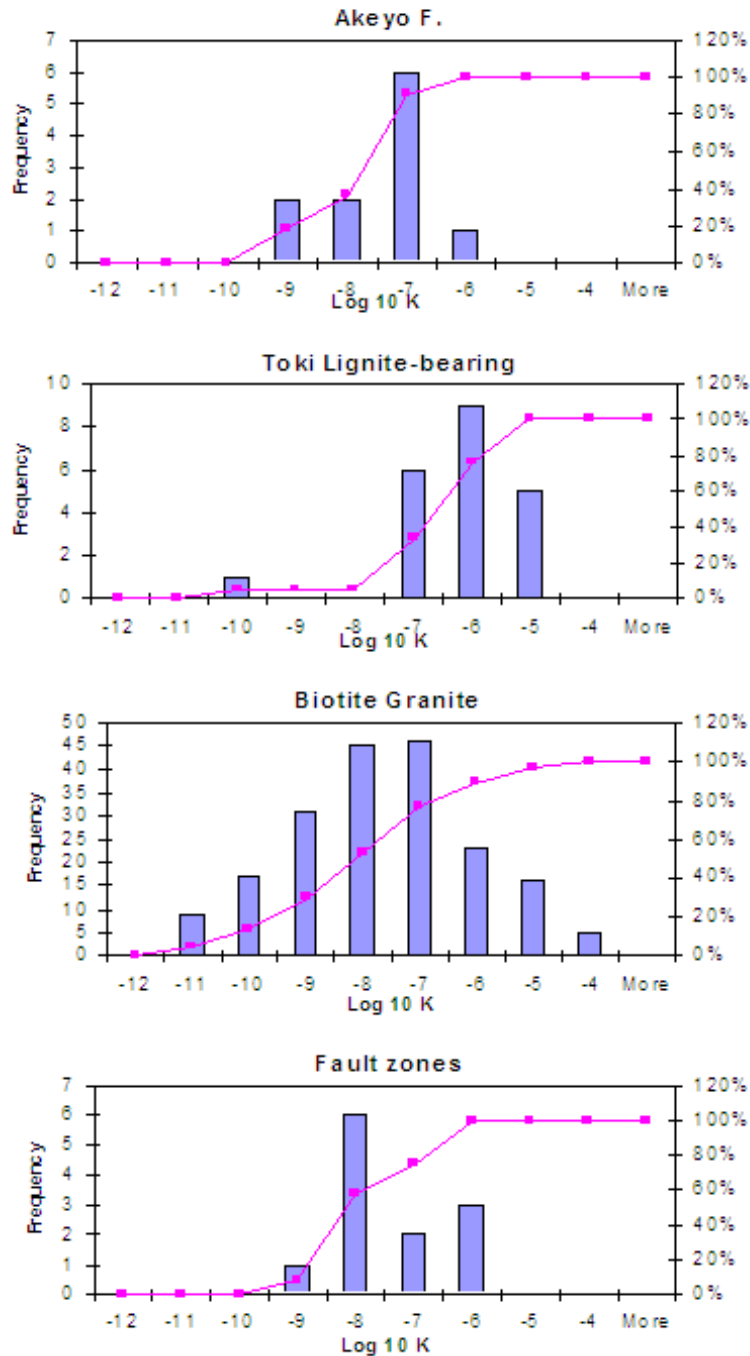
Fig. 5.23. Distribution of log K obtained from slug tests and pumping tests. Each conductivity value is weighted by the length of the test interval. The line shows the cumulative distribution function

Finite element grid conductivity values were drawn from stochastic distributions for each lithological layer (that is each material type in the model). For the granitic rocks, distributions were constructed by re-sampling field measurements. For the sedimentary rocks, there are not enough measurements for a given material type to make re-sampling viable, so log-normal distributions were used.

Table 5.4 summarizes the material types and conductivity distributions used in the model. To investigate whether the K distributions showed a spatial correlation structure between the finite elements and the lithofacies scale, K values versus depth profiles for individual wells were created, and then these profiles were compared among wells. The results (Fig. 5.23) suggest that K is not strongly spatially correlated at this scale, so field measurements within each material type were randomly shuffled before being assigned to the finite elements. Permeability is simply the product of hydraulic conductivity and the ratio of water viscosity μ to specific gravity ρg, which is a constant for an isothermal system.

Counting the fractures observed in borehole images enables fracture density d (number of fractures per meter) to be estimated. We assume that fracture spacing b is inversely related to fracture density

$$b = \frac{1}{d} \tag{5.1}$$

Porosity ϕ is estimated as the ratio of average aperture of all apertures, w, to fracture spacing b

$$\phi = \frac{w}{b} \tag{5.2}$$

The relationship between w and K_f, the individual fracture conductivity, is obtained from the parallel-plate assumption for fracture [National Research Council Committee on Fracture Characterization and Fluid Flow, 1996].

$$\frac{w^2}{12\mu} = K_f \tag{5.3}$$

Since the effective continuum conductivity K is related to K_f according to

$$K = K_f \left(\frac{w}{b}\right) \tag{5.4}$$

we get the well-known cubic law relating w and K

$$K = \frac{w^3}{12\mu b} \tag{5.5}$$

We combine equations (5.1), (5.2) and (5.5) to write ϕ in terms of K and d

$$\phi = \left(12 K \mu d^2\right)^{\frac{1}{3}} \tag{5.6}$$

As has been demonstrated in Chapter 2.0 of this thesis, fracture density measurements are sparse and no obvious correlation between d and K was found. Also, d measurements from lithological layers were combined to determine a mean fraction of 7.95 m^{-1} and standard deviation of 5.0 m^{-1}. For most of the lithological layers, d values were drawn from a normal distribution with these moments, which is truncated at a small number (0.01 m^{-1}) to ensure that d is always positive.

Table 5.5. Properties for starting 9 km by 9 km ECM model (from Doughty and Karasaki, 2002)

Geolayer	Porosity	Hydraulic Conductivity (m/s)	
		Within Materials	Between Materials
Sedimentary (Seto+Mizunami)	0.2	6.3×10^{-8}	6.3×10^{-10}
Weathered granite	7.3×10^{-3}	1.0×10^{-7}	1.0×10^{-9}
Granite	3.4×10^{-3}	1.0×10^{-8}	1.0×10^{-10}
Deep granite	3.4×10^{-3}	1.0×10^{-9}	5.0×10^{-11}
Tsukiyoshi fault core	8.4×10^{-4}	1.0×10^{-10}	1.0×10^{-10}
Tsukiyoshi fault (hanging wall sandwich)	7.6×10^{-3}	2.7×10^{-6}	1.0×10^{-8}
Tsukiyoshi fault (foot wall sandwich)	7.6×10^{-3}	2.7×10^{-6}	1.0×10^{-8}
Other faults	3.0×10^{-3}	1.0×10^{-6}	5.0×10^{-9}

For each finite element, after K and d had been drawn from the appropriate distribution, equation (5.6) is applied to determine ϕ. The resulting model porosity statistics are summarized in Table 5.5.

Note that for sediments and granites 'within material' permeability is generally K_{hor}, the horizontal component of permeability and 'between material' permeability is generally K_{ver}, the vertical component of permeability, whereas in faults 'within material' permeability is generally K_{ver} and 'between material' permeability is generally K_{hor}

.

5.2   Construction of the Numerical Model

The numerical simulator Feflow (Diersch, 2005a) is used for the flow and transport calculations. The hydrogeological system contains two main aquifers separated by weathered granite. The top hydro-stratigraphic unit is considered to be a Quaternary sedimentary confined aquifer. The second aquifer located below the weathered granite is a granitic. Field data shows the heads in the Quaternary sediments overlying the granite to hardly respond

to the excavation (pumping) activity and thus the granite formation can be treated as confined. The pressure response does not go beyond the Tsukiyoshi fault and the granite is covered by the sediments with a low vertical permeability, which makes the granite formation confined. Thus the granite formation was modelled as a confined aquifer.

Feflow is a general purpose finite element code that simulates saturated/unsaturated seepage flow and transport, based on the geological units in the model and 3-D distribution of fractures. Depending on the design of the mesh, Feflow can represent individual fractures or fracture networks explicitly, using the so-called discrete feature approach (Diersch, 2005b) or through an effective continuum formulation as done in this study. Feflow applies governing equations, including Darcy's law, taking unsaturated and saturated flow conditions into consideration using the continuity equation for groundwater flow in porous media (i.e., conservation of mass of fluid and solid continua, mass conservation of contaminants and chemical constituents, momentum and energy conservation of fluid and solid continua).

Three-dimensional finite element meshes are developed for the groundwater flow based on geological units in the conceptual model and 3-D distribution of fractures. Three-dimensional meshes are formed taking into consideration the boundaries of the geological units that are shown in Table 5.5.

The 3-D mesh is shown in Fig. 5.24. Local refinement is applied around the wells and shafts as well as around faults.

Using the mesh, the 3-D distribution of fractures described in Section 5.1 is statistically developed in granite to construct an effective continuum model. Each finite element represents an effective fractured continuum with permeability and porosity assigned sta-
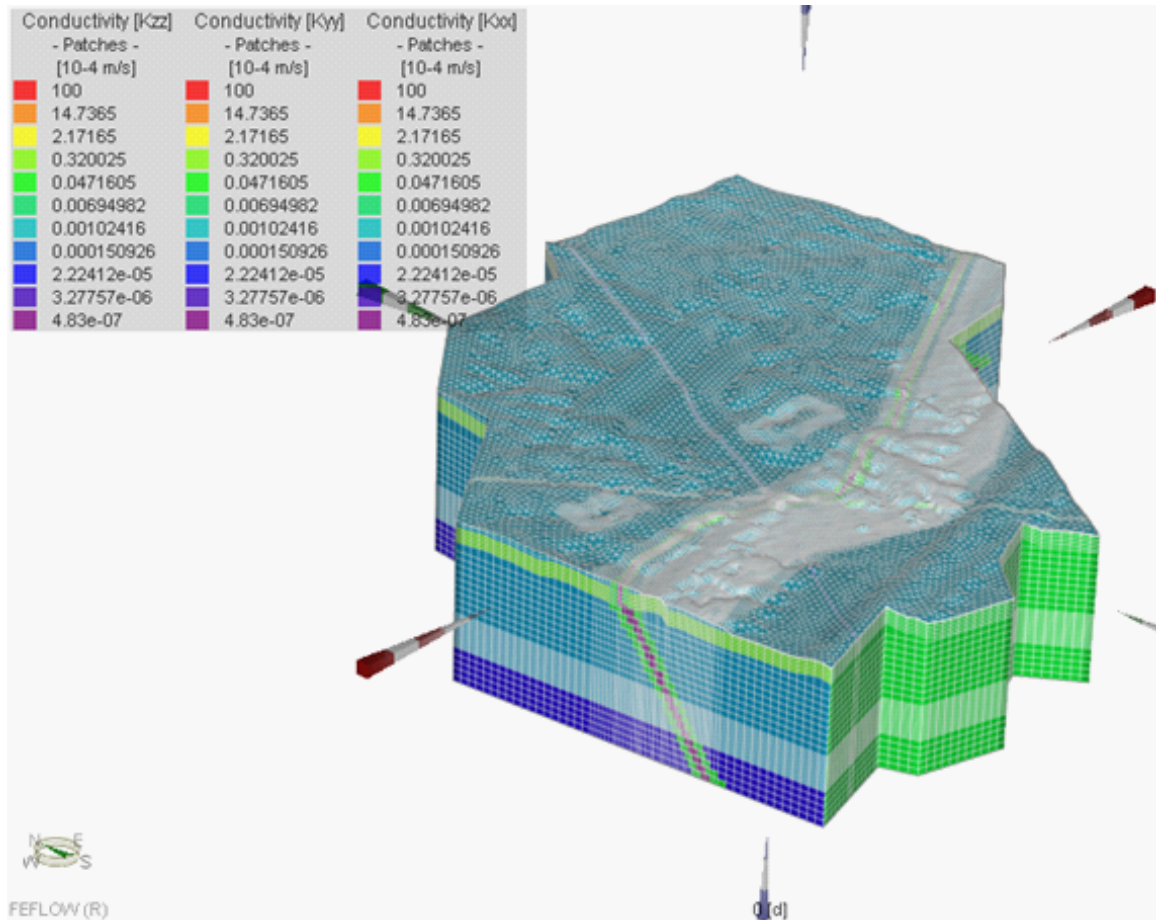
Fig. 5.24. Local mesh refinement along the main fault (fault represented as a 'sandwich' with the low permeability core and the high permeability damage zone on either side of the core), around the pumping shafts and two hypothetical contaminant sites

tistically. The hydraulic conductivity, K, is determined from slug tests and pumping tests conducted using packed-off intervals in boreholes. Because many of the intervals used for the tests are of the same order as the vertical extent of the finite elements making the model, there is no need to scale up or scale down the K values measured during the well tests, and they therefore represent the effective continuum conductivities.

For the granite rocks and fault zones, weighting the conductivity values by the length of the test interval shifts the values towards higher conductivities, implying that long test intervals are likely to be associated with high conductivity values. If test intervals are chosen to reflect features observed in the rock, then this relationship supports the concept that high conductivity fractures tend to be more spatially extensive than low conductivity fractures.

Porosity ϕ is calculated as the product of fracture aperture w and fracture density d, with aperture determined from equation (5.6). Note that the effective continuum conductivity K is related to the actual conductivity of an individual fracture K_f according to equation (5.4).

As has been demonstrated in Chapter 2, fracture measurements are sparse and no correlation between fracture density and conductivity was found.

5.3 Initial and Boundary Conditions

Initial conditions for the steady-state simulations are chosen as a matter of convenience, that is, they do not affect the final model result, only how efficiently the computer reaches it. The initial conditions for the shaft excavations are taken from steady-state head distri-

butions. The steady-state distributions obtained (see Fig. 6.31 to Fig. 6.41) do a good job matching observed head distributions throughout the 9 km by 9 km model area.

The top boundary: although the groundwater recharge from a mathematical point of view is rather a boundary condition, it is handled as a material property in Feflow. Recharge at the top takes precipitation, evaporation and run-off into consideration. The recharge rate of 102.2 mm/year, the mean calculated by JAEA from observations carried out from 1990 to 1997 in the vicinity of Tono Mine, was applied to the steady state groundwater simulation. The Tono Mine is an abandoned mine within the study area. The results showed head distributions that are higher than the actual observations. This recharge rate value was changed to 90 mm/year so that the simulated results would match the field data. The ground surface is assumed to be a free-seepage surface with unrestricted inflow and outflow of water possible.

The lateral boundaries of the model are chosen on local geography. Along the western and northern boundaries, the model follows ridgelines and is a no-flow (closed) boundary, to represent the watershed divide. However, it is not clear whether these ridgelines always coincide with the watershed boundaries, because of geological structures. Nonetheless, a previous study (Saegusa et al., 1998) of groundwater flow encompassing the model area indicates that water flows from the north to the south and is controlled by regional topography. As the groundwater flow roughly follows topography, an assumption is made that these ridgelines represent boundary streamlines. No exchange of water is expected over these boundaries and therefore a no flow boundary condition is assumed. However, one may argue that it could be better to set the northern boundary on the Kiso River to the

north. Then the water level along the river would then be used as the value for a first-kind hydraulic boundary condition. The effect of putting the northern boundary of the model on the Kiso River is not investigated in this thesis, but should be investigated in future.

The Toki River completely controls the head along the southern and eastern boundaries. The elevations of the river surface are used as the constant head values assigned to the southern boundary. A further assumption is made that the Toki River might actually be flowing on top of a high permeability fault (i.e., the river might actually flow along a fault), and therefore the material directly beneath the river is treated as high permeability material.

For the transient calculations in response to the shafts excavation, two shafts are being excavated and located in the southern part of the model. These shafts together with a pumping rate of 500 m^3/day are located in the MIU construction site. Finally, the Tono mine is specified as a constant mass sink and the average flow rate out of the mine was set at 0.57 kg/sec, according to the data.

Chapter 6
Steady-State Analysis

The groundwater flow simulation in this thesis uses the saturated/unsaturated seepage low analysis code (Feflow) for an equivalent heterogeneous continuum media. The ground water simulations are based on the hydrogeological investigations described in Chapter 2 of the present work and the flow parameters described in Chapter 4. Specifically, data in Table 5.5 were used for the initial or starting model.

Steady-state simulations were carried out with the purpose of understanding the groundwater hydrogeology in the study area and to establish the initial conditions to predict the effects of shaft excavation. Thus, in this section we analyse the Tono basin before it was disturbed by the production or excavation of the shafts. Steady-state head profiles are available from 11 wells within the 9 km by 9 km model area.

6.1 Model Calibration

The starting model was developed by calibrating to steady state heads in the 11 wells mentioned above, using the effective continuum model. The permeability and recharge rate are modified to improve the match (note that steady-state profiles do not depend on porosity). The steady-state head distributions were then calculated to compare with observed data and serve as initial conditions and boundary conditions for the subsequent transient response to shaft excavation. The results of the simulations using the ECM are shown in Fig. 6.26 to Fig. 6.30 and Fig. 6.31 to Fig. 6.41. The hydraulic head at depth over much of the Tono
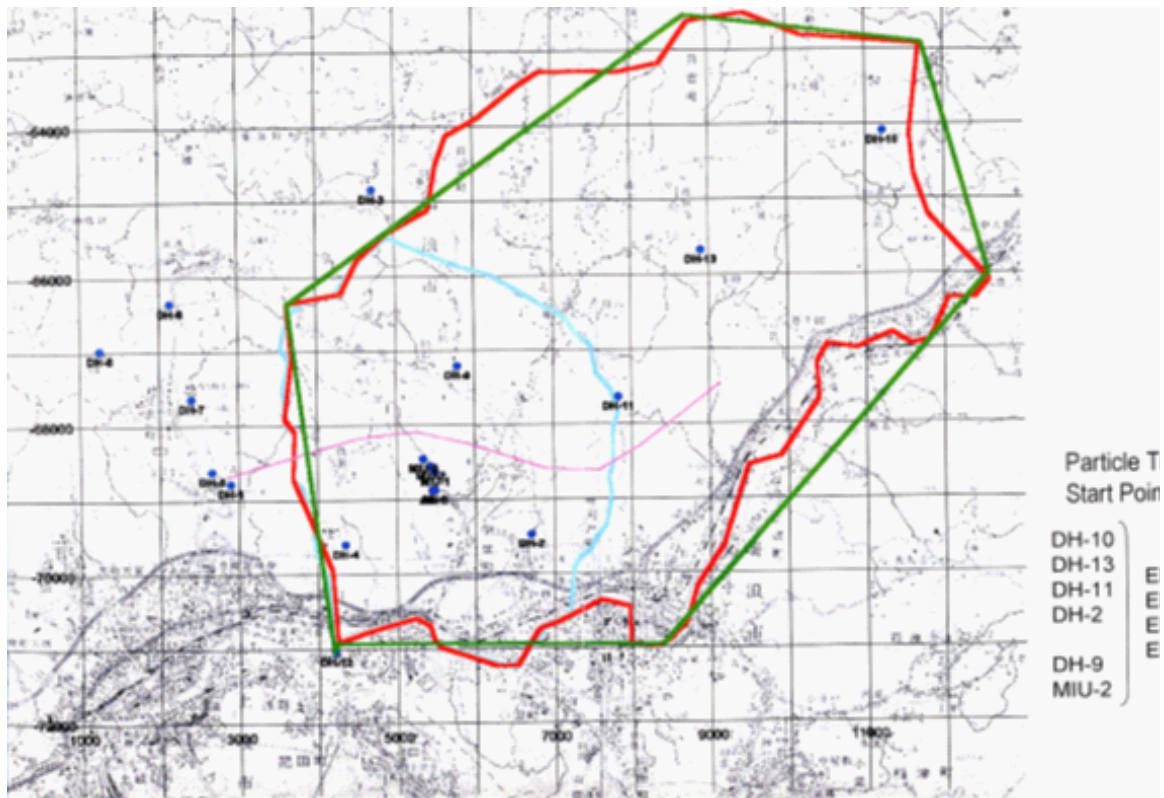
Fig. 6.25. Plan view of the model's lateral boundary (red), superimposed on the digital topography map of the area. Some of the boreholes (blue dots) for water pressure response and the Tsukiyoshi fault (purple line) are also shown. The blue boundary is for the earlier 4 km by 6 km model.

basin is near the surface elevation. The heads in the study area generally decrease from north to south indicating that water generally flows from north to south. Figure 23 clearly shows the effects of the faults on the hydrology in the study area. Most profiles show constant head with depth, with higher head north of the Tsukiyoshi fault (wells DH-9, DH-11, and DH-13).

Modelled heads at the 10 wells are shown in Fig. 6.31 to Fig. 6.41, which indicates that the model heads in the Mizunami area match observations much better than in Doughty and Karasaki, (2009) (marked D&K2009 in Fig. 6.31 to Fig. 6.41). In particular, the match between data and model heads at DH-2 shows much improvement over Doughty and Karasaki, (2009). At MIU-2 and MIU-3, where the Tsukiyoshi fault is intersected, there is an abrupt change in head values on opposite sides of the fault (Fig. 6.32 and Fig. 6.33). In the MIU-3 well (Fig. 6.33), this step change is quite clear and shows a head difference of about 40 m between the northern and southern side of the Tsukiyoshi fault. These two wells (MIU-2 and MIU-3) cross the dipping Tsukiyoshi fault, as evidenced by higher heads at depth. This demonstrates that the Tsukiyoshi fault acts as a barrier to flow. In general, while the simulated values are still slightly higher than the field data values as in Doughty and Karasaki (2008, 2009), the results shown here are a significant improvement on their results. This could be attributed to local mesh refinement around the faults and wells. Also, in this study the top boundary of the model was specified as a constant recharge, different from the constant head boundary condition of Doughty and Karasaki (2010). Overall, the calibration results for the steady-state simulation show a good match to field data.
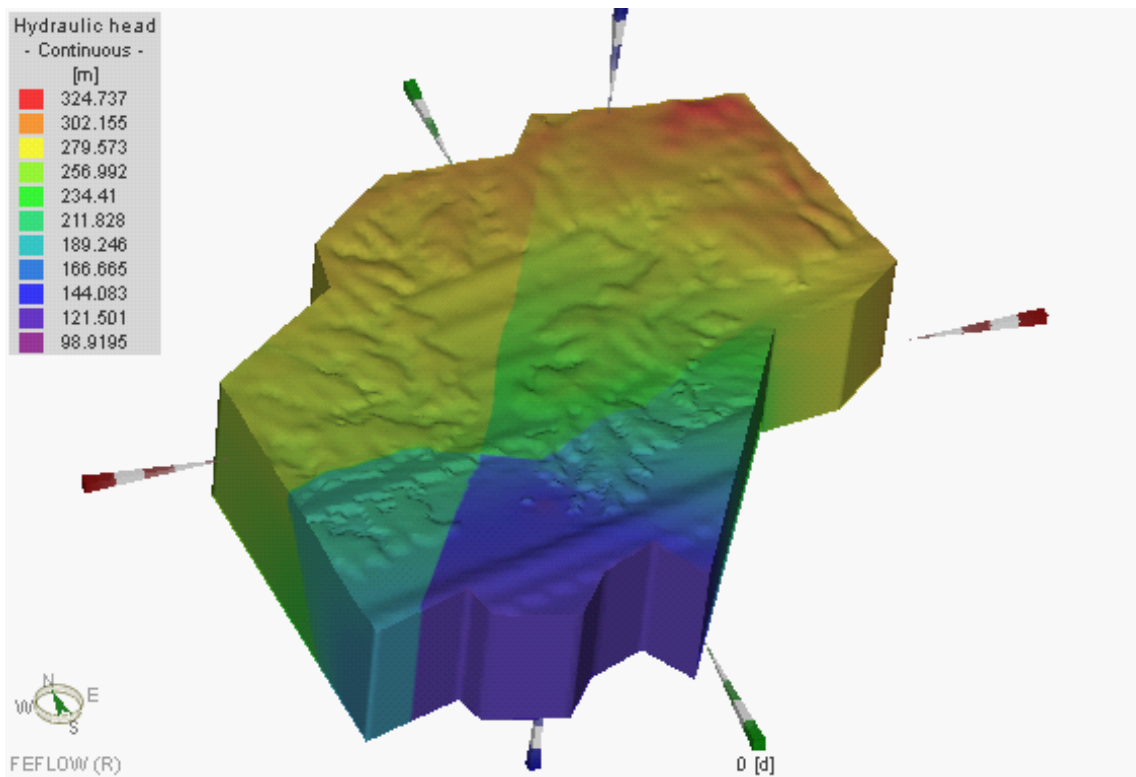
Fig. 6.26. Three-dimensional hydraulic head distribution in the study area. The hydraulic head distribution is marked by colours only. The uneven area on the top boundary is the topography.
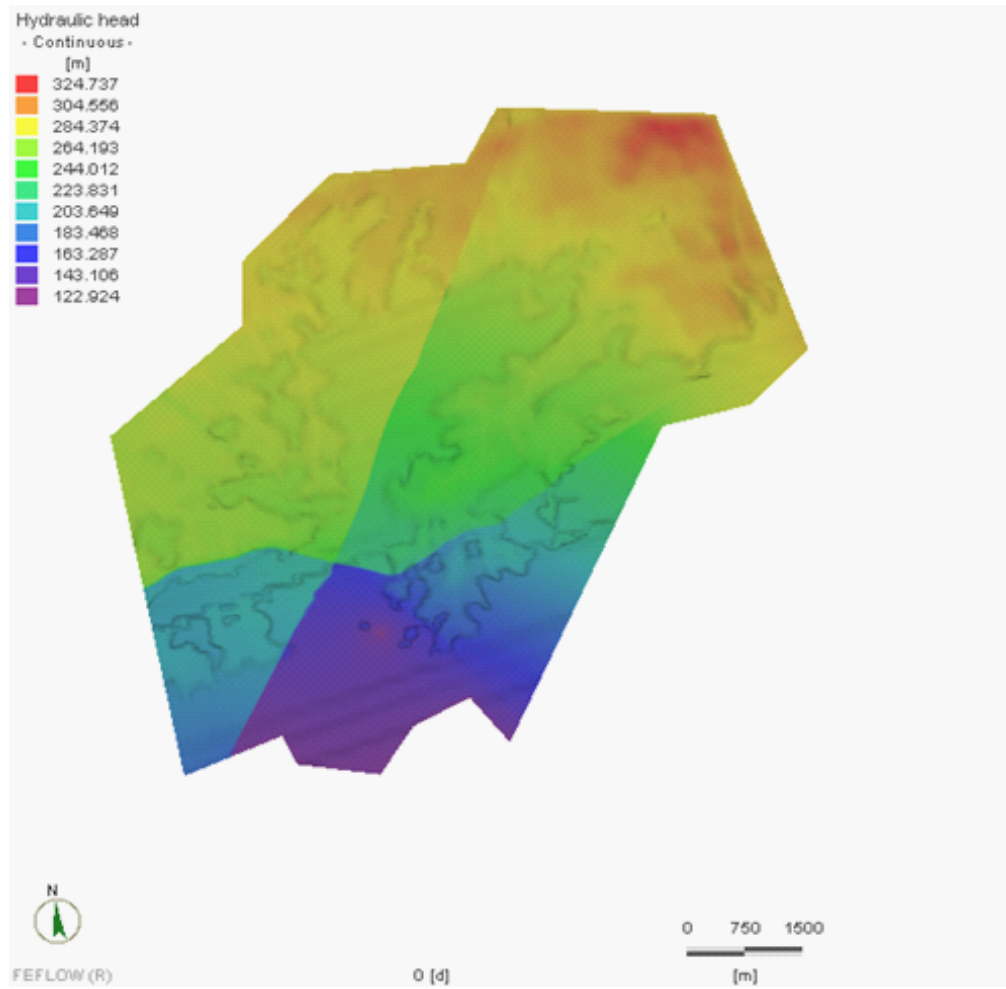
Fig. 6.27. Steady-state head distribution at the ground surface. Note that the head distribution is shown only by the colours; the other artefacts show the topography
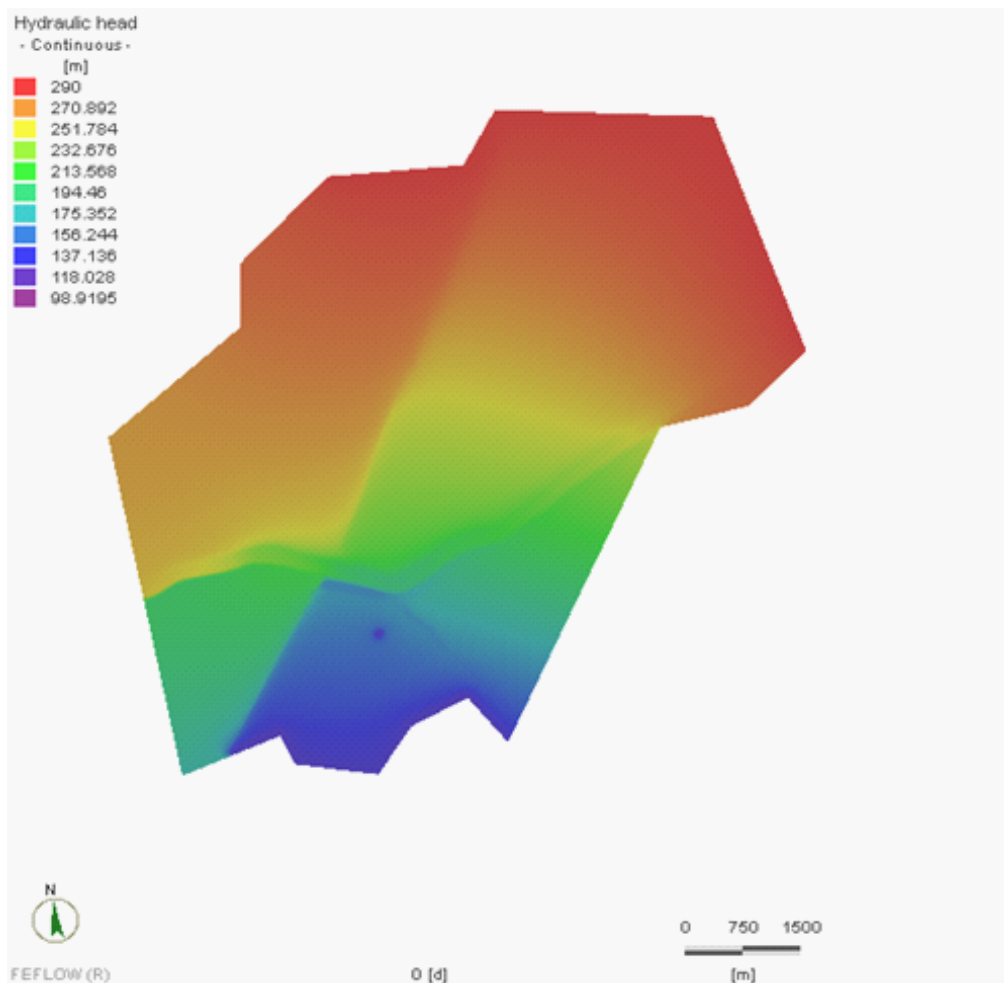
Fig. 6.28. Steady-state head distribution at -100 masl
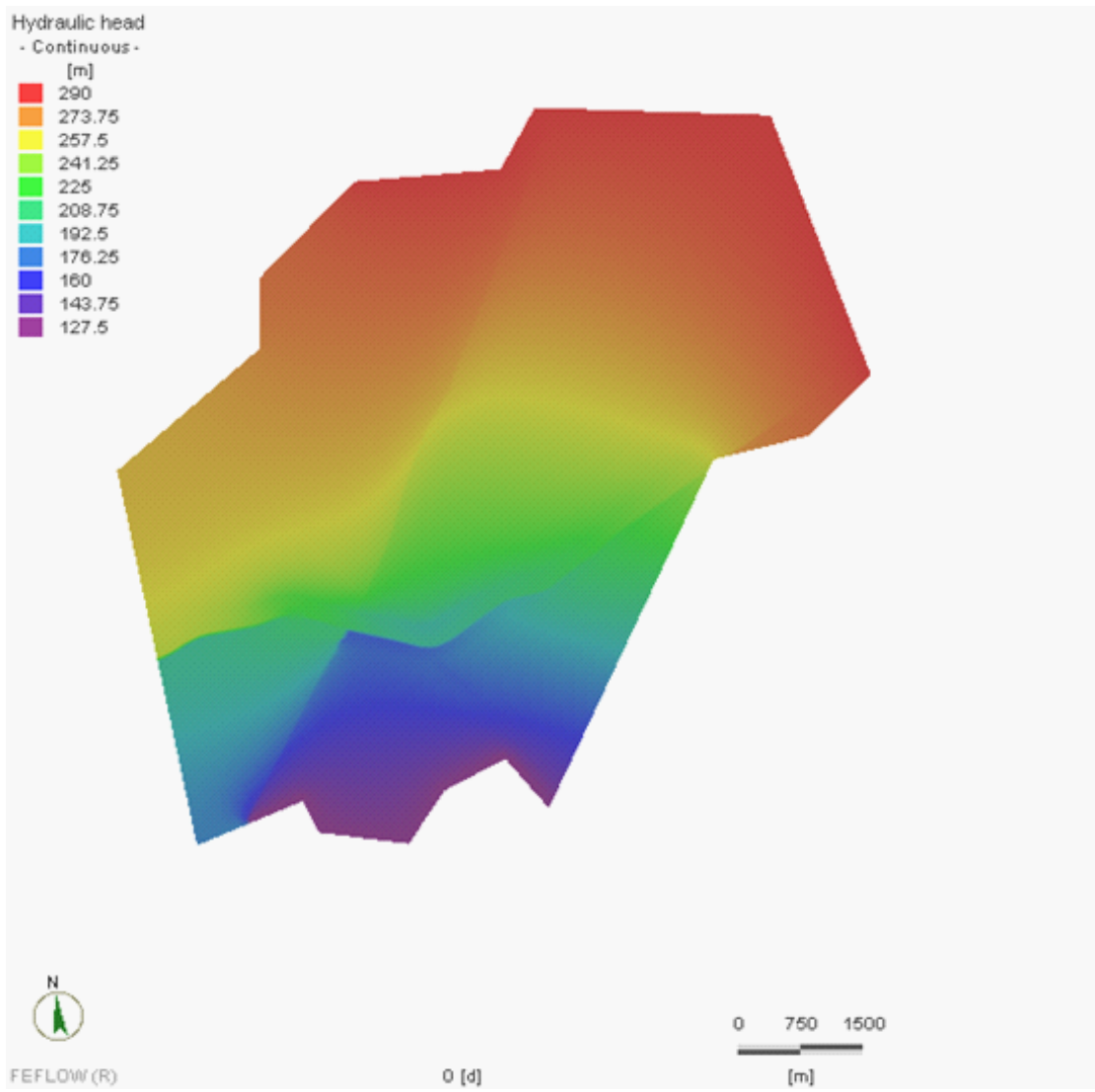
Fig. 6.29. Steady-state head distribution at -300 masl
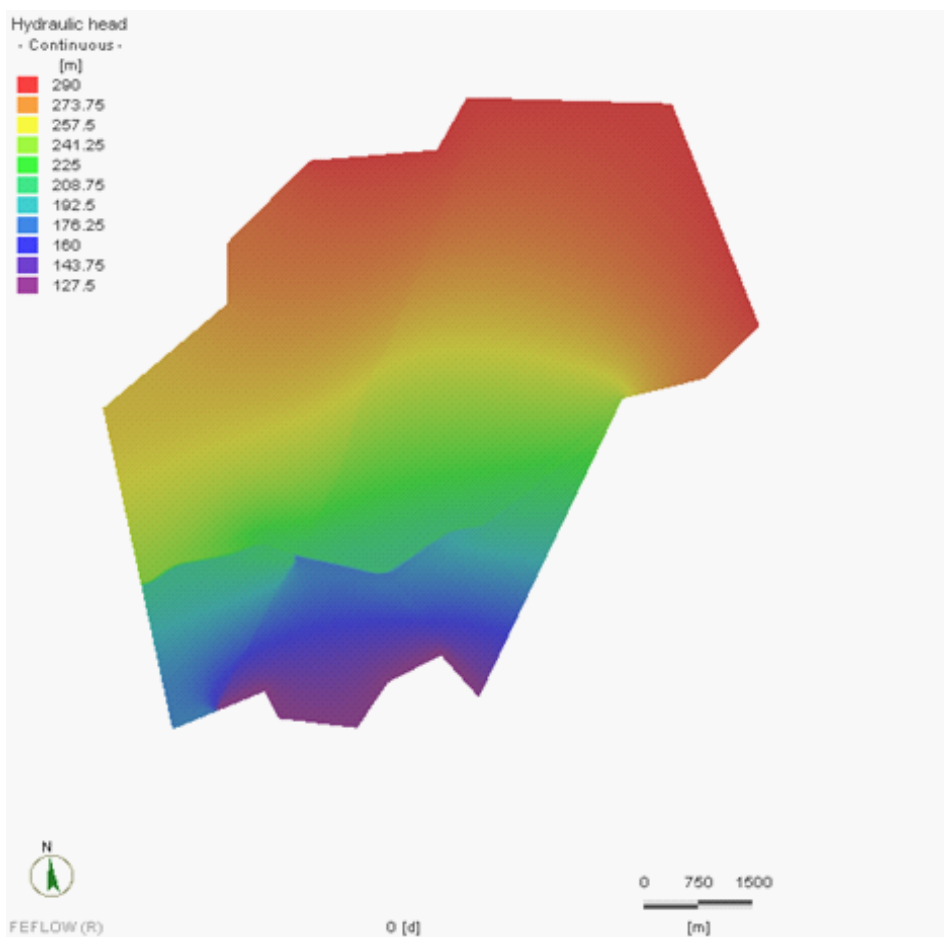
Fig. 6.30. Steady-state head distribution at -700 masl

Fig. 6.31. Steady-state head profiles observed and calculated in MIU-1

Fig. 6.32. Steady-state profiles observed and calculated in MIU-2

Fig. 6.33. Steady-state head profiles observed and calculated in MIU-3

Fig. 6.34. Steady-state head profiles observed and calculated in AN-1

Fig. 6.35. Steady-state head profiles observed and modelled in AN-3

Fig. 6.36. Steady-state head profiles observed and modelled in DH-9

Fig. 6.37. Steady-state head profiles observed and modelled in DH-11
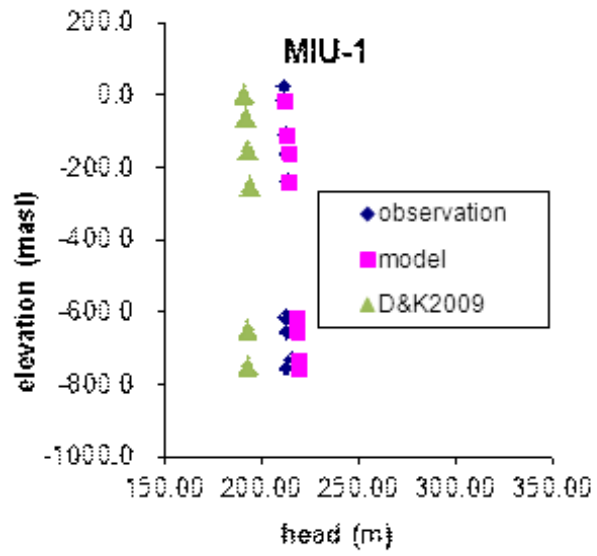
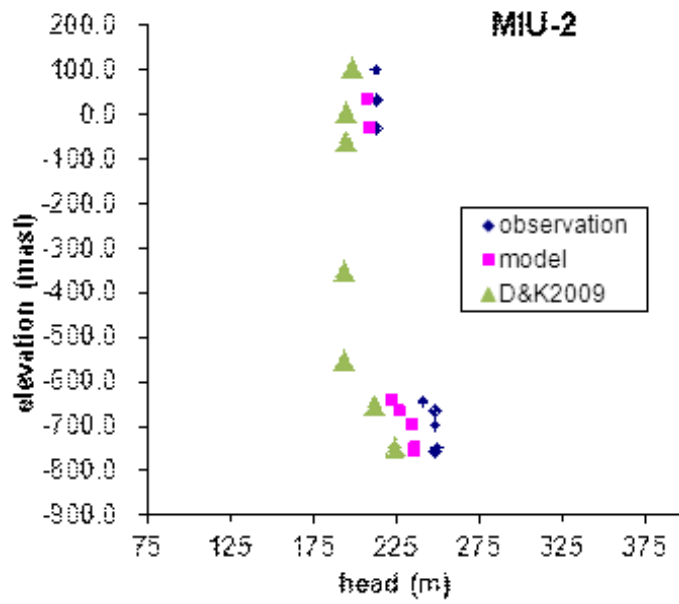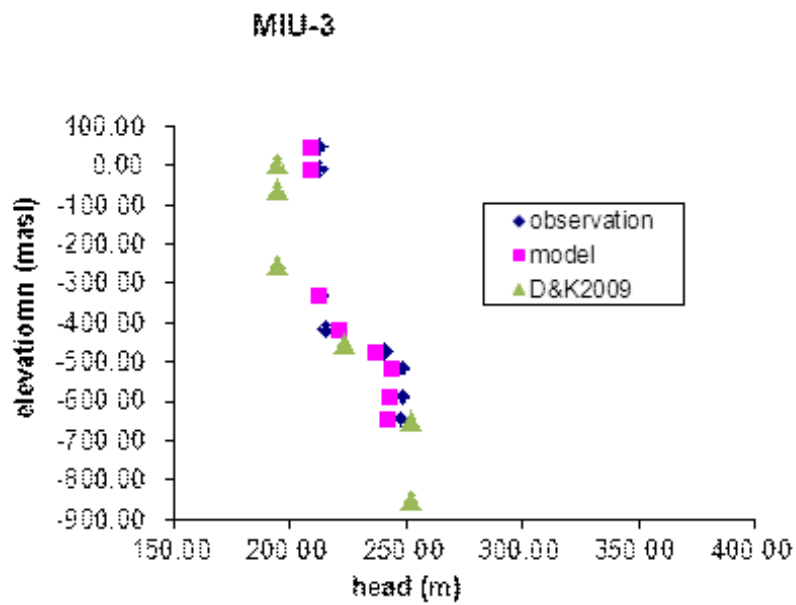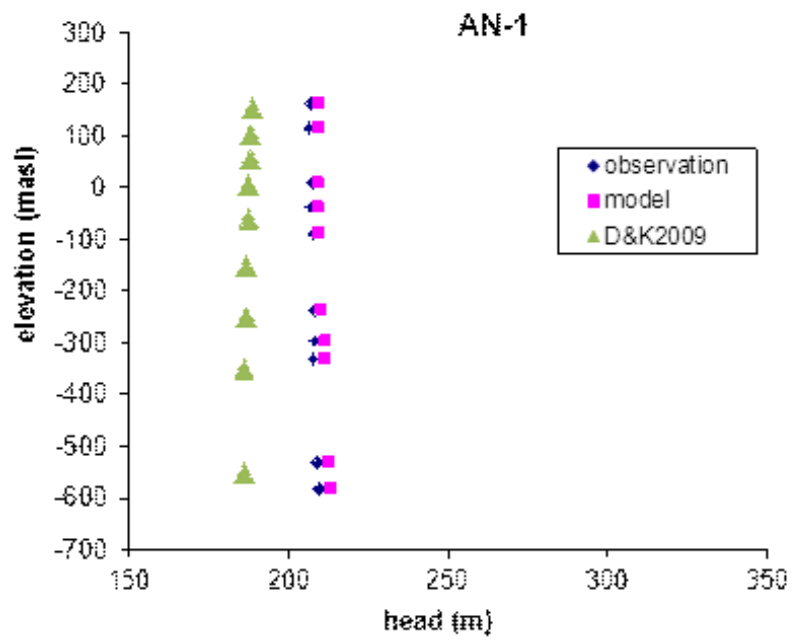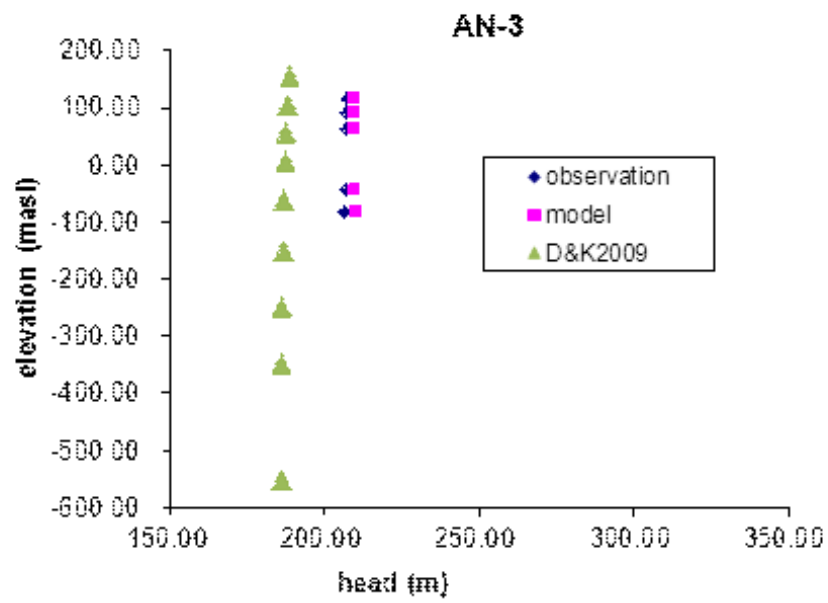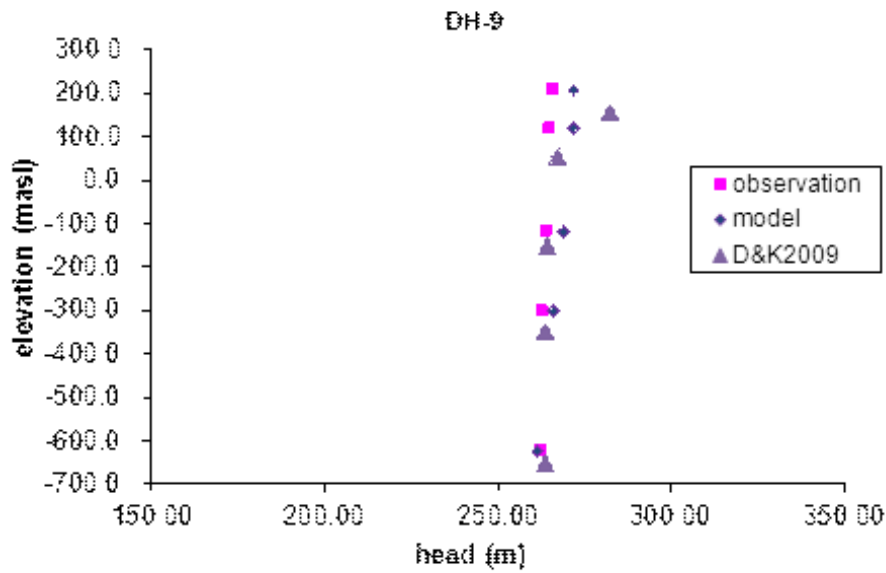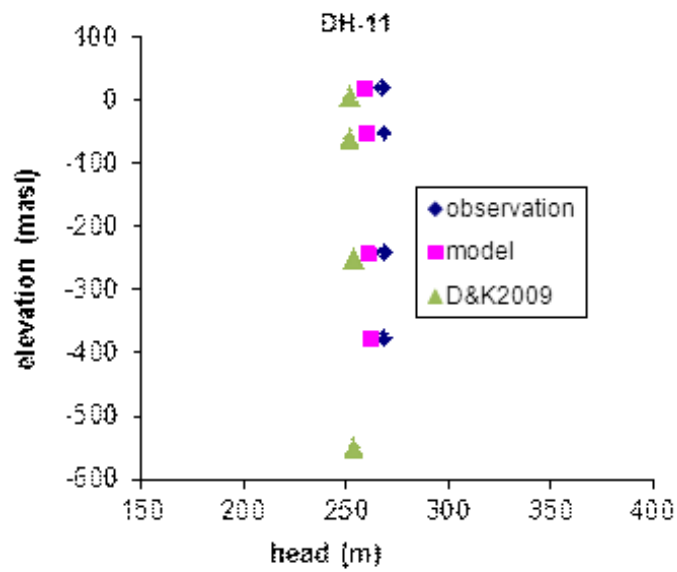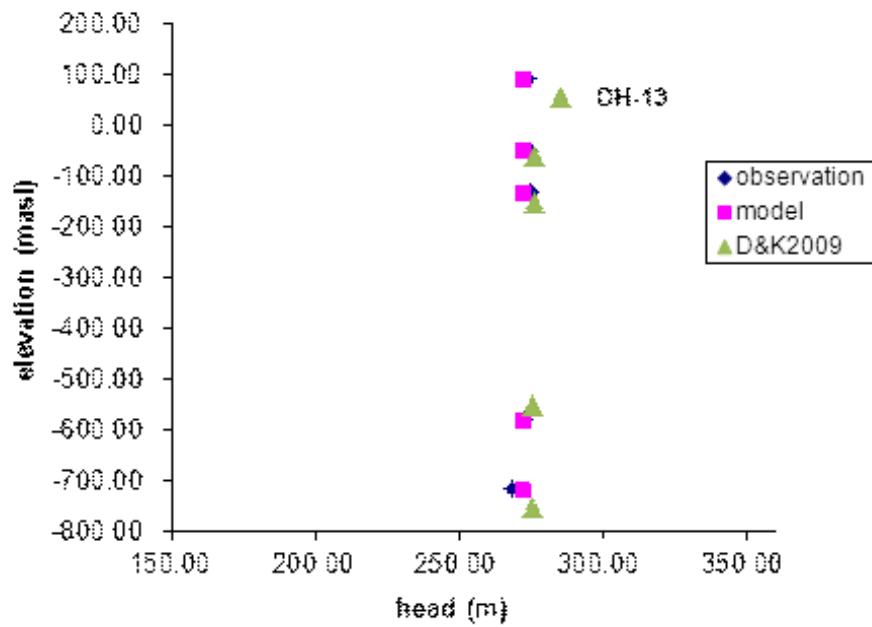Fig. 6.38. Steady-state head profiles observed and modelled in DH-13
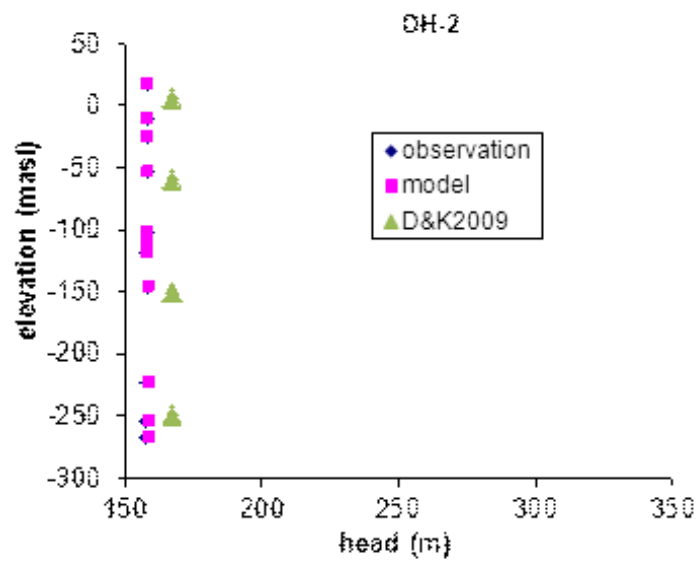
Fig. 6.39. Steady-state head profiles observed and modelled in DH-2
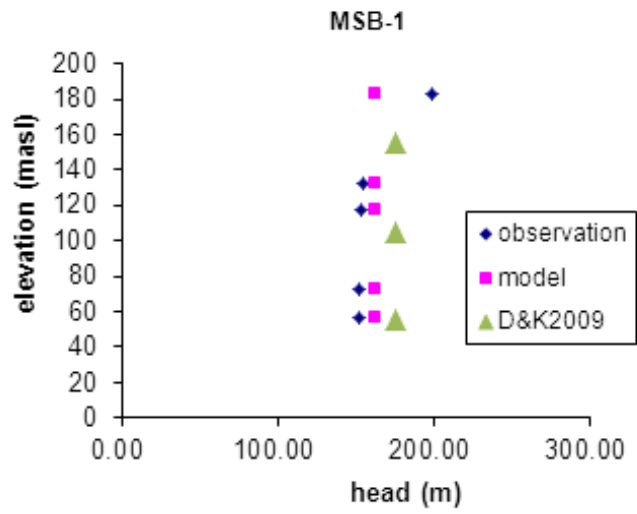
Fig. 6.40. Steady-state head profiles observed and modelled in MSB-1
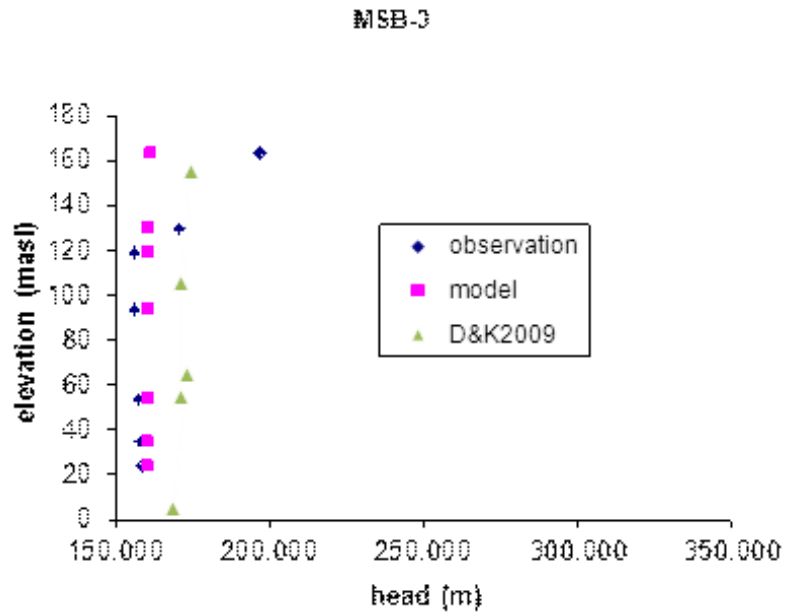
Fig. 6.41. Steady-state head profiles observed and modelled in MSB-3

Chapter 7
Transient Analysis

Hydraulic head was monitored at the Tono site at multiple depths in nine wells while two shafts (the main shaft and ventilation shaft) were excavated from the surface to $200m$ depth. The monitoring of the heads at the nine wells was specifically aimed at providing estimates for fracture properties such as the intrinsic permeability and porosity of the formation being characterized. In this study, the head responses at these wells were analysed to produce an effective porosity of the granitic rock. In general, for fractured formations with low matrix permeability, the parameter estimates determined using pressure response data are reasonable estimates for fracture properties, assuming the matrix is at a high liquid saturation and the fractures are predominantly water filled.

7.1 Transient Response to Excavation

In this study, pressure response transients were analysed to produce the effective porosity of the granitic rock. The numerical flow and transport simulator Feflow (Diersch, 2005a) was used, along with the inversion and statistical analysis code PEST (Doherty et al., 1994). The results of the steady-state (natural-state) simulation were used as the initial conditions to the transient simulation of the transient response to excavation, which uses the ECM, and assumes that the fractures and matrix are in equilibrium.

The transient responses to excavation were modelled using Feflow. In order to model the increasing depth of the shafts, time-varying material properties were used. A fully dis-

cretized well approach was used, and the pumping shafts were implemented as second-kind flow boundary conditions (BC). Next, a very high hydraulic conductivity and a porosity of 1.0 were assigned to those elements that are parts of the shaft to ensure free flow within the shaft. To simulate the shaft that moves deeper during the simulation, the so-called T-lists in Feflow Classic were used to ensure that elements that are located below the bottom of the shaft when the simulation starts, but which will be part of the shaft at a later time during the simulation, will have a high conductivity and a porosity of 1.0 once the shaft is extended and they belong to the shaft.

As mentioned above, second-kind BCs were applied for the shaft. In this case, care was taken to make sure that the abstraction was placed at the exact depth as needed, and therefore a slice was placed at the exact location. The set-up looks as follows: boundary conditions were assigned on all slices that represent the bottom of the shaft at a certain time during the simulation. For each 'bottom', separate time series needed to be applied. The time series was set up so that the BCs are inactive (0 m/d) when they do not represent the bottom, and so that they are active with the correct flux when they represent the bottom of the shaft.

Results were compared to the actual responses observed in the field and are shown in Fig. 7.42 to Fig.7.50. In general, all wells show some agreement between observed and modelled responses. The differences are mainly due to the fact we did not have very accurate pumping rate data. In the model we used average values for the pumping rate, whereas it can be seen from the observation data that the pumping rate was not constant and there were times when the water levels recovered.
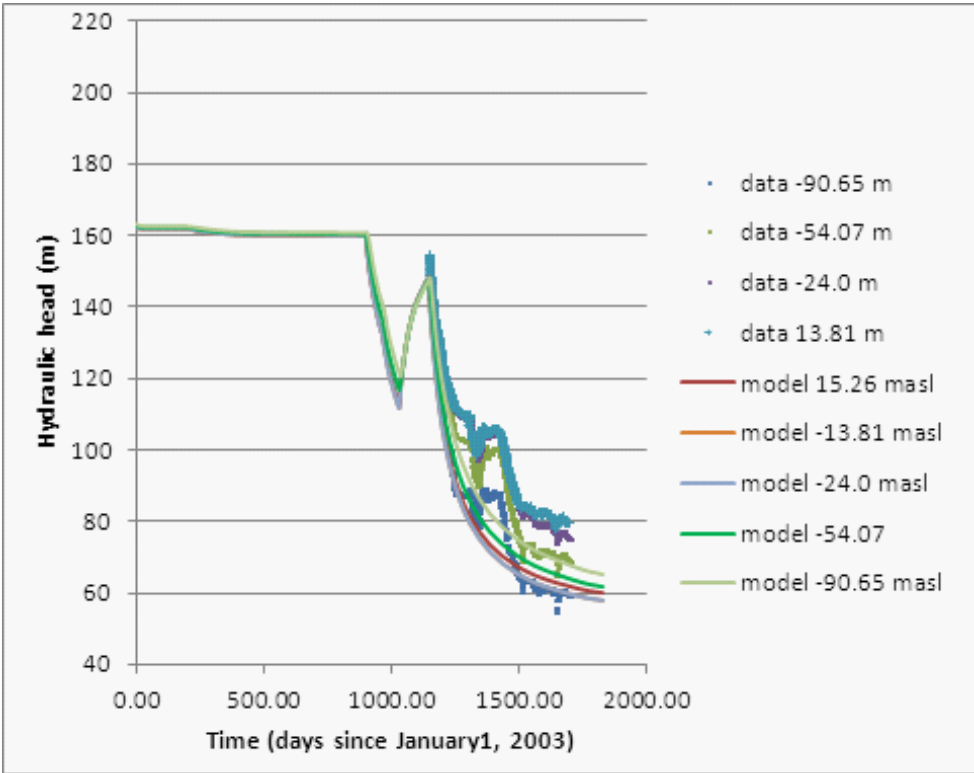
Fig. 7.42. Transient responses to excavation in borehole 05ME06
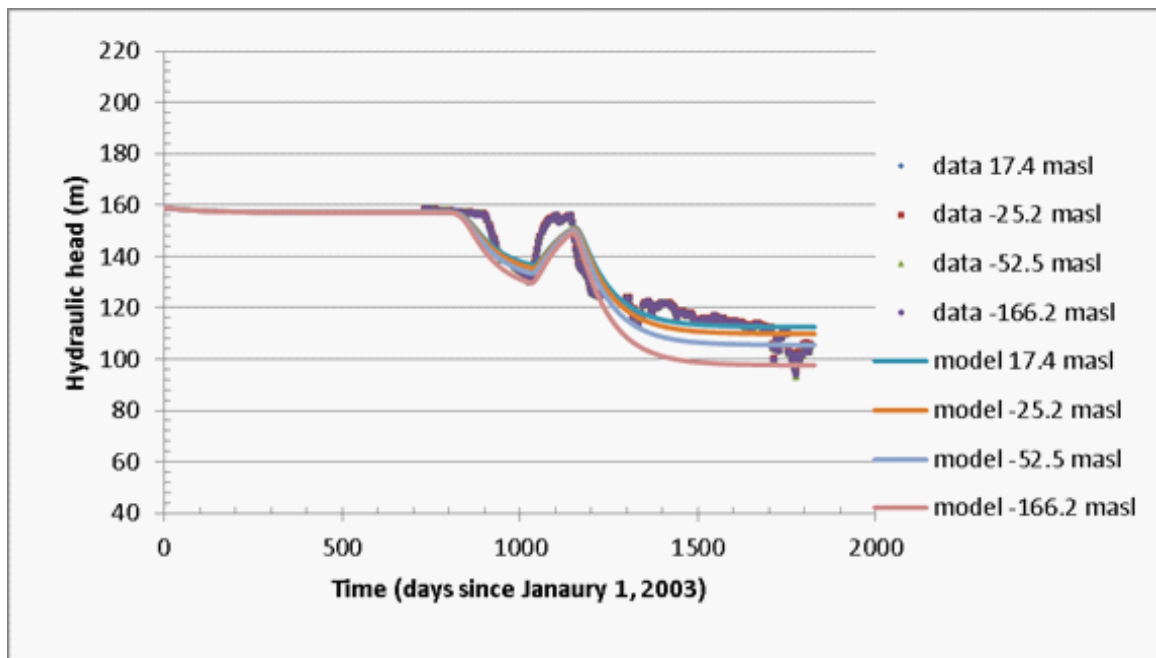
Fig. 7.43. Transient responses to excavation in borehole DH-2
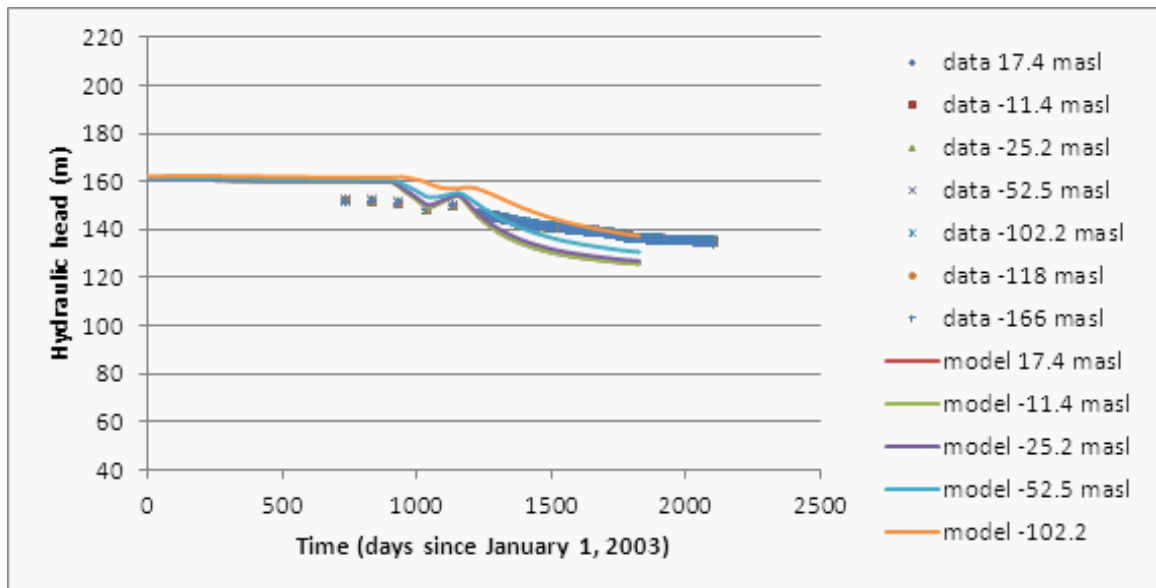
Fig. 7.44. Transient responses to excavation in borehole DH-15
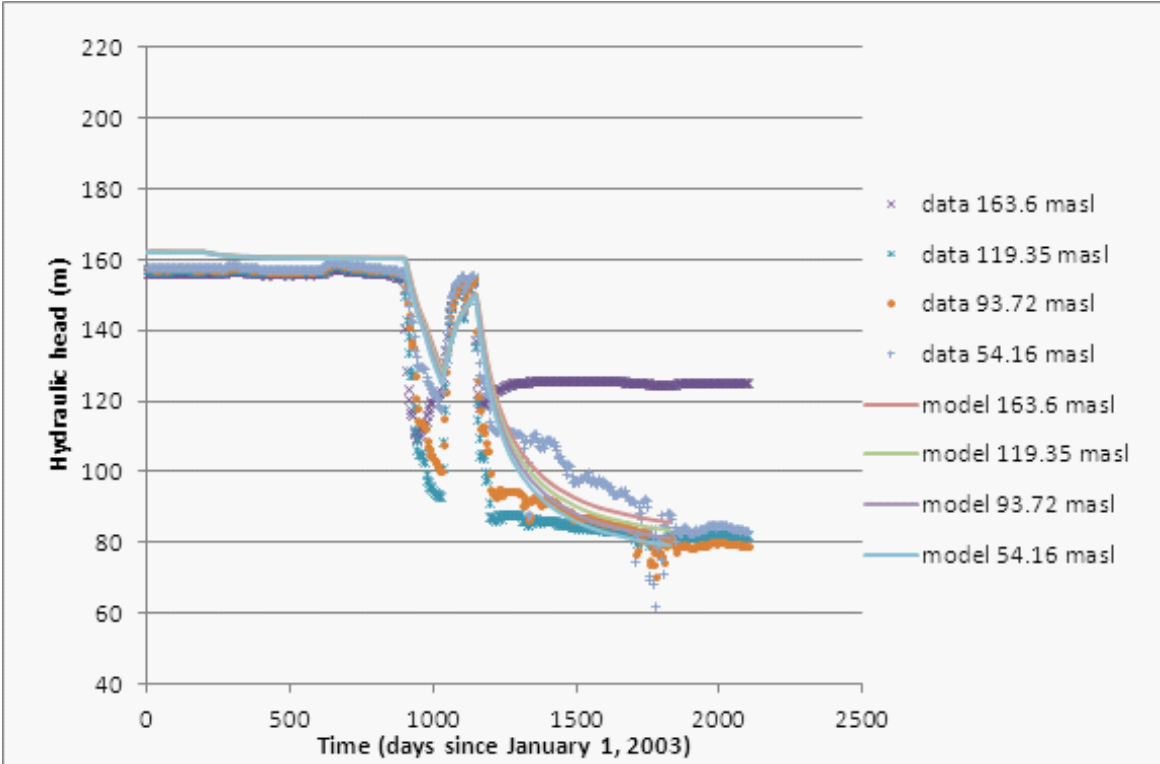
Fig. 7.45. Transient responses to shaft excavation in borehole MSB-3
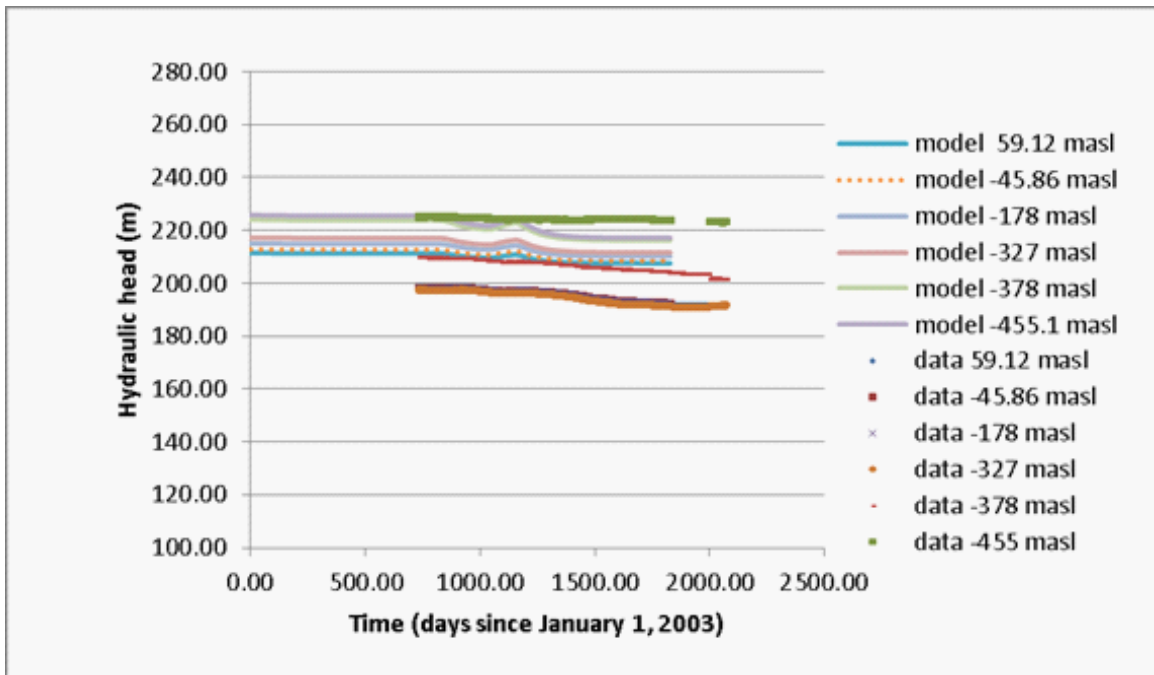
Fig. 7.46. Transient responses to shaft excavation in borehole MIU-4
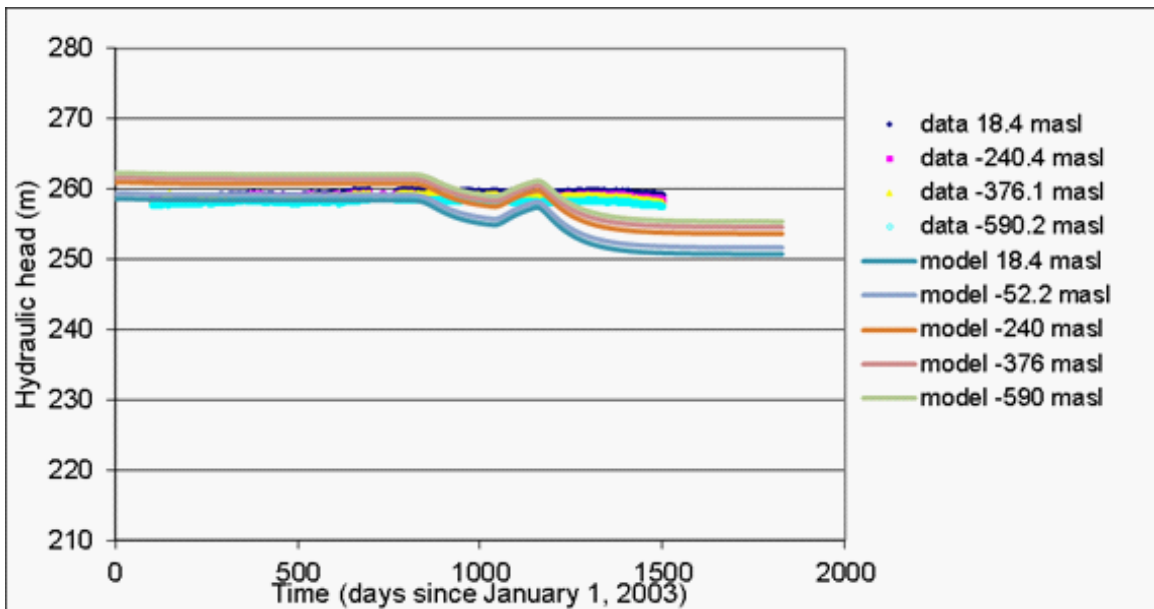
Fig. 7.47. Transient responses to shaft excavation in borehole DH-11
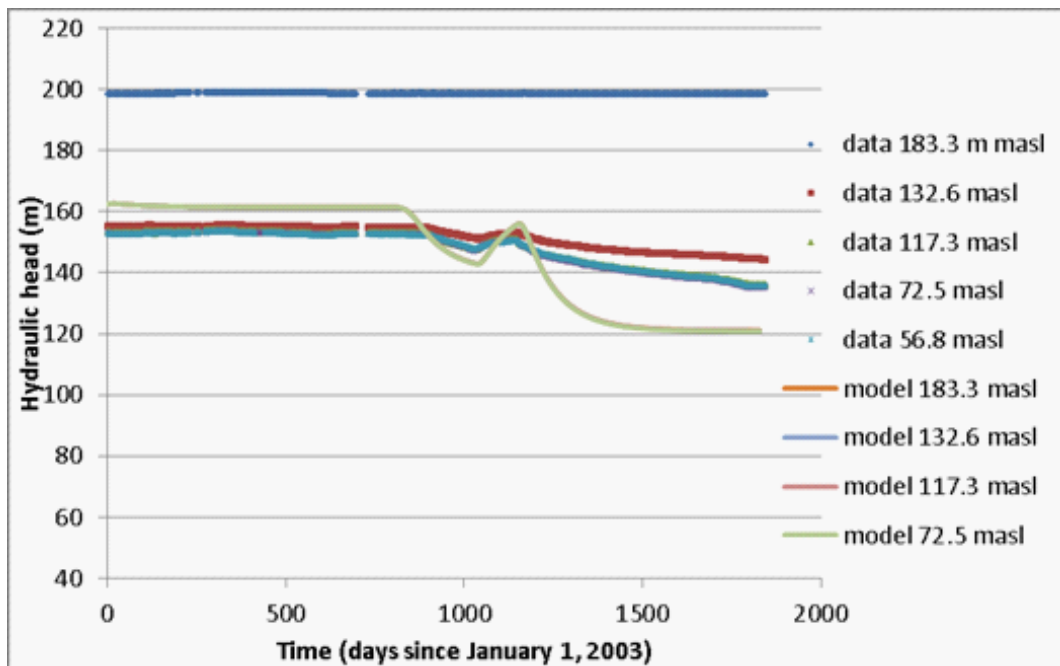
Fig. 7.48. Transient responses to shaft excavation in borehole MSB-1
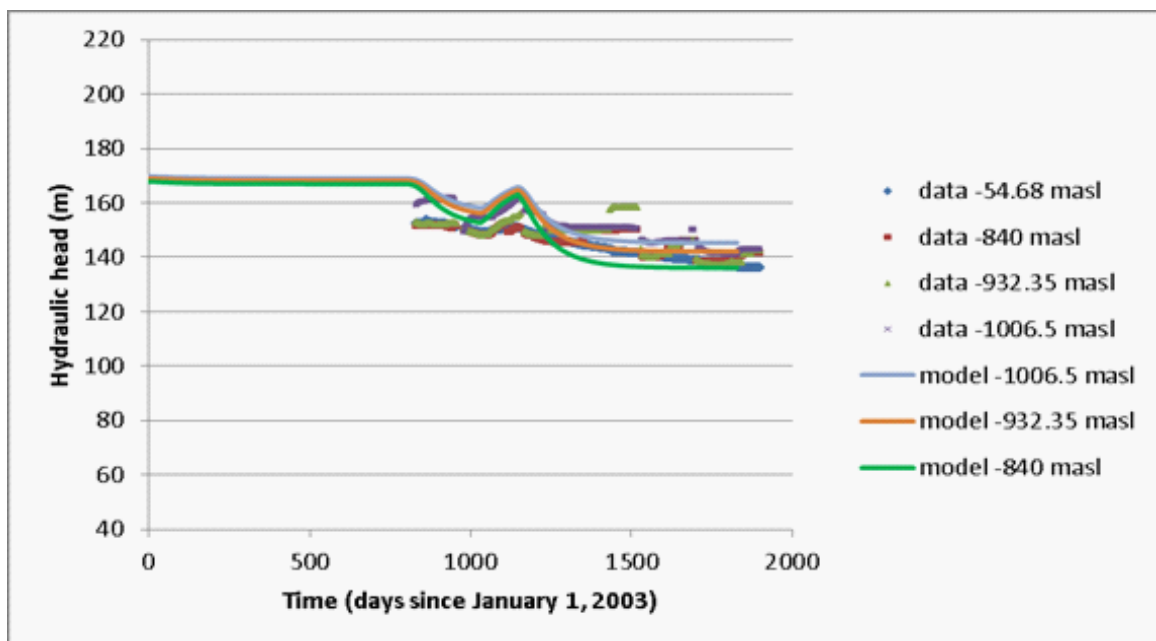
Fig. 7.49. Transient responses to shaft excavation in borehole MIZ-1
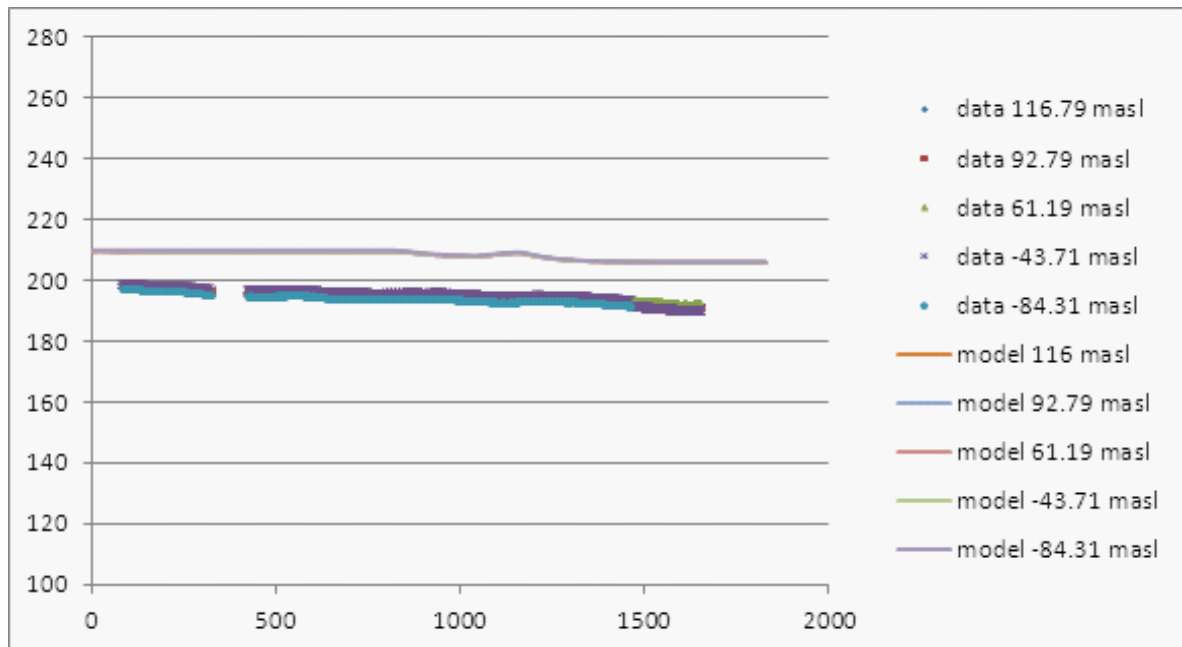
Fig. 7.50. Transient response to shaft excavation in borehole AN-3

One interesting feature of the observation data is that the responses in boreholes closer to a fault (DH-2 and DH-15) are vertically invariant. Our hypothesis is that those boreholes are located in the damage zone of the fault, with high permeability vertical fractures. Interpretations of the responses in these boreholes suggest that the head is approximately equal to the land surface in the damage zone. This has already been demonstrated in the steady-state analysis in the previous chapter. This hydrostatic condition does not suggest that water is not flowing; rather, it suggests that flow is topographically controlled with the head closely coupled to the land surface. The potentiometric surface in the damage zone of the Tsukiyoshi fault suggests the vertical permeability of the vertical fractures is relatively higher than one would expect from matrix permeability alone. Therefore, the

vertical fractures seem to be equilibrating heads between otherwise unconnected upper sedimentary layers and granite.

Another notable feature shown in these plots (DH-2 and DH-15) is that the model's responses tend to differ more at different depths than do the field data. For example, in well DH-2 only the shallowest sensor shows no response, whereas the model predicts a very limited response in all sensors in the sediments, and a relatively high response in the granite. In MIZ-1, the model shows a big response in weathered granite, but very little response in deeper granite, whereas all sensors actually respond similarly.

7.2   Parameter Estimation

The numerical inversion simulator PEST (Doherty et al., 1994) is used to estimate the effective porosity (although PEST estimates the specific storage from which the effective porosity is calculated) of the granite by matching pressure response to measured pressure recovery transient curves. PEST estimates elements of a parameter vector, $\mathbf{p}$, based on observations summarized in vector $\mathbf{z}^*$, by minimizing an objective function $\mathbf{S}$, which is a function of the residual vector $\mathbf{r}$. For example, in the inversion presented herein, the elements of $\mathbf{p}$ are the storage coefficients. Vector $\mathbf{z}$ contains the pressure at discrete points in time, where the measured quantities are indicated by, $\mathbf{z}^*$ and the simulated results are represented by $\mathbf{z}$. The residual vector $\mathbf{r}$ contains the measured and calculated system response; the latter is a function of parameter vector $\mathbf{p}$. The objective function, $\mathbf{S}$, is a weighted least-squares measure of the misfit between the data and the model calculation. Minimization of the of the objective function, $\mathbf{S}$, is based on local linearization of the model output by

calculating partial derivatives of the system response with respect to the parameters. The
Levenberg-Marquart modification of the Gauss-Newton algorithm is used to iteratively up-
date the parameter vector. Details of the inverse modeling theory as implemented in PEST,
the objective functions, minimization algorithms, residual and error analysis and extensive
references are given by Doherty et al. (1994).

The response of water levels in wells that penetrate confined aquifers to earth tides
and fluctuations in atmospheric pressure has been known, recorded and studied by several
researchers (Bredehoeft, 1967, Bordvarsson, 1970, Narasimhan et al., 1984; Van der Kamp
and Gale, 1983; Hsieh et al., 1988).

In modeling the transient flow in response to excavation it is necessary to assign
a specific storage Ss value to each element in the grid block. For fractured crystalline
granite, following Van der Kamp and Gale (1983) and assuming that the rock matrix is
incompressible, the specific storage S_s is defined as

$$S_s = \rho g \left(\phi \beta_w + \alpha \right) \tag{7.7}$$

where ϕ is the porosity, β_w is the compressibility of water ($4.5 \times 10^{-6} 1/kPa$) and
α is the compressibility of the rock. It should be noted that β_w and α are equivalent to
$\frac{1}{K_f}$ and $\frac{1}{K}$ in the notation of Van der Kamp and Gale (1983). A pair of equations showing
the interaction of stress σ and fluid pressure p in the presence of fluid flow was derived by
Rice and Cleary (1976) using the results of Biot (1941) and Nur and Byerlee (1971). They
are

$$K\nabla^2 p = S_s \frac{\partial}{\partial t}(p - \beta\sigma_t) \tag{7.8}$$

and

$$\nabla^2\sigma_t = \lambda\nabla^2 p \tag{7.9}$$

where λ is Lame's constant, K is the hydraulic conductivity, β is a parameter that defines the portion of the stress increment born by the fluid and σ_t is the mean normal stress. Equations (7.8) and (7.9) are the basic constitutive equations for the interaction of pore pressure and stress in a porous medium. No shear stress is included in Equations (7.8) and (7.9) because the assumption is made that shear stresses do not lead to any net dilation. Equation (7.8) defines the response of a porous medium to applied stresses. In 'undrained' conditions, that is, if there is no flow of water induced by stress changes (except between neighboring pores), then $\nabla^2 p = 0$ and $p = \beta\sigma_t$. Thus the pore pressure transients in the undrained case give a direct measure of changes in the mean normal stress. These results suggest that under appropriate conditions boreholes can be used as stress meters.

Van der Kemp and Gale (1983) did a comprehensive analysis of stress changes applied over a large area—those due to earth tides and to barometric pressure changes. In this thesis, long-term pressure responses observed in various boreholes after excavation of a 7 m diameter shaft are used to estimate the effective porosity of the fractured granite.

Analysis of a previous well test conducted at the MIU site found $S_s = 10^{-7}\ 1/m$ (Takeuchi et al., 2001) for granitic rocks. For a typical granite porosity value of 4.0×10^{-4}, assuming $S_s = 10^{-7} m^{-1}$ in Equation (7.9) yields $\alpha = 9.8 \times 10^{-8} m^{-1}$. This value of α is much bigger than $\phi\beta_w$, implying that well-test analysis would be unlikely to provide much

information on ϕ itself, and the values of S_s in Table 2.2 support this. The values in Table 2.2 are too small, smaller than for a solid hard rock or water. Limitations of the ability of the shot pump test to provide reliable values of S_s have been documented previously (Karasaki, 1987) and this analysis supports this. However, it may still be useful to compare general features of the slug-tests S_s values in Table 2 with theoretical values based on Equation (7.9), to investigate the interplay of water (β_w) and rock (α) compressibilities.

In general, if Equation (7.7) under-predicts field values of S_s, one could increase either ϕ or α. For the granitic rocks it has been found that, to achieve $S_s = 10^{-7}m^{-1}$, the value of should be $\alpha = 9.8 \times 10^{-8}m^{-1}$, along with the typical value for $\phi = 4.0 \times 10^{-4}$ for granite. Formally, ϕ could simply be increased from 4.0×10^{-4} to 0.022, while assuming α to be negligible. However, this approach would not be physically motivated. Because ϕ cannot be greater than one, in order to increase S_s significantly, α must be non-zero.

Here we propose a new constitutive equation that relates the fracture porosity to storage capacity of a large volume of fractured rock. The following assumptions are made:

1.   The rock matrix of granite is essentially incompressible.

2.   The storage comes from fractures.

3.   The amount of water that comes out of storage is proportional to the number of fractures, that is, porosity and inversely proportional to the fracture stiffness.

4.   Fracture stiffness is uniform the given rock type (granite) and is much smaller than that of the rock matrix.

A 'normalized' rock compressibility

$$\alpha' = \alpha/\phi \tag{7.10}$$

that does not vary much between rock types is assumed. For a rock that is regularly

crossed by a single set of fracture joints, Goodman (1989) has shown that is possible to

calculate elastic constants for an equivalent continuous material representative of the rock

mass. If the normal stiffness of the rock is k_n and the fractures are assumed to be regularly

spaced by a distance S, Goodman (1989) has shown that

$$\frac{1}{E_n} = \frac{1}{E} + \frac{1}{k_n S} \tag{7.11}$$

where E_n is the modulus of elasticity of the equivalent continuous material and E

is the modulus of elasticity of the intact rock. For granitic rock that is densely fractured

in several directions, Equation (7.11) can be used to a 'reduced modulus' representing the

fractured rock mass. If we assume that the granitic rock is highly fractured such as those

found at Tono site, then the fracture spacing S is very small and Equation (7.11) can be

approximated by:

$$\alpha = \frac{1}{E_n} = \frac{1}{k_n} \tag{7.12}$$

In their technical note, Zangerl et al. (2008) list the fracture stiffness values of

granitic rock obtained from analysis of published laboratory and in-situ tests. Table 1 of

their paper lists what they term the stiffness characteristic $\left(\frac{dk_n}{d\sigma'_n}\right)$, where

$$k_n = \left(\frac{dk_n}{d\sigma'_n} \right) d\sigma'_n \tag{7.13}$$

and σ'_n is the normal stress. Using Equation (7.13), the normal stiffness of the fracture k_n at any effective normal stress level σ'_n was calculated and α obtained from it using Equation (7.12).

For simulations of the responses to shaft excavation and using Equation (7.9), Equation (7.7) is re-written as

$$S_s = \phi\beta_w + \alpha = \phi \left(\beta_w + \alpha' \right) \tag{7.14}$$

In this study inversion calculations using PEST were carried out in order to estimate the large-scale effective porosity ϕ and from it derive the 'normalized' rock compressibility α' of the granite based on the long-term pressure responses.

Specific storage is defined as the volume of water produced when pressure is changed (reduced) by a unit over a unit volume of rock, which includes fracture and matrix. For fractured granite, water should come from the deforming fracture than from the matrix itself. Fracture stiffness should be much smaller than that of the matrix. Thus, the amount of water expelled from fractured granite should be proportional to the fractional volume of fractures in the unit volume of rock. Granted, the unit in this case is very large, thus requiring a large-scale pump test. Testing on a core is not relevant and would not work.

As mentioned in Section 5.2, the study area was modelled as a confined formation. The approach proposed in this thesis is based on the actual field data collected when a large volume of fractured rock mass was directly stressed by a massive, long-term pump test, as

Table 7.6. Calculated values of specific storage obtained using the data from Zangerl et al. (2008) and the porosity obtained from inversion calculations

Rock type, fracture type	Fracture dimensions	$\sigma'_{n,\max}$ (MPa)	α_n (1/Pa)	$\alpha' = \alpha/\phi$ (1/Pa)	S_s (1/m)
Charcoal granite, artificial fracture	11.2x24.8 cm	7.0	6.8E-6	1.91E-4	6.80E-6
Carnmenellis, clean natural fracture	5.1x10.2 cm	4.0	8.93E-6	2.51E-4	8.93E-6
Charcoal black granite, clean natural fracture	10 cm diameter	30.0	4.12E-7	1.16E-5	4.12E-7
Charcoal black granite, clean natural fracture	15 cm diameter	30.0	4.44E-7	1.25E-5	4.45E-7
Charcoal black granite, clean natural fracture	19.3 cm diameter	30.0	6.29E-7	1.77E-5	6.29E-7
Charcoal black granite, clean natural fracture	29.4 cm diameter	24.0	9.06E-7	2.54E-5	9.06E-7
Granodiorite, natural fracture coated with iron-oxide and pyrite	28.2x25.4 cm	20.0	2.27E-6	6.38E-5	2.27E-6
Pinawa granite, natural fracture	15.9 cm diameter	30.0	5.85E-7	1.64E-5	5.85E-7
Stripa granite, natural fracture	15.4 cm diameter	20.0	1.79E-6	5.02E-5	1.79E-6

described in Chapter 5. The pressure responses throughout the site reflect the permeability and storage capacity of a large volume of the fractured rock. An inversion calculation using Feflow/PEST was carried out in order to estimate the large-scale effective porosity, ϕ, of the granite, based on the long-term pressure responses to shaft excavation monitored at several boreholes in the study area. The inversions calculations gave a result of $\phi = 3.56 \times 10^{-2}$ for the large-scale granite in the study area. Using Equation (7.14), this value of ϕ and selected values of $\alpha_n = \frac{1}{k_n}$ for different types of granite from Zangerl, et al., (2008), the calculated S_s values are shown in Table 7.6. These values of S_s are much higher than those found from core testing (which gives just the matrix porosity) (Takeuchi et al., 2001), demonstrating the importance of the scale of the pumping test.

Table 7.7 summarizes the key elements of the models developed by five research groups that participated in the original JAEA project (Sawada et al., 2001). Two major features distinguish the models: how the fracture-network porosity was chosen, and how permeable the Tsukiyoshi fault is.

Table 7.7. Key features of different research groups' models (Sawada et al., 2001)

Organization (model name)	Model type	Hydraulic conductivity (m/s)	Fracture porosity	Tsukiyoshi fault	Travel time (years)
Ndiweni thesis (Felow +PEST)	Effective continuum with a few faults modelled explicitly	From well tests assigned stochastically, Avg =1e-7	From numerical inversion based on long-term pressure responses, ϕ=3.56E-2	Moderate barrier	5–1500
Lawrence Berkeley National Lab TOUGH2	Effective continuum with a few faults modelled explicitly	From well tests assigned stochastically, Avg =1E-7	From fracture density and conductivity 2E-6-3E-3 Avg=4E-4	Moderate barrier	1–25
Taisei Corporation (EQUI_FLOW)	Effective continuum based on fracture network	From zones virtual well-test analysis, assigned stochastically Avg =5E-8	From fracture density and transmissivity Avg =1E-4	Complete barrier	0.25–66
Saitama University (Don-Chan)	Channel network (faults as anisotropic porous media)	3E-8	Assumed, 0.01 0.01	Moderate or complete barrier	300–40000
Sandia National Laboratories (POR_SALSA)	Effective continuum with few faults modelled explicitly	From well tests, constant by zone, 5E-9 - 5E-6 mostly 5E-8	Assumed 0.005 – 0.1, mostly 0.01	Moderate barrier	150–2500

Porosity is either calculated from fracture density and hydraulic conductivity values (Berkeley Lab, Taisei; values range from 10^{-6} to 10^{-3}) or is chosen from generic values for typical rock materials (Sandia Lab and Saitama University; values range from 0.01 to 0.1). The porosity value determined in this thesis is 3.56×10^{-2} and lies within the porosity ranges used by the different groups. It should be noted that it is the only porosity value that is based on large-scale observation data, that is, transient pressure responses to shaft excavation. Other groups just used generic data for solid granite or simply made up the porosity values, or used porosity values sampled down the well. The primary effect of

porosity is on the travel time through the model, with travel time roughly proportional to porosity.

Chapter 8
Impact of the Tsukiyoshi Fault on Transport

The transport of energy (heat transport) and dissolved substances in groundwater is influenced by various processes. These can include advection, diffusion-dispersion, and sorption, but also chemical and biological degradation. Hydrodynamic dispersion encompasses the physical phenomena of diffusion and hydrodynamic dispersion. Furthermore, dissolved substances are influenced by sorption, chemical and biological degradation. Transport and storage of an ideal tracer (without any sorption, nor chemical, nor biological degradation) only occurs in fractures while storage occurs mainly in the rock matrix. The transient transport mass balance equation in a saturated aquifer for a contaminant at any point within the aquifer is given by

$$\frac{\partial c}{\partial t} + \nabla.(c\mathbf{V} - \mathbf{D}\nabla c) = R + Q(c^* - c) \tag{8.15}$$

where

$$\mathbf{D} = \alpha_{ij}\mathbf{V} + D \tag{8.16}$$

and c is the contaminant concentration, c^* is the contaminant concentration at source, $\mathbf{V}$ is the fluid velocity, α_{ij} is the dynamic dispersivity, D is the effective molecular diffusion coefficient and R represents all non-conservative transport processes such as sorption, chemical and biological degradation. In Equation 8.15, an assumption is made that the concentration of the contaminant is rather, so that the fluid's density remains unaffected by changes in c.

Table 8.8. Parameters used in the transport calculations

Effective porosity	3.56×10^{-2}
Molecular diffusion coeffient	$1.21 \times 10^{-9}\ m^2 s^{-1}$
Transverse dispersivity	$0.001\ m$
Longitudinal dispersivity	$0.01\ m$
Fracture pore velocity	$0.5\ md^{-1}$

In order to analyse the impact of the Tsukiyoshi fault on the transport of contaminants in the basin, fictitious particles are released in the study area. The porosity obtained from inversion calculations using observed pressure response data was used in the transport calculations. It must be note that there are no contaminants in the Tono basin, but in order to demonstrate the effect of the fault on possible contaminants fictitious particles were released in the study area. First, the particle tracking was used to investigate the effects of the fault on pathlines. Only advective and diffusion transport of the particles was considered. The properties used in the analysis are listeed in Table 8.8. The input data of Table 8.8 are taken from thosed used by Wu and Pruess (2000) while the effective porosity and fracture pore velocity were determined in the flow calculations in this thesis. The results are shown in Fig. 8.51.

Particles are released from the area marked yellow in Fig. 8.51, and move in a horizontal direction until they reach the Tsukiyoshi fault, where the horizontal trend is interrupted and the fluid is sent toward the surface. The particles then cross over the fault in the weathered granite, which has a higher permeability than the fault core. It is noteworthy that the particles follow the high-permeability damage zone as they move toward the surface. This a clear demonstration of the fault acting as a barrier to horizontal flow and transport as well as enhancing vertical flow and transport.
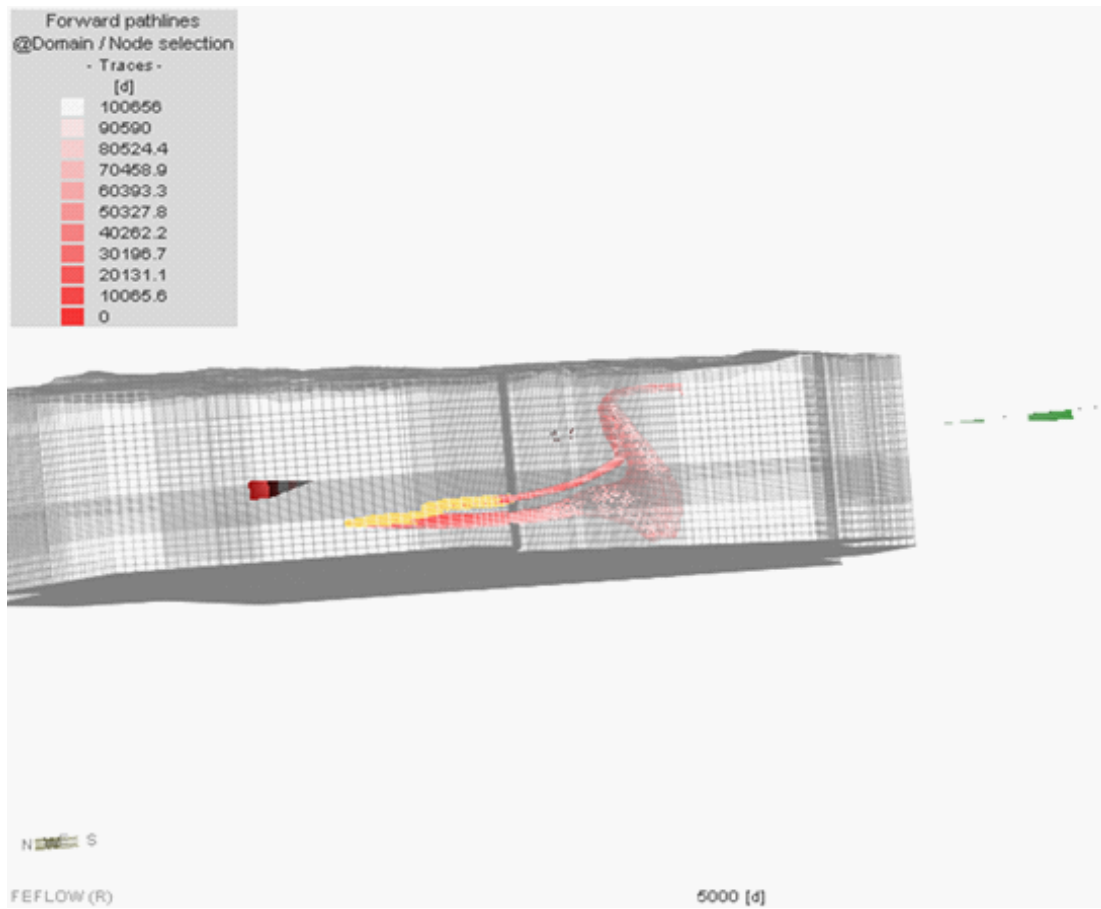
Fig. 8.51. Pathlines showing how the fault influences flow in the basin

The pathline-based evaluation does not take into account any mixing processes due to diffusion and mechanical dispersion. For this purpose, a full transport calculation was carried out. The results are shown in Fig. 8.52 and Fig. 8.53.

As can be seen in Fig. 8.52 and Fig. 8.53, the contaminant plume follows the direction shown in the pathlines of Fig. 8.51, where the high-permeability damage zone acts as a conduit for contaminants in the vertical direction. However, Fig. 8.53 shows that there is little or no contaminant plume within the low-permeability fault core, which further demonstrates that the fault core acts as barrier to lateral flow.

Fig. 8.53 also shows another interesting feature of the contaminant transport: on the northern side of the fault, the plume is transported from the release points in a horizontal direction. When the flow is interrupted by the Tsukiyoshi fault, the plume follows a downward direction along the vertical fractures in the damage zone. When it gets to the bottom boundary of the model (the no-flow boundary) it changes direction (just like the pathlines of Fig. 8.51) and is then transported towards the surface and only crosses over the fault in the weathered granite. This shows that most of the transport here is by advection, as it follows the direction of water flow. However, at the bottom of the model, where the water slows down as it changes direction, it is clear that there is some mixing and that contaminants are crossing over the fault at depth. This is explained by the fact that as the water slows down and changes direction, diffusion becomes the dominant mode of transport.
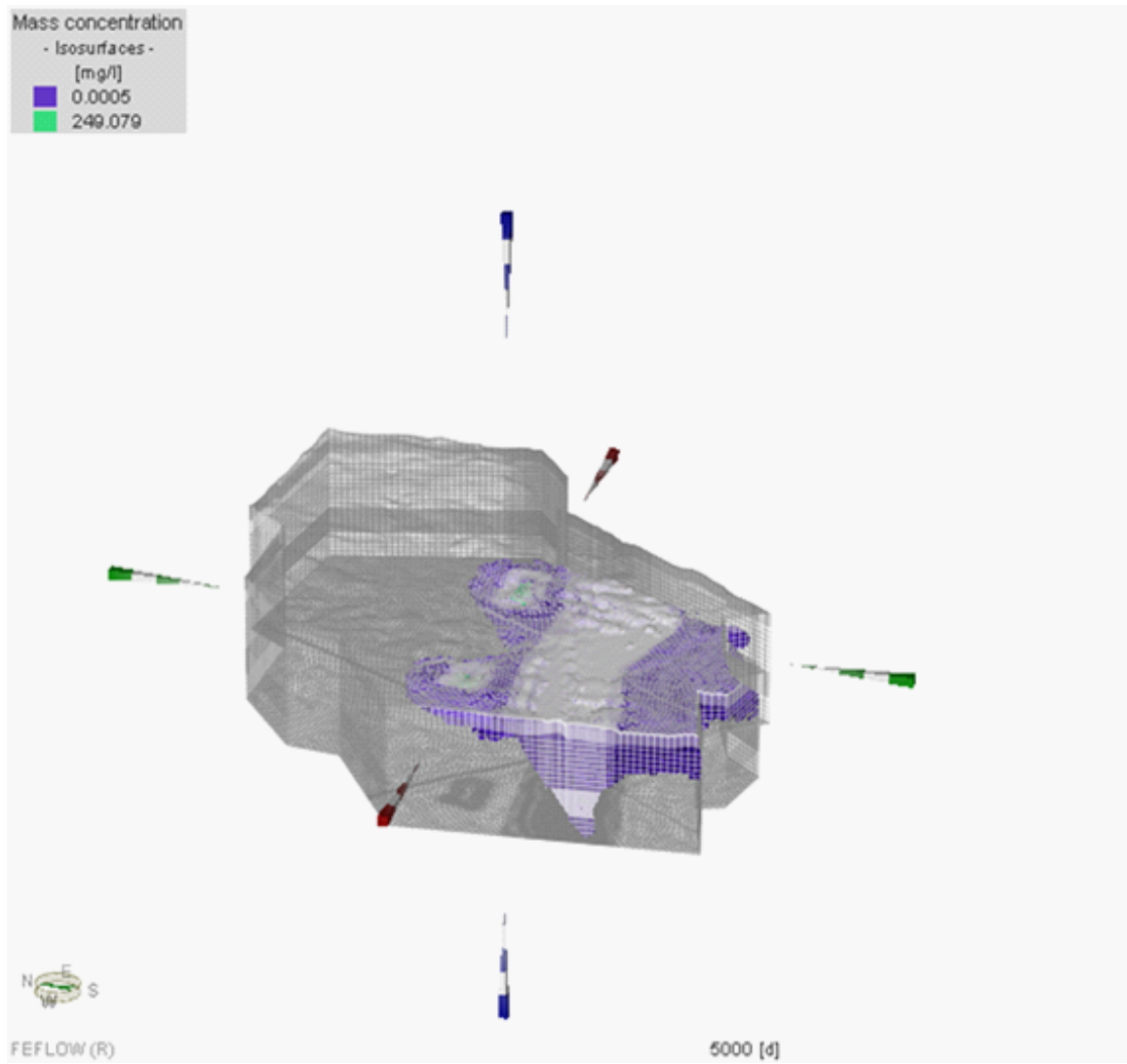
Fig. 8.52. Distribution of the contaminant plume released from the hypothetical contaminant sites (green), showing the effect of the Tsukiyoshi fault.
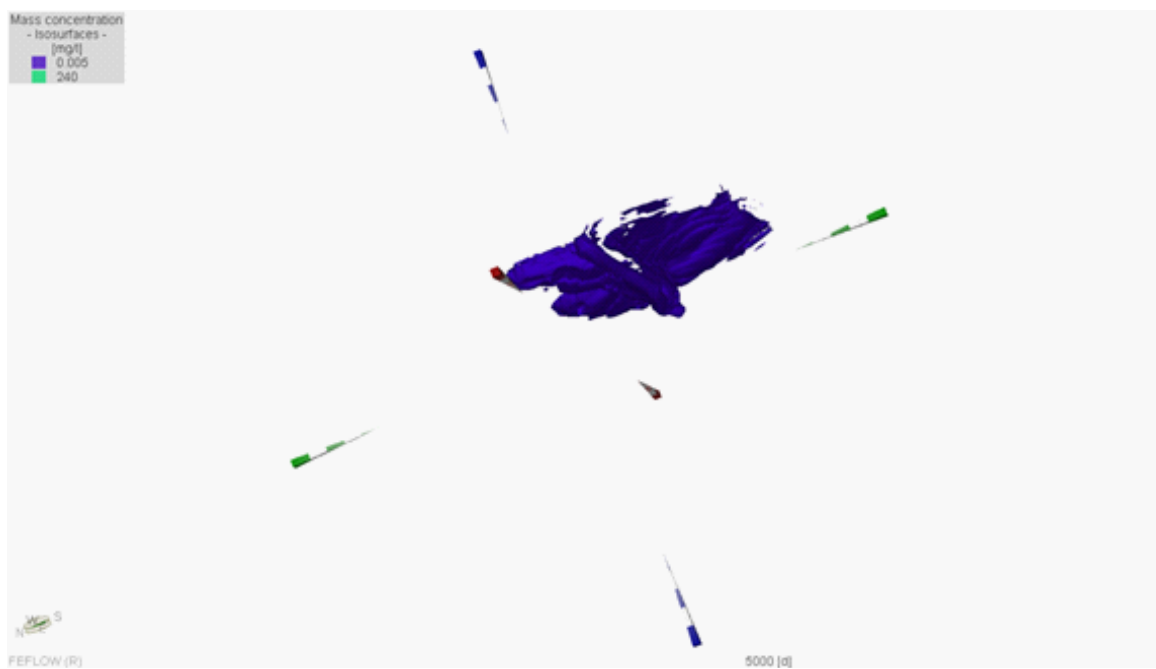
Fig. 8.53. Distribution of the contaminant plume released from the hypothetical contaminant sites (green in Figure 51), showing the effect of the Tsukiyoshi fault. Here the mesh has been removed to show detail in the fault zone.

Chapter 9
Conclusions

The impact of the Tsukiyoshi fault on groundwater movement in the Tono basin is clearly demonstrated in this study. Thus, in general, in order to improve the groundwater flow model, the exact relationship between tectonic structures (faults) and hydrogeology needed to be clarified. Using field data and numerical modelling, this thesis has evaluated the effects of vertical anisotropy on flow and transport in the Tono basin in a rigorous way by incorporating anisotropy into the model, and has explained the observations and numerical modelling results indicating a hydrostatic condition in a highly anisotropic fault.

Fracture data from the Mizunami Underground Rock Laboratory (URL) site have been examined and an attempt to find a direct correlation between geologic/geometric attributes of a fracture and associated permeability of the sectioned borehole intervals that contain the fractures is made. The results show clearly that there is no direct correlation between fracture density and permeability. Thus, the traditional approach of discrete fracture network modelling, where fractures are binned by dip and orientation into sets and the permeability assumed to be a function of fracture density, needs to be improved. The density of the fractures is not the main issue; their connection seems to be the main feature responsible for water conduction.

Steady-state numerical modelling results show head differences of approximately 40 m between the north and south of the fault. Boreholes that penetrate the fault also show higher heads at depth, indicating that the fault acts as a barrier to flow. Proximity to the

Tsukiyoshi fault is found to be a key attribute that determines the ability of a fracture to conduct water. We consider the pressure response to two shafts pumping in the upper parts of the fractured granitic formation near the fault. The response to pumping is monitored at two boreholes (DH-15 and DH-2) on the same side of the fault as the pumping shafts. The responses at the two boreholes are vertically invariant and highlight the effects of enhanced vertical permeability around the fault.

An important conclusion of this thesis is that the Tsukiyoshi fault in the Tono basin controls the hydrology. It acts as strong barrier to lateral groundwater flow while vertical flow is enhanced. The hydrogeological build-up of this fault is strongly anisotropic. At the location of this fault zone, normally unconnected aquifers are hydraulically coupled, making vertical interchange of groundwater between the upper sediments and the basement granitic rock possible. This sort of mechanism has been demonstrated here to have serious implications for the spread of contaminated groundwater, which may intrude into other aquifers through vertical flow along the fault. This has serious implications, in for example, deep geological storage of spent nuclear fuel or carbon sequestration.

Inversion calculations were carried out to estimate the large-scale hydraulic effective porosity of the granite based on the long-term observed pressure responses. Effective porosity $\phi = 3.56 \times 10^{-2}$ was obtained in these calculations based on real regional-scale observed pressure response data. This was found to be larger than the value obtained by Takeuchi *et al*. (2001) from short pump tests, and larger than the mean porosity value used by different groups (Sawada et al., 2001) which were obtained from porosities sampled along the well itself while other groups just used generic solid granite porosity values.

Porosity values obtained from testing on the core and sampling along a well only give the matrix porosity and therefore are not suitable for use at a regional scale in fractured formations. At a regional scale, the unit in this case is very large, thus requiring a large-scale pump test. The monitoring of transient pressure responses to shaft excavation was effectively large-scale, long-term pump testing. Thus the use of pressure response data to invert for porosity gives promising and reasonable results. Although heuristic, the above argument makes perfect sense. This concept is new and, ideally, should be developed in conjunction with laboratory experiments, though there is an insurmountable problem of scale. The problem of correctly estimating the fracture porosity at a large scale (kilometres) is well known. One approach is to scale up using the discrete fracture network concept. However, past efforts have failed miserably, as cited in this thesis. Conducting tracer tests in such a large scale is practically impossible, besides the geometry has to be known/assumed to interpret tracer tests to calculate porosity.

The approach used in this thesis is based on actual field data where a large volume of fractured rock mass was directly stressed by massive, long term "pump test." The pressure responses throughout the site reflect the permeability and storage capacity of a large volume of the fracture rock.

For the Tono basin, this study explored the hypothesis that the main fault provides the vertical conduits for flow and is at the same time a barrier to horizontal flow. The results show that this is plausible. However, the effects of smaller faults in the basin have not been assessed in detail. Smaller faults are frequent in the study area and therefore will probably have a strong cumulative effect on the aquifer structure and small-scale ground-

water systems. Observation wells are widely spaced to give sufficient information to make
a reconstruction of the flow pattern near these smaller faults. It is expected that the cumu-
lative effect of a set of these small faults that are induced by the regional stress field, should
result in a regional anisotropy of the permeability. Further thorough analysis of pumping
tests and the sinking of more observation networks should be carried out to reveal such
regional anisotropy. Hydraulic head patterns and their fluctuations over time should give
information on the underlying geological build-up of the basin and could reveal structures
that would otherwise be difficult to detect.

References

Adler, P.M., and J.-F. Thovert, *Fractures and Fracture Networks*, Kluwer Acad., Norwell, Mass., 1999.

Aifantis, E.C., On Barrenblatt's problem, *Int. J. Eng. Sci.*, 18, 857-867, 1980.

Andreoli, M. A. G., Raubenheimer, E., Meyer, W. C. M. and Dzanga, P. (2006) *Gearing for Geological Disposal of High-Level Radioactive Waste in South Africa: Current Status and Research Trends*. P. A. Witherspoon and G. S. Bodvarsson LBNL-59808.

Arbogast, T., J. Douglas, and U. Hornung, Derivation of the double-porosity model of a single phase flow via homogenisation theory, *SIAM J. Math. Anal.*, 21, 823-836.

Baker, W.J., 1955, Flow in fissured formations, Proc. Fourth World Petroleum Congress, Section II, 379-393.

Barenblatt, G.I. and Zheltov, Y.P., 1960, *On fundamental Equations of Flow of h\Homogeneous Liquids in Naturally Fractured Rocks*, Dokl. Akad. Nauk. USSR 132, No. 3, 545-548.

Barenblatt, G.I., Zheltov, Y.P., and Kochina, I.N., 1960, Basic concepts in the theory of seepage of homogeneous liquids in fractured rocks, *Prik. Matem, i Meckh*. 24, No. 5, 852-864.

Bear, J., *Modeling flow and contaminant transport in fractured rocks, in Flow and Contaminant Transport in Fractured Rock*, edited by J. Bear, C.-F. Tsang and G. de Marsily, pp 1-37, Academic, San Diego, California, 1993.

Bear, J., 1972, *Dynamics of Fluids in Porous Media*, Elsevier, New York, 1972.

Berkowitz, B., J. Bear, and C. Braester, Continuum models for contaminant transport in fractured porous formations, *Water Resources Research*, 24 No. 8, pp. 1224-1236, American Geophysical Union, Washington D.C. 1988.

Bixel, H.C., and Van Poolen, H.K., 1967, Pressure drawdown on buildup in the presence of radial discontinuities, *Soc. Pet. Eng. J.*, Sept., 301-309; *Trans. AIME* 240.

Bodvarsson, G., 1970, Confined fluids as strain meters, *J. Geophys. Res.*, 75, 2711-2718.

Bredehoeft, J.D., 1967, Response of well-aquifer systems to earth tides, *J. Geophys. Res.*, 72, 3075-3087.

Charlaix, E.A., A criterion for percolation threshold in a random array of plates, *Solid State Communications*, 50(11):999-1002, 1985.

Chen, Z.-X., 1989, Transient flow of slightly compressible fluids through double porosity, double-permeability systems - A state of the art review, *Transport in Porous Media* 4 (1989), 147-184.

Chen, Z.-X., 1990, Analytical solutions for double-porosity, double-permeability and layered systems, *Journal of Petroleum Science and Engineering* 5 (1990) 1-24.

Dershowitz, W.S., and C. Fidelibus, Derivation of equivalent pipe network analogues for three-dimensional discrete fracture networks by the boundary element method, *Water Resour, Res.*, 35, 2685-2691,1999.

Diersch, H.-J.G., 2005a, *Interactive, graphics-based finite element simulation system FE-FLOW for modeling groundwater flow, contaminant mass and heat transport processes.* Release 5.2, User's Manual, WASY Ltd., Berlin, 2005.

Diersch, H.-J.G., 2005b, *Interactive, graphics-based finite element simulation system FE-FLOW for modeling groundwater flow, contaminant mass and heat transport processes*. Release 5.2, Reference Manual, WASY Ltd., Berlin, 2005.

de Marsily, G., Flow and transport in fractured rocks: connectivity and scale effects, *Proc. Int. Assoc. of Hydrogeologists: Hydrogeology of rocks of low permeability*, Tucson, AZ., 17:267-277, 1985.

Doherty, J., Brebber, L., and Whyte, P., 1994, *PEST - model independent parameter estimation, User's Manual*, Watermark Computing, Corinda, Australia.

Doughty, C., and Karasaki, K., 1999, Using an effective continuum model for flow and transport in fractured rock: The H-12 flow comparison, *Rep. LBNL–44966*, Lawrence Berkeley National Lab., Berkeley.

Doughty, C., 1999, Investigation of conceptual and numerical approaches for evaluating moisture, gas, chemical and heat transport in fractured rock. *J. Contam. Hydrol.* 38, 69-106.

Doughty, C., and Karasaki, K, 2001, Evaluation of uncertainties due to hydrogeological modeling and groundwater flow analysis: Effective continuum model using TOUGH2, Lawrence Berkeley National Lab., Berkeley.

Doughty, C., and Karasaki, K, 2002, Evaluation of uncertainties due to hydrogeological modeling and groundwater flow analysis: steady state flow, transient flow and thermal analysis, *Rep. LBNL–51894*, Lawrence Berkeley National Lab., Berkeley.

Doughty, C. and K. Karasaki, 2003, Evaluation of uncertainties due to hydrogeological modeling and groundwater flow analysis: constraining the model with pressure data, *Project Report, March, 2003*.

Doughty, C., and Karasaki, K, 2005, Evaluation of uncertainties due to hydrogeological modeling and groundwater flow analysis: 9x9 km dual porosity model of the Tono site, Lawrence Berkeley National Lab., Berkeley.

Doughty, C. and K. Karasaki, 2009, Preliminary Results from 9x9 km TOUGH2 model of shaft excavation, *Project Report, November 18, 2008.*

Doughty, C. and K. Karasaki, 2010, Improvement of the Southern Portion of the 9kmx9km TOUGH2 model of the Tono region, *Project report, March 2010*.

Fara, H.D., and Scheidegger, A.E., 1961, Statistical geometry of porous media, *J. Geophys. Res.*, 66, 3279-3284.

Freeze, R.A., 1975, A stochastic-conceptual analysis of one-dimensional groundwater flow in non-uniform homogeneous media, *Water Resour. Res.*, 11(5), 725-741.

Goodman, R.E., *Introduction to Rock Mechanics*, Second Edition, John Wiley & Sons, 1989.

Hubbert, M.K., 1956, Darcy's law and the field equations of the flow of underground fluids, *Trans. Am. Inst. Min. Metall. Pet. Eng.* 207, 222-239.

Huitt, J.L., 1956, Fluid flow in simulated fractures, *J. Am. Inst, Chem. Eng*. 2 259-264.

Hsieh, P.A., Bredehoeft, J.D. and Rojstaczer, 1988, Response of well aquifer system to the earth tides: Problem revisited, *Water Resour. Res*., 24(3), 468-472.

IAEA (2007) *Factors Affecting Public and Political Acceptance for the Implementation of Geological Disposal TECDOC-1566*. International Atomic Energy Agency, Vienna, Austria.

Ijiri, Y., Saegusa, H., Sawada, A., Ono, M., Watanabe, K., Karasaki, K., Doughty, C., Shimo M., and Fumimura K., 2009, Evaluation of uncertainties from different modeling approaches applied to analyze regional groundwater flow in the Tono area of Japan, *Journal of Contaminant Hydrology* 103, 2009, 168-181.

Iwatsuki, T., Satake, H., Metcalfe, R., Yoshida, H., Hama, K., 2002, Isotopic and morphological features of fracture calcite from granitic rocks of the Tono area, Japan: a promising palaeohydrogeological tool, *Applied geochemistry* 17, 1241-1257.

Iwatsuki, T., Yoshida, H., 1999, Groundwater chemistry and fracture mineralogy in the basement granitic rock in the Tono uranium mine area, Gifu Prefecture, Japan – groundwater composition, Eh evolution analysis by fracture filling minerals, *Geochemical Journal* 33, 19-32.

Karasaki, K., *Well Test Analysis in Fractured Media*, PhD thesis, Department of Material Science and Mineral Engineering, University of Calif., Berkeley, *Rep. LBL-21442*, Lawrence Berkeley National Lab., Berkeley, Calif., 1987.

Karasaki, K., Onishi, C., Gasperikova, E., Goto, J., Tsuchi, H., Miwa, T., Ueta, K., Kiho, K., and Miyakawa, K., 2010, Development of characterization technology for fault zone hydrology, 13th International Conference on Environmental Remediation and Radioactive Waste Management, I*CEM10*, October 3-7, 2010, Tsukuba, Japan.

Karasaki, K., Long, J.S., and Witherspoon, P.A., 1988, A new analytical model for fracture-dominated reservoirs, *Soc. Pet. Eng. J.*, March, 242-250.

Karasaki, K., Ito, K., Wu, Y-S., Shimo, M., Sawada, A., Maekawa, K., Hatanaka, K., 2009, Uncertainty reduction of hydrogeologic models using data from surface investigation.

Kazemi, H., 1969, Pressure transient analysis of naturally fractured reservoirs with uniform fracture distribution, *Soc. Pet. Eng. J., Dec.*, 451-462; Trans. AIME 246.

Kumazaki, N., Ikeda, K., Goto, J., Mukai, K., Iwatsuki, T., Furue, R., 2003, Synthesis of the shallow borehole investigations at the MIU construction site, *Japan Nuclear Fuel Cycle Development Institute Report TN7400*, pp 2003-2005.

Larkin, B.K., 1963, Solutions to the diffusion equation for region bound by a circular discontinuity, *Soc. Pet. Eng. J.*, June., 113-115; Trans. AIME 228.

Levy, T., 1988, Ecoulement d'un fluide dans un milieu poreux fissure, *C.R. Acad. Sci. Paris*, 306, 1413-1417, 1988.

Levy, T., 1990, Filtration in a porous fissured rock: Influence of the fissures connectivity, *Eur. J. Mech*. B9, 309-327, 1990.

Lomize, G.M., 1951, Seepage Through Fractured Rocks, *Gosenergoizdat*, Moscow.

Long, J.S., Remer, J.S., Wilson, C.R., and Witherspoon, P.A., 1982, Porous media equivalents for networks of discontinuous fractures, *Water Resour. Res*. 18, No. 3, 645-658.

Long, J.S., and Witherspoon, P.A., 1985, The relationship of the degree of interconnection to permeability in fracture networks, *J. Geophys. Res*. vo. 90, No. B4, pp. 3087-3098.

Long, J.S., and Billaux, D.M., 1987, From field data to fracture network modeling: an example incorporating spatial structure, *Water Resour. Res*. 23, No. 7, 1201-1216.

Muskat, M., 1937, Use of data on build-up hole pressures, *Trans. AIME* 123, 44-48.

Muskat, M., 1949, *Physical Principles of Oil Production*, McGraw-Hill, New York.

Nakano, K., Amano, K., Takeuchi, S., Ikeda, K., Saegusa, H., Hama, K., Kumazaki, N., Iwatsuki, T., Yabuuchi, S., Sato, T., 2003, Working program for MIZ-1 borehole investigations, *Japan Nuclear Fuel Cycle Development Institute Report TN7400*, pp 2002-2008.

National Research Council Committee on Fracture Characterization and Fluid Flow, Rock failures and Fluid flow: contemporary understanding and applications, *National Academy Press*, Washington D.C., 1996.

Narasimhan, T.N., B.Y. Kanehiro, and P.A. Witherspoon, 1984, Interpretation of earth tide response of three deep, confined aquifers, *J. Geophys. Res*., 89(B3), 1913-1924.

Neretnieks, I., 1980, Diffusion in the rock matrix: an important factor in radionuclide retardation, *J. of Geophys. Res.* 85, B8, 4379-4397.

Odeh, A.S., 1965, Unsteady state behaviour of naturally fractured reservoirs, Soc. Pet. Eng. J., March, 60-64; *Trans. AIME* 234.

OECD/NEA (2002) GEOTRAP: Radionuclide Migration in Geologic, Heterogeneous Media. Nuclear Energy Agency, Organisation for Economic Co-Operation and Development, OECD Publications, 2, rue André-Pascal, 75775 Paris Cedex 16, France.

Oyamada, K., and Ikeda T., 1999, Uncertainty analysis on hydrologic modeling in heterogeneous media (CORE Collaborative Study), *Japan Nuclear Fuel Cycle Development Institute, TJ1400* 99-023.

Panfilov, M., Main modes of porous flows through highly heterogeneous media, *Sov. Phys. Dokl., Engl. Transl.*, 35, 225-227, 1990.

Panfilov, M., Averaged mode-type transition in flows through multiple heterogeneous media, *C.R. Acad. Sci. Paris*, 318, 1437-1443, 1994.

Parsons, R.W., 1966, Permeability of idealized fractured rock, *Soc. Pet. Eng. J.*, June, 126-136; Trans. AIME 246

Pinder, G.F., P.S. Huyakom, and E.A. Sudicky, *Simulation of flow and transport in fractured porous media, in Flow and Contaminant Transport in Fractured Rock*, edited by J. Bear, C.-F. Tsang and G. de Marsily, pp 395-435, Academic, San Diego, Calif. 1993.

Pruess, K., Narasimhan, T.N., 1985, A practical approach for modelling fluid and heat flow in fractured porous media, *Soc. Pet. Eng. J.*, 25 (l), 14-16.

Ramey, H.J. Jr., 1970, Approximate solutions for unsteady liquid flow in composite reservoirs, *J. Canadian Pet. Tech.*, March, 32-37.

Robinson, P.C., *Connectivity, flow and transport in network models of fractured media*, Ph.D. thesis, Oxford. Rep. TP 1072, Atomic Energy Research Authority, Harwell, UK, 1984.

Romm, E.S., 1966, *Flow Characteristics in Fractured Rocks*, Nedra, Moscow.

Saegusa, H., Inaba, H., Koide, K, Ogata, N., 1998, Simulation of regional scale groundwater flow in Tono area, *PNC TN*7410 98-004.

Saga, B., and Runchal, A., 1982, Permeability of fractured rock: Effect of fracture size and data uncertainties, *Water Resour. Res*. 18, No. 2, 266-274.

Sawada, A., Saegusa H., Takeuchi, S., Nakano, K, and Ijiri, Y, 2001, Evaluation of uncertainties due to hydrogeological modeling and groundwater flow analysis, in proceedings, Symposium on flow problems in fractured rocks, *Japanese Geotechnical Society*, Sept. 2001.

Sawada, A., H. Saegusa, K. Nakano, and H. Osawa, 2003, A study of uncertainties for evaluating groundwater flow by multiple modeling approaches, in proceedings, 32nd *Japanese Rock Mechanics Symposium*, Tokyo, 2003.

Sawada, A., Ohnishi, Y., Ohtsu, H., Ijiri, Y., Nishiyama, S., 2002, Applicability of the concept of fractal to fracture network model in rock mass, ed. by Choy, Ryu, Jeon and Moon. *Rock engineering problems and approaches in underground construction*, vol.1, pp 203-210 ISBN 89-53134-0-4 94530.

Schwartz, F.W., Smith, L., and Crowe, A.S., 1983, A stochastic analysis of macroscopic dispersion in fractured media, *Water Resour. Res.* 19, No. 5, 1253-1265.

Schweitzer, G. and Robbins, K. (Ed.) (2008) Setting the Stage for International Spent Nuclear Fuel Storage Facilities: *International Workshop Proceedings. National Academies Press*.

Snow, D.T., 1965, *A Parallel Plate Model of Fractured Permeable Media*, Ph.D. thesis, University of California, Berkeley.

Snow, D.T., 1969, Anisotropic permeability of fractured media, *Water Resour. Res*. 5, No. 6, 1273.

Takeuchi, S., Shimo, M., Nishijima, N, Goto, K., 2001, Investigation of hydraulic properties near the fault by pressure interference tests using 1000 m depth boreholes, *The 31st Japanese Rock Mechanics Symposium*, pp. 296-300, 2001.

Terzaghi, K., *Theoretical Soil Mechanics*, John Wiley and Sons, New York (1943) ISBN 0-471-85305-4.

Theis, C.V., 1935, The relation between the lowering of the piezometric surface and the rate and duration of discharge of a well using groundwater storage, *Trans. Amer. Geophys. Union* 16, 519-524.

Toth, J., Groundwater in sedimentary (clastic rocks), paper presented at the *National Symposium on Groundwater Hydrology, San Francisco, Calif.*, Nov. 6-8 1967.

Uozumi, N., Murakami, S., Oishi, Y., Kawamura, H., 2005, Drilling investigations in Mizunami Underground Research Laboratory Project, *Japan Nuclear Fuel Cycle Development Institute Report TJ7400*, pp 2005-2091.

Van der Kamp, G., and J.E. Gale, 1983, Theory of earth tide and barometric effects in porous formations with compressible grains, *Water Resour. Res.*, 19(2), 535-544.

Van Golf-Racht, T.D., 1982, *Fundamentals of Fractured Reservoir Engineering, Developments in Petroleum Science*, 12 Elsevier Scientific, Amsterdam, Oxford, New York.

Warren, J.R., and Root, P.J., 1963, The behavior of naturally fractured reservoirs, *Soc. Pet. Eng. J.*, Sept., 245-255; *Trans. AIME* 228.

Wilson, C.R., and Witherspoon, P.A, 1974, Steady state flow in rigid networks of fractures, *Water Resour. Res.* 10, No. 2, 328-335.

Wu, Y. -S., and K. Pruess, 2000, Numerical simulation of non-isothermal multiphase tracer transport in heterogeneous fractured porous media, Advances in Water Resources, 23 (2000), 699 -723.

Zangerl, C, K.F. Evans, Eberhardt, E., and S. Loew, Normal stiffness of fractures in granitic rock: A compilation of laboratory and in-situ experiements, *Int. J. Rock Mechanics and Mining Sciences*, 45(2008), 1500-1507.

Zimmerman, R.W., T. Hadgu, and G.S. Bodvarsson, 1996, Coupling of the semi-analytical dual-porosity simulation procedure to the LBNL/USGS site-scale model of the unsaturated zone at Yucca Mountain, Yucca Mountain Project Milestone 2GLF101M, Lawrence Berkeley National Laboratory, Berkeley, CA.